

**The nuclear envelope proteins Kugelkern and Narf
and their putative role in aging**

Dissertation

for the award of the degree

“Doctor rerum naturalium (Dr.rer.nat.)”

in the GGNB program “Genes and Development”

Division of Mathematics and Natural Sciences

at the Georg-August-University Göttingen

submitted by

Maria Kriebel

from Aschersleben, Germany

Göttingen, January 2018

revised version October 2018

MEMBERS OF THE THESIS COMMITTEE

Prof. Jörg Großhans (Supervisor, reviewer)

Department of Developmental Biochemistry, University of Göttingen

Prof. Reinhard Schuh (Reviewer)

Department of Molecular Developmental Biology, Max Planck Institute for Biophysical Chemistry, Göttingen

Prof. Harald Hermann-Lerdon

Department of Molecular Genetics, German Cancer Research Center, Heidelberg

MEMBERS OF THE EXAMINATION BOARD

Prof. Gregor Bucher

Department of Evolutionary Developmental Genetics, University of Göttingen

Prof. Bernd Wollnik

Department of Human Genetics, University of Göttingen

PD Dr. Halyna Shcherbata

Department of Gene expression and signaling, Max Planck Institute for Biophysical Chemistry, Göttingen

Date of the oral examination: 13.03.2018

AFFIDAVIT

I hereby declare that I wrote this thesis “The nuclear envelope proteins Kugelkern and Narf and their putative role in aging “on my own with no other sources and aids than indicated.

Maria Kriebel

Göttingen, 31.01.2018

TABLE OF CONTENT

Acknowledgments	1 -
Abbreviations	2 -
1 Abstract	6 -
2 Introduction	7 -
2.1 Nuclear lamins	7 -
2.2 Lamin A mutations and Hutchinson-Gilford progeria syndrome.....	9 -
2.3 <i>Drosophila</i> as a model to study aging	10 -
2.4 Narf - a new progeria gene?	11 -
2.5 Narf like genes have a common ancestor and play a role in Fe-S protein biogenesis	12 -
2.6 Role of Narf-like genes in sensing oxygen.....	13 -
2.7 Role of Narf-like genes in aging.....	14 -
3 Aim of the study	15 -
4 Results	16 -
4.1 Identification of novel Kuk interaction partners.....	16 -
4.1.1 Characterization of $\Delta 15$ a kuk deficient fly line.....	16 -
4.1.2 Nuclear elongation is missing in $\Delta 15$ embryos	17 -
4.1.3 Gene expression is altered in <i>kuk</i> -depleted embryos.....	19 -
4.1.4 Survival rate is affected in <i>kuk</i> -depleted animals	20 -
4.2 Identification of biochemical interaction partners of Kuk.....	22 -
4.2.1 GFP-Kuk transgenes did not rescue the <i>kuk</i> loss of function phenotype- 22 -	
4.2.2 Proteolytic cleavage of GFP-Kuk.....	23 -
4.2.3 Nuclei solubilization promoted further degradation.....	26 -
4.2.4 Biochemical properties of GFP-Kuk (C567S)	28 -
4.3 Identification of genetic interaction partners of Kugelkern.....	30 -
4.3.1 Morphological defects upon Kugelkern overexpression were primary independent of apoptosis.....	31 -
4.3.2 Genetic interaction partners of Kuk remain undiscovered	35 -
4.4 The role of Narf in nuclear morphogenesis and aging	37 -
4.4.1 Generation of a Narf specific antibody.....	37 -
4.4.2 Narf localized to the nuclear envelope	39 -
4.4.3 Narf has a function during <i>Drosophila</i> development	41 -

4.4.4	The lethal allele NC 38 probably resulted in nonsense-mediated decay-	43 -
4.4.5	Genomic transgenes mimicing the human patient situation.....	- 44 -
4.4.6	Increase of genomic copies of Narf might positively affect viability -	46 -
4.4.7	Ubiquitous overexpression of Narf had beneficial effects on lifespan-	49 -
4.4.8	Using the CRISPR approach for generating a Narf null allele.....	- 50 -
4.4.9	The GeneSwitch Gal4 system was used to muscle specifically express GFP in a dose dependent manner	- 52 -
4.4.10	The GeneSwitch system was used to muscle specifically overexpress Narf.....	- 55 -
4.4.11	Overexpression of Narf increased nuclear size in muscle cells.....	- 56 -
4.4.12	Muscle specific overexpression of Narf affected negative geotaxis behavior	- 58 -
4.4.13	Muscle specific overexpression of Narf affected <i>Drosophila</i> lifespan-	60 -
4.4.14	Knock-down of Narf did not significantly increase nuclear size in muscle cells	- 63 -
4.4.15	Muscle specific knock-down of Narf during adulthood affected lifespan.....	- 65 -
4.4.16	Narf is essential during adult stage.....	- 67 -
4.4.17	Gene expression is changed in Narf overexpressing or down regulating situations.....	- 69 -
4.4.18	Klp68D is a Narf interaction partner	- 71 -
4.5	Is Narf involved in aging in <i>C. elegans</i> ?	- 72 -
4.5.1	Oxygen sensitivity of <i>oxy-4</i> mutants	- 72 -
4.5.2	<i>oxy-4</i> mutants showed a developmental delay under normal conditions-	73 -
4.5.3	Unchanged muscle structure in <i>oxy-4</i> mutants	- 74 -
4.5.4	Nuclei morphology and Ce-lamin farnesylation were not affected in <i>oxy-4</i> mutants	- 77 -
4.5.5	Do Oxy-4 and Ce-lamin act via the same pathway?	- 79 -
5	Discussion	- 82 -
5.1	Kugelkern and its role in aging.....	- 82 -
5.1.1	The <i>kuk</i> deficient fly line $\Delta 15$ might still contain recessive mutation(s)-	82 -
5.1.2	Proteolytic cleavage might be mediated by PEST-sequences.....	- 83 -
5.2	Narf is involved in aging in <i>Drosophila</i>	- 84 -

5.2.1	Narf might have an essential role in Fe-S protein maturation.....	85 -
5.2.2	Lifespan analyses as a tool to study aging.....	86 -
5.2.3	Narf overexpression might increase intracellular stress defense mechanisms	87 -
5.2.4	An altered Narf expression in muscle cells probably leads to redox imbalance.....	91 -
5.2.5	The human mutation might represent a loss-of function allele	94 -
6	Materials and Methods	95 -
6.1	Materials	95 -
6.1.1	General Buffers	95 -
6.1.2	Chemical reagents	95 -
6.1.3	Laboratory services.....	95 -
6.1.4	Antibiotics	95 -
6.1.5	Enzymes and Kits	96 -
6.1.6	Chromatography	96 -
6.1.7	Fly stocks.....	97 -
6.1.8	Worm strains and RNAi-vectors used in this study	98 -
6.1.9	Media for flies	99 -
6.1.10	Media for <i>C.elegans</i>	99 -
6.1.11	Bacterial cell lines	100 -
6.1.12	Media for bacterial culture	100 -
6.1.13	Oligonucleotides.....	100 -
6.1.14	Plasmid constructs	103 -
6.1.15	Primary antibodies.....	105 -
6.1.16	Secondary antibodies.....	106 -
6.1.17	Software.....	107 -
6.1.18	Equipment.....	107 -
6.1.19	Other materials	108 -
6.2	Methods	110 -
6.2.1	DNA methods	110 -
6.2.2	RNA methods	113 -
6.2.3	Biochemical methods	114 -
6.2.4	Antibodygeneration	117 -

6.2.5	Staining methods	- 124 -
6.2.6	Fly work methods	- 127 -
6.2.7	Worm work methods	- 129 -
6.2.8	Microscopy	- 130 -
7	References	- 132 -
8	Supplement Data	- 145 -
	List of Figures	- 157 -
	List of Tables.....	- 159 -
	Curriculum Vitae.....	Fehler! Textmarke nicht definiert.

Acknowledgments

First of all I would like to thank Prof. Jörg Großhans for giving me the opportunity to do my PhD in his laboratory and to get the chance to carry out a project within the aging field. I am very thankful for all the discussions, his support and his positive thinking during the 4 years of my PhD.

I would like to thank my thesis committee members Prof. Reinhard Schuh and Prof. Harald Herrmann-Lerdon for their suggestions and constructive criticism during our meetings. I am thankful to Prof. Bernd Wollnik for sharing the Narf-project with me.

I would like to thank Prof. Yosef Gruenbaum, who gave me the opportunity to work in his laboratory and getting the chance to work with *C.elegans*, another very fascinating model organism. Special thanks go to Ph.D. Noam Zuela, Chayki Charar, Tam Yadid, Jehudith Dorfmann and Perah Spann, who introduced me in to the *C.elegans* methods and supported me during my stay. I would also like to thank Prof. Henrik Bringmann, as I was allowed to finish my *C.elegans* project in his laboratory. In addition, I would like to thank the Boehringer Ingelheim Founds for the funding of the *C.elegans* project in Israel.

Furthermore, I am grateful to all members of the Department of Developmental Biochemistry for the nice working atmosphere and our regular seminars. I would like to thank the TAL lab for performing the RNAseq analysis and their helpful discussions.

A special thank goes to all members of the “fly group”. I am happy that I had the chance to work with all of you together. I really enjoyed our friendly and cooperative environment! I am thankful to Dr. Michaela Clever and Dr. Roman Petrovsky for sharing their results, their supportive discussions and ideas during our “monday” meetings. I would like to express thanks to Long Li for his friendship and for helping me to take care of my fly cages at the weekend. I am thankful to Johannes Sattmann for assisting me with the lifespan analyses. Furthermore I would like to show gratitude to Anja Schmidt and Dr. Franziska Winkler, who helped me a lot during my PhD and shared their expertise with me whenever I needed advice.

I am also very thankful to Dr. Deqing Kong, Dr. Katja Kriebel, Dr. Maja Gere and Dr. Zhiyi Lv, who were willing to read parts of my first versioned thesis. Thank you for your patience and suggestions!

I would like to thank my family for their support and believe in me. And last but not least I am very grateful to Florian Rest, for his endless support and understanding.

Abbreviations

%	percent
Δ	deletion
°C	degree Celsius
μ	micro-
A	ampere
aa	amino acid (s)
Ab	antibody
Amp	Ampicillin
ATP	adenosine triphosphate
bp	base pairs
BSA	bovine serum albumin
<i>C. elegans</i>	<i>Caenorhabditis elegans</i>
cDNA	complementary DNA
cm	centimeter
Co-IP	Co-immunoprecipitation
CV	column volume (s)
d	day (s)
D.m.	<i>Drosophila melanogaster</i>
Da	Dalton
DAPI	4', 6' – Diamidino-2-phenylindole
DEPC	diethyl pyrocarbonate
ddH ₂ O	double distilled water
DNA	deoxyribonucleic acid
DTT	1,4-dithiothreitol
<i>E.coli</i>	<i>Escherichia coli</i>
EDTA	ethylenediaminetetraacetic acid
<i>et al.</i>	latin phrase for "and others"
FG	phenylalanine-glycine
FRAP	fluorescence recovery after photobleaching
FRT	flippase recognition target
FTase	Farnesyltransferase
FTI	farnesyl transferase inhibitor

Abbreviations

fwd	forward
g	gram (s)
G0	parental generation
GFP	green fluorescent protein
gp	guinea pig
h	hour (s)
H/R	histidine/arginine
HCL	<i>hydrochloric acid</i>
HeLa	Henrietta Lack cells
HEPES	4-(2-hydroxyethyl)-1-piperazineethanesulfonic acid
HGPS	Hutchinson-Gilford progeria syndrome
His	histidine
<i>in vitro</i>	latin phrase for "within the glass"
<i>in vivo</i>	latin phrase for "within the living"
<i>in silico</i>	latin phrase for "performed on computer"
INM	inner nuclear membrane
IOP1	mammalian iron-only hydrogenase-like protein 1 (Narf-like)
IOP2	mammalian iron-only hydrogenase-like protein 2 (Narf)
IPTG	Isopropyl- β -D-thiogalactopyranoside
kb	kilobases
<i>kuk</i>	<i>kugelkern</i> gene
Kuk	Kugelkern protein
l	litre (s)
L1/L2/L3	larval stages 1, 2 and 3
LB	Luria-Bertani medium
LMN	lamin gene
m	milli, meter-
M	molar
MCS	multiple cloning site
MEFs	mouse embryonic fibroblasts
min	minute (s)
mRNA	messenger RNA
MW	molecular weight

Abbreviations

MWOC	molecular weight cut-off
n	nano
NaOH	Sodium hydroxide
Narf	nuclear prelamin a recognition factor protein
NarfL	Narf-like
NGM	nematode growth medium
NLS	nuclear localization signal
NPC(s)	nuclear pore complex (es)
Nup	Nucleoporin
OD	optical density
PA-isoform	protein isoform A
PBS	phosphate buffered saline
PCR	polymerase chain reaction
pH	potential of hydrogen
PMSF	phenylmethylsulfonyl fluoride
PTM	post-translational modification
qRT-PCR	quantitative real-time PCR
r	rabbit
rev	reverse
RNA	ribonucleic acid
RNAi	RNA interference
RNAseq	RNA sequencing
ROS	reactive oxygen species
RT	room temperature
RU	Mifepristone
s	second (s)
<i>S. cerevisiae</i>	<i>Saccharomyces cerevisiae</i>
SDS	<i>sodium dodecyl sulfate</i>
SDS-PAGE	SDS-polyacrylamide gel electrophoresis
TAE	<i>buffer</i> solution of Tris base, acetic acid and EDTA
TCA	trichloroacetic acid
Tris	<i>tris</i> (hydroxymethyl)aminomethane
U	Unit (s)

Abbreviations

UAS	upstream activating sequence
V	Volt
v/v	volume per volume
VDRC	Vienna <i>Drosophila</i> RNAi Center
w/v	weight per volume
WT	wild-type
xg	g-force
Y2H	yeast two-hybrid

1 Abstract

Lamins are type V intermediate filaments and represent the major constituent of the nuclear lamina. Mutations in the laminA/C gene as well as in other nuclear envelope associated proteins lead to a series of human genetic disorders, so-called laminopathies. The most prominent laminopathy is the Hutchinson-Gilford progeria syndrome (HGPS). HGPS patients appear prematurely aged developing aging-related conditions such as osteoporosis, loss of subcutaneous fat and cardiovascular disease already during childhood. Many of the HGPS patients contain a single point mutation in the lamin A/C gene which affects the maturation process and leads to the expression of a permanently farnesylated Prelamin A, called Progerin. Progerin accumulates at the nuclear periphery and leads to a variety of cellular and nuclear defects like a disorganization of heterochromatin structure, an increase in DNA damage and defects in nuclear morphology. Despite the insights in the clinical symptoms and the genetic basis of HGPS and other laminopathies, the molecular and cellular mechanism that leads to accelerated aging is unknown and remains a topic of ongoing research.

The Großhans lab has developed a HGPS model in *Drosophila*, using lamin Dm0 and Kuk, a nuclear protein which shares structural and functional features to lamins. As farnesylation plays a major role in the disease mechanism, I screened for genetic and biochemical interaction partners of Kuk. I focused on Narf, which has previously been identified as a Lamin binding partner that depends on farnesylation. Furthermore a dominant *de novo* mutation was recently identified within the human Narf protein causing HGPS related symptoms (Prof. Wollnik, personal communication). Narf is an evolutionary conserved protein with a homologue in *Drosophila*. As Narf is thought to interact specifically with the farnesylated Prelamin A in humans, I hypothesized that Narf interacts with Lamin Dm0 or Kugelkern in *Drosophila*. Beside mapping and complementation analysis, nothing was known about the function of Narf in *Drosophila*. In order to study the cell biological and developmental functions of Narf, I established *Drosophila* as a model system. I characterized point mutations and generated several tools like an antibody as well as genomic and inducible transgenes. Narf localizes to the nuclear envelope and is essential for development as well as during adulthood. Narf function may rely to its role in Fe-S protein maturation. I demonstrated that Narf is involved in aging-related processes as loss-of function experiments decreased *Drosophila*'s lifespan whereas constitutively higher expression by multiple genomic copies or UAS overexpression led to a prolongation in lifespan. How Narf might contribute to these processes is not clear yet. RNA sequencing analyses points to a role in oxidative stress response. My data suggest a role of Narf in the regulation of stress defense mechanisms which are required for the maintenance of a cellular redox homeostasis needed for aging.

2 Introduction

2.1 Nuclear lamins

The defining property of eukaryotic cells is a nucleus. The nucleus consists of an outer nuclear membrane and an inner nuclear membrane which are fused together at sites of the nuclear pore complexes, allowing the exchange of molecules between the cytoplasm and the nucleoplasm. Metazoan cells additionally contain the nuclear lamina which is underlying the inner nuclear membrane and consist predominantly of lamins which are evolutionary conserved type V intermediate filament proteins. Lamins are required for the maintenance of the nuclear shape and involved in numerous nuclear functions (reviewed in Gruenbaum et al., 2003, Dechat et al, 2010, Gruenbaum and Foisner 2015, Vidak and Foisner 2016).

Two different types of lamins can be found, namely A- and B- type lamins. A-type lamins are encoded by the LMNA gene in which lamin A and lamin C represent the major isoforms. They are generated by alternative splicing and differ in their C-terminus. A-type lamins are tissue specific expressed. Conversely, B-type lamins are constitutively expressed and are essential for developmental processes. B-type lamins, comprising lamin B1 and B2, are encoded by two distinct genes, namely LMNB1 and LMNB2 (Eckersley-Maslin et al., 2013, Dechat et al., 2010).

Nuclear lamins share a conserved polypeptide structure which comprises a variable head domain, a α -helical coiled-coil rod domain and a globular tail domain including an Ig-fold motif, the nuclear localization signal (NLS) and the CaaX motif (Stuurman et al., 1998) (Figure 1 A). B-type lamins and lamin A, but not lamin C, originate from premature lamins and contain a CaaX motif (C- cysteine residue, aa – aliphatic residues, X- any amino acid) (Liu et al., 2006, Sinensky et al., 1994) (Figure 1 B-C). During lamin maturation the cysteine within the CaaX-motif is farnesylated which is mediated by a farnesyltransferase (FTase). The next processing step includes the cleavage of the last three carboxyl terminal aminoacids (aaX) by the proteases FACE1/ZMSPTE24 or FACE2/Rce1. Finally, a carboxymethylation of the farnesylated cysteine takes place which is mediated by the isoprenyl-cysteine-carboxy-methyltransferase (ICMT). B-type lamins are not further processed and stay farnesylated. Lamin A maturation is completed by a further cleavage of the last 15 carboxy terminal aminoacids, which lead to a removal of the farnesylated and carboxymethylated

cysteine by FACE1/ZMPSTE24 (Pendas et al 2002, Rusinol and Sinensky 2006, Young et al 2005) (Figure 1 B).

The farnesylated and carboxymethylated CaaX- motif mediates the association of lamins with the inner nuclear membrane (INM). B-type lamins keep the CaaX- motif after processing which lead to a predominant localization to the nuclear envelope. A-type lamins instead lack the farnesyl group in their matured form, which causes a localization to the nuclear envelope as well as to the nucleoplasm (Dechat et al., 2010, Kolb et al., 2011, Moir et al., 2000).

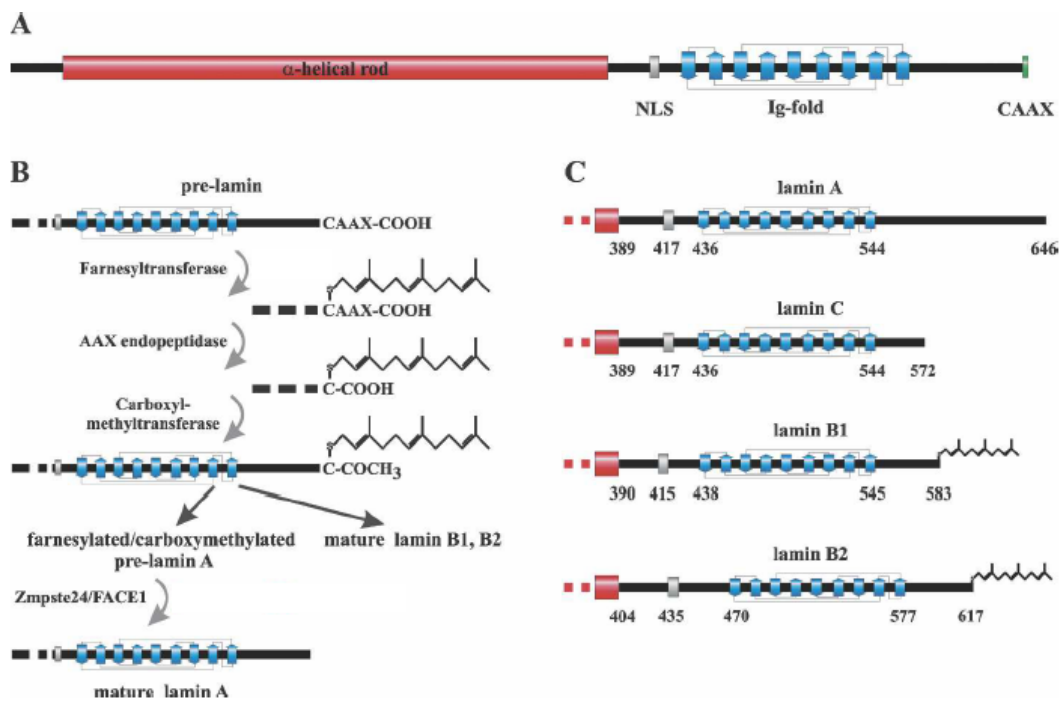


Figure 1: Nuclear lamins share a conserved structure

(A) Illustration of the lamin A structure. Lamins consist of a variable head domain (not shown), α helical coiled-coil rod domain (red) and a globular tail domain (blue), including the nuclear localization signal (NLS, grey) and the CaaX-motif (green). (B) Overview of the processing steps of the premature lamins A, B1 and B2. The processing includes three major steps: first the farnesylation of the cysteine within the CaaX-motif by a farnesyltransferase (FTase), second the cleavage of the last three carboxyl terminal amino acids (aaX) by an endopeptidase (FACE1/ZMPSTE24 or FACE2/Rce1) and third the carboxymethylation of the farnesylated cysteine by an isoprenyl-cysteine-carboxy-methyltransferase (ICMT). B-type lamins are not further processed and stay farnesylated. Lamin A maturation is completed by a cleavage step of the last 15 carboxy terminal amino acids, including the farnesylated and carboxymethylated cysteine by FACE1/ZMPSTE24. (C) Overview of the C-terminal differences in matured lamins. Mature lamin A and lamin C do not possess a farnesylation motif at their C-terminal end. The reasons are the cleavage of farnesylation for lamin A during maturation and

the lack of a CaaX motif for lamin C. However, B-type lamins stay farnesylated and carboxymethylated (modified to Dechat et al., 2008).

2.2 Lamin A mutations and Hutchinson-Gilford progeria syndrome

A series of human genetic disorders, so-called laminopathies are caused by mutations in genes coding for proteins of the nuclear lamina, including lamin A/C. More than 500 mutations are reported until now, which give rise to striated muscles diseases, adipose tissue diseases, peripheral nerve diseases and accelerating aging disorders (reviewed in Broers et al., 2006). The most prominent laminopathy is the Hutchinson-Gilford progeria syndrome (HGPS), which affects 1 in 4-8 million newborns (Progeria Research Foundation). Patients with HGPS appear prematurely aged and develop aging-related conditions already during childhood.

Most of the HGPS patients contain a single point mutation within exon 11 (1824C>T, p.G608G). This mutation causes the activation of a cryptic splice site which lead to an internal deletion of 50 amino acids and by this to a disruption of the premature lamin A processing. The consequence is the generation of a mutant Prelamin A, called Progerin. Progerin is permanently farnesylated, in contrast to normal Lamin A, as the internal deletion also affects the FACE1/ZMPSTE24 cleavage site (De Sandre-Giovannoli et. al., 2003, Eriksson et al., 2003, Pollex and Hegele 2004, Moulson et. al., 2007). Progerin is accumulating at the nuclear periphery as a consequence to its permanent farnesylation, which mediates the association to the inner nuclear membrane. This leads to severe cellular defects like disorganized heterochromatin, increased DNA damage and defects in nuclear morphology (Dechat et al., 2007, Kitten and Nigg 1991, Krohne 1998, Capell et al., 2005, Gonzalez-Suarez et. al., 2009, Scadaffi et al., 2005). Progerin expression can be also found in physiologically aged humans, suggesting that Progerin contributes to normal aging, too (McClintock et al., 2007). Currently, clinical trials with HGPS patients have been ongoing for a few years with inhibitors of the farnesyl transferase (Young et al., 2006, Gordon et al., 2013, Young et al., 2013, Ullrich et al., 2013). Less clear than the clinical symptoms and the genetic basis of HGPS and other laminopathies, is the molecular and cellular mechanism that leads to accelerated aging. Several models, such as reduced mechanical stability, dysfunctional nuclear transport, impaired chromatin organization and increased DNA

damage have been proposed, but none of these models provides a full explanation (reviewed in Gosh and Zhou 2014, Gruenbaum and Foisner 2015).

2.3 *Drosophila* as a model to study aging

Aging processes are a field of extensive research, whereby *Drosophila* is used as a model system to study lamins in general but also to mimic distinct *lamin* mutations causing human diseases (e.g. Schulze et al., 2009, Munoz-Alarcon et al., 2007, Dialynas et al., 2015). Compared to humans, where two types of lamins can be found, most of the invertebrates possess only one B-type lamin. However, *Drosophila* represents an exception among invertebrates as two lamins, lamin Dm0 and lamin C are expressed. Lamin Dm0 is grouped to B-type lamins by the presence of a CaaX-motif and its ubiquitous expression during development. Lamin C is classified as an A-type lamin, lacking a CaaX box and being expressed in a developmentally regulated manner (Erber et al., 1999, Gruenbaum et al., 1988, Bossie and Sanders, 1993, Riemer et al., 1995).

Drosophila contains a second farnesylated nuclear protein next to the farnesylated B-type lamin Dm0, which is named Kugelkern (Kuk) due to its function in nuclear morphogenesis (Brandt et al., 2006). The Grosshans lab has established a *Drosophila* HGPS model (Brandt et al., 2006, 2008), in which this mechanism can be studied in a genetically tractable organisms. Kuk is localized to the nuclear side of inner nuclear membrane and causes ruffled and overlobulated nuclei, a reduction in heterochromatin and shortened mean lifespan of flies similar to lamin Dm0 (Brandt et al., 2008). Overexpression of the farnesylated Kuk in *Drosophila* and Lamin proteins in humans induce similar aging related phenotypes (Figure 2). Thus, it might be beneficial to study the function and activity of Kuk in order to enhance the understanding of premature aging in HGPS.

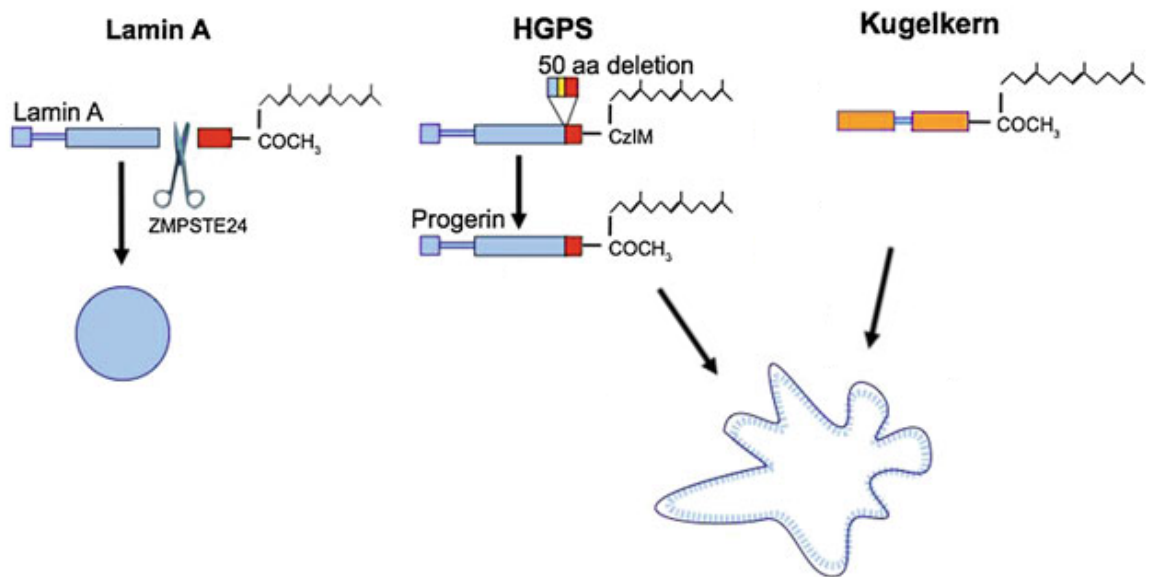


Figure 2: The effect of farnesylated nuclear proteins on nuclear morphology

The normal processing of Pre-lamin A includes the removal of the farnesylated cysteine within the CaaX-motif by a FACE1/ZMPSTE24 mediated cleavage of the last 15 carboxy terminal amino acids (red). This last processing step is disrupted in HGPS patients due to an internal deletion of 50 aminoacids (blue-yellow-red box) which is caused by a single point mutation (yellow). This leads to a mutant Pre-lamin A, called Progerin. Expression of this mutant protein leads to accumulation at the inner nuclear membrane and causes cellular defects like disorganized heterochromatin, increased DNA damage and defects in nuclear morphology. Same effects have been observed in *Drosophila melanogaster* overexpressing Kugelkern (Kuk), a nuclear protein that do not belong to lamins. Kuk shares structural similarities like a putative coiled-coil region (blue), a nuclear localization signal (not shown) and a farnesylated CaaX-motif. Not conserved features are shown in orange (modified to Brandt and Vilcinskis, 2013).

2.4 Narf - a new progeria gene?

The group of Prof Bernd Wollnik (Institute for Human Genetics, Göttingen) recently identified a dominant *de novo* mutation in the protein Narf in a Turkish patient with symptoms related to HGPS, mimicking clinical features (e.g. reduced subcutaneous fat, mild osteoporosis) and nuclear morphology (e.g. ruffled nuclei) (personal communication Prof. Wollnik). Initially Narf was identified as a binding partner of farnesylated Prelamin A. Narf binds the carboxyl-terminal tail of Prelamin A dependent on farnesylation (Barton and Worman, 1999). The authors proposed that Narf could be a co-factor of ZMPSTE and might be important for Lamin A processing or might act as an anchor for farnesylated Prelamin A to organize nuclear proteins.

2.5 Narf like genes have a common ancestor and play a role in Fe-S biogenesis

Narf-like genes are quite conserved as they share a common ancestor with [Fe] -only hydrogenases. Due to this they are also known as eukaryotic hydrogenase like proteins. Hydrogenases in general are enzymes in anaerobic organisms, which are needed for anaerobic respiration as they are catalyzing the oxidation of molecular hydrogen: $2\text{H}^+ + 2\text{e}^- \rightleftharpoons \text{H}_2$ (reviewed in Nicolet et al., 2002).

However, Narf-like genes do not produce hydrogen anymore and it is supposed that they developed new functions during development (Hackstein, 2005). One of the best characterized Narf-like genes is the yeast homologue *nar1*. Nar1 belongs to the group of Fe-S-proteins and is essentially required for the maturation of cytosolic and nuclear Fe-S proteins (Balk et. al., 2004, 2005). Fe-S protein biogenesis is a quite conserved mechanism and Fe-S proteins are involved in a variety of processes including oxygen sensing, electron transport, Fe-S protein maturation and transcriptional regulation (Nakamura et al., 2013, reviewed in Johnson et al., 2005).

In mammalian, the two orthologous Narf (nuclear prelamin A recognition factor) or IOP2 (iron-only hydrogenase-like protein 2) and Narf-like or IOP1 are known. It was shown in HeLa cells and MEFs (mouse embrionic fibroblasts) that IOP1 is involved in biogenesis of mammalian cytosolic Fe-S protein as a knockdown situation is affecting the activity of different cytosolic Fe-S proteins but has no effect of tested mitochondrial Fe-S proteins or non Fe-S proteins (Song et al., 2009; Song and Lee, 2008, 2011). The described effects were shown to be specific for IOP1 as a knockdown for IOP2/Narf did not affect Fe-S protein maturation (Song and Lee, 2008). The effect of an IOP1 depletion in mice leads to lethality during early embryogenesis as well as in adults if the knock-out was performed in an inducible way (Song and Lee, 2011). On the molecular level it was described that IOP1 depletion in MEFs selectively activates intracellular signaling pathways like caspase dependent apoptosis and stress kinase p38 mediated autophagy (Song and Lee, 2011). Comparable with yeast, it was described in Hela cells that a knockdown of IOP1 leads to a global decrease in protein synthesis which finally leads to a growth impairment and a decreased cell viability (Song and Lee, 2008).

2.6 Role of Narf-like genes in sensing oxygen

Loss of function studies performed for Narf-like genes revealed a sensitivity against oxygen. Growth defects during development at high concentrations as well as under normoxic conditions were observed for example in *C. elegans* (*oxy-4*), *S. cerevisiae* (Nar1) and *A. thaliana* (Gollum) (Cavazza et al., 2008; Fujii et al., 2009; Mondy et al., 2014).

In yeast, Nar1 mutant cells exhibited a higher level of reactive oxygen species (ROS) even in non-stressed situations, which is even more increased at high concentrations of oxygen. One explanation for this finding was given by the observation that a loss of Nar1 leads to a decrease of mitochondrial SOD2 mRNA level, one of the superoxide detoxifying genes and critically required for efficient oxidative stress protection in yeast (Steinman, 1980; Sturtz et al., 2001; Zhao et al., 2014). It was supposed that a loss of Nar1 causes a defect in the maturation of several Fe-S protein, which consequently damages mitochondria and leads to a decrease in SOD2 (Zhao et al., 2014). In plant and yeast growth arrest can be rescued with hypoxic conditions (Cavazza et al., 2008; Fujii et al., 2009), suggesting that Nar1 and Gollum might be involved within an oxygen sensitive step in Fe-S protein maturation or are not essential at low oxygen concentrations. However, complementation of the plant Gollum gene within in a Nar1 yeast mutant strain was not achieved, meaning that they either functions in different pathway or interact with different interaction partner (Cavazza et al., 2008).

In mammalian cells an additional oxygen response pathway was linked to IOP1. It was shown that a knockdown of IOP1 (Narf-like) but not of IOP2 (Narf) results in an up regulation of HIF1 α (hypoxia inducible factor 1 α), which is a key transcription factor under hypoxic conditions (Huang et al., 2007). The HIF transcription factor functions as a heterodimer and consist of α - and β -subunits. In case of hypoxia, the subunits are dimerizing and translocate to the nucleus to allow gene expression (reviewed in Semenza, 1999). Under normoxic conditions, proline residues of the HIF1 α subunit are permanently hydroxylated by a family of PHDs (proline hydroxylase domain-containing protein), which marks HIF1 α and finally leads to its degradation (Bruick and McKnight, 2001; Ivan et al., 2001; Jaakkola et al., 2001; Salceda and Caro, 1997). A Yeast-two-hybrid assay showed that IOP1 and PHD2 are direct interaction partners, showing a function of IOP1 under normoxic and hypoxic conditions (Huang et al., 2007). A shRNA approach of IOP1 in hyperoxia resistant HeLa cells caused increased oxygen sensitivity and identified IOP1 to be active also under

hyperoxic conditions. The increase in oxygen resistance was achieved by the up regulation of IOP1 mRNA and protein levels (Corbin et al., 2015). Fe-S proteins are sensitive against ROS and oxygen as the iron is easily oxidized (reviewed in Johnson et al., 2005). It was shown that IOP1 was able to protect the cytosolic and nuclear Fe-S proteins in presence of high oxygen and thereby overcome the problem of oxidative stress (Corbin et al., 2015).

2.7 Role of Narf-like genes in aging

A link between Fe-S protein maturation and genome stability was made in 2012. It was shown that depletion of IOP1 in HEK293 cells leads to a defective maturation of XPD, which is a component of the transcription factor complex TFIIH and involved in nucleotide excision repair (Gari et al., 2012, Rudolf et al., 2006, Stehling et al., 2012). Several other nuclear Fe-S proteins are known to play a role in DNA repair, replication and telomere length. It is likely that a defect in Fe-S protein maturation affects multiple DNA repair pathways which finally leads to genomic integrity a known characteristic of aging (Gari et al., 2012, Stehling et al., 2012).

Lifespan analyses in *C.elegans* and yeast, demonstrated the role of Narf-like genes in aging (Fujii et al., 2009, Zhao et al., 2014). The reasons for a decrease in lifespan were made by an increased sensitivity to oxygen. It is a well-known fact that oxygen and the resulting reactive oxygen species (ROS) are involved in the damage of DNA, proteins and lipids. By this oxidative stress leads to accelerated aging. An interesting link between vertebrates and invertebrates was given by the observation that the mutant allele of the *C.elegans* ortholog Oxy-4 possesses an amino acid exchange at exactly the same position like it was described for human Narf/IOP2 (Fujii et al., 2009, personal communication Prof. Wollnik). Besides, of being a binding partner of farnesylated Prelamin A nothing is known for Narf/IOP2. As Narf and IOP1 differ in protein localization and are not able to complement each other, it is supposed that they do not have the same functions, hypothesizing a direct role of Narf/IOP2 in aging (Barton and Worman, 1999, Song and Lee, 2008, 2011). However, the molecular mechanism of how Narf-like genes affect the lifespan are not well characterized yet.

3 Aim of the study

Overexpression of the farnesylated Kuk induces cellular defects that lead to aging related phenotypes. One aim of this thesis was the identification of Kuk binding partners or complexes and to determine the role of farnesylation. Furthermore, CG17683 the *Drosophila* homologue of the human Narf was analyzed. As Narf is an already identified Lamin binding partner and dependent on farnesylation it was hypothesized that CG17683 specifically interacts with Lamin Dm0 or Kugelkern in *Drosophila*. Beside mapping and complementation analysis, the function of Narf in *Drosophila* has not been studied. Due to this, the function of Narf during development, the connection of Narf in aging in *Drosophila* and the effect of Narf to the farnesylation or subcellular distribution of Kugelkern and/or Lamin Dm0 was analyzed.

4 Results

4.1 Identification of novel Kuk interaction partners

The *Drosophila* protein Kugelkern (Kuk) is the only known nuclear envelope protein, excluding lamins, which also contains a CaaX-motif enabling farnesylation. It was shown that Kuk shares further structural similarities with lamins, like a nuclear-localization signal (NLS) and a putative coiled-coil domain. Kuk is characterized through an early zygotic gene-expression and is required for nuclear elongation. An overexpression of Kuk causes overlobulated nuclei and is connected to accelerated aging phenotypes in adult flies (Brandt et al., 2006, 2008). It is hypothesized that these effects are partially dependent on Kuk-farnesylation, suggesting the mediation of a distinct protein-complex formation. The aim of this study was the identification of farnesylation dependent interaction partners of Kuk and to determine the role of farnesylation in protein complex formation.

4.1.1 Characterization of $\Delta 15$ a kuk deficient fly line

To study Kugelkern function a deletion mutant was generated by the Großhans laboratory. Therefore, a w^+ marked transposon was mobilized and a lethal point mutation within CG5169 (GckIII) was complemented with a genomic rescue construct (Brandt et al., 2006). However, the deletion breakpoints were not fully characterized yet. To narrow down the breakpoints, genomic DNA of *kuk* deficient flies ($\Delta 15$) was isolated and PCR reactions comprising the *kuk* neighboring regions were performed. A long range PCR, using the oligonucleotides MK26 and MK29, revealed a size difference of the wild type PCR product compared to the mutant gene locus. Sequencing analyses confirmed that the depletion of the *kuk* deficient line comprises a gene region of 5.5 kb with an additional insertion of 465 bp from the originally inserted P-element vector. An illustration of the described characterization is shown in Figure 3. The sequencing results of the deletions breakpoints are shown in Supplement Figure 1.

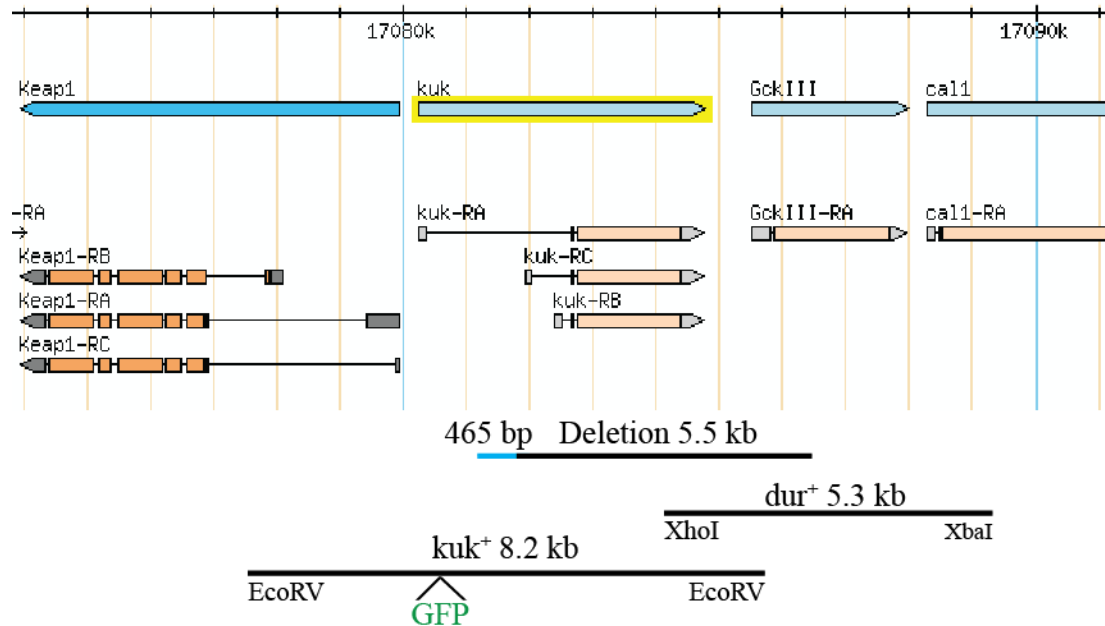


Figure 3: The deletion of a *kuk* deficient line comprise 5.5 kb within the genomic locus

The genomic breakpoints of the deletions were analyzed by PCR, including the neighboring genes of *kuk*. Final characterization was done by a long range PCR (MK26/MK29) followed by a subsequent sequencing analysis. The sequencing results revealed a depletion of ~ 5.5 kb within the genomic locus of *kuk* and *GckIII* (*dur*). Furthermore, an insertion of 465 bp due to initially performed transposon remobilization was found. Furthermore the rescue constructs of *dur* (*GckIII*) and *kuk* are depicted. Scheme of the genomic region was modified according to <http://flybase.org/reports/FBgn0038476>.

4.1.2 Nuclear elongation is missing in $\Delta 15$ embryos

Original Kugelkern loss of function data were produced using a heterozygous $\Delta 15$ fly strain, which was kept over deficiency, as recessive lethal mutations existed in combination with the *kuk* depletion (Brandt et al., 2006). Meanwhile, the chromosome was cleaned, secondary lethal effects were removed and a homozygous $\Delta 15$ fly strain was established (M. Clever). Western blot analysis of mutant embryo extract revealed that the *kuk* deficient fly line $\Delta 15$ represents a protein null allele (Figure 4 A). To verify if homozygous $\Delta 15$ flies still show the described *kuk* phenotype of round shaped nuclei at the end of cellularization, an embryo immunostaining was performed (Figure 4 B). A staining against lamin Dm0 was used as a marker for the nuclear envelope, whereas Slam indicates the cellularization progress. In wild type embryos a progressive elongation of round shaped nuclei can be observed over time starting with the furrow invagination. Compared to this, nuclei in *kuk* depleted embryos stayed rounded and formed multiple nuclei layers. As the

aim of this study was the identification of farnesylation dependent Kuk interaction-partners, I further examined the nuclear morphology phenotype of a non-farnesylable mutant (KukC567S) within a $\Delta 15$ background. This transgene encodes for a cysteine to serine exchange (C567S) within the CaaX-motif of the native *kuk*. It is shown that the expression level of the mutant protein and its wild type homolog are comparable (Figure 4 A). The missing farnesylation was confirmed in a SDS-Page, due to the smaller molecular mass of KukC567S and the induced band shift. Thus, the mutant Kuk protein is not sufficient to rescue the $\Delta 15$ phenotype. Previous studies showed that expression of a non-farnesylated KukCS protein in wild-type flies caused a clear localization to the nuclear envelope. This was reasoned by homo-dimerization with farnesylated, endogenous Kuk-protein (Brandt et al., 2008). In a background without endogenous Kuk ($\Delta 15$), the GFP-tagged KukC567S is mislocated to the nucleoplasm compared to the typical nuclear rim localization of the GFP tagged wild type Kuk (Figure 4 C).

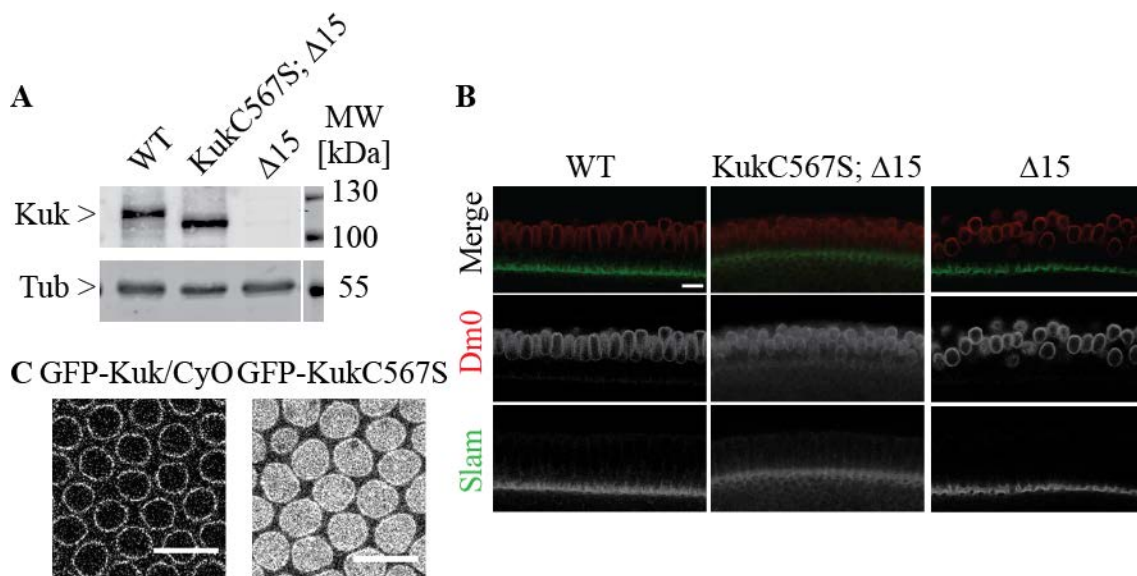


Figure 4: The *kuk* deficient line $\Delta 15$ represents a protein null allele

(A) Western blot analysis of wild-type and $\Delta 15$ embryo extracts revealed that $\Delta 15$ is a Kuk-protein null allele. Tubulin was used as loading control. Embryo extract of KukC567S samples showed a band shift due to the loss of farnesylation. Western blot analysis was performed with the extract of 20 embryos. (B) Side view of an embryo immunofluorescence staining at the end of cellularization stained for lamin Dm0 and Slam. Wild type embryos showed the nuclear elongation phenotype, whereas $\Delta 15$ and KukC567S; $\Delta 15$ embryos remained rounded. Scale bar: 10 μ m (C) Top view from live-imaging of a genomic GFP-Kuk wild type allele and a non-farnesylable GFP-KukC567S mutant. The farnesylated wild type allele localized to the nuclear envelope, whereas the mutant protein is found predominantly within the nucleoplasm. Both genomic transgenes were expressed in a *kuk* deficient background ($\Delta 15$). Scale bar: 10 μ m.

4.1.3 Gene expression is altered in *kuk*-depleted embryos

To validate if gene expression is affected by the loss of *kuk*, RNA sequencing analyses were performed. *kuk*-depleted embryos showed a change in their genome-wide expression profile during cellularization compared to wild type embryos (Brandt et al., 2006). In this transcriptome analyses embryos from stage 5 to 7 were examined and a down regulation of early zygotic genes like *slam*, *nullo* and *frühstart* have been observed. In this study $\Delta 15$ and wild type control embryos were collected after 6-8 hours referring to stage 11 and 12. 670 genes were differentially expressed in *kuk*-depleted embryos. The top 50 up- and down-regulated candidates based on their log₂fold were selected. These 100 candidates were further sorted based on the p-value and the base Mean (p-value $\geq 1.01 \cdot 10^{-3}$, base Mean < 17.65 for up regulated and < 46.39 for down regulated genes). By this it was possible to narrow down 50 candidate genes (Supplement Table: 1). A functional classification was performed using the Panther software (www.pantherdb.org). With this 20 genes were successfully grouped, whereas 30 genes were not further classified (Figure 5). One of the unclassified genes is *kuk*, which is strongly down regulated in $\Delta 15$ embryos and was used as control. Compared to the previously performed analysis by Brandt et al., an enrichment for genes containing a catalytic activity (group 3) was found. Out of these, 5 candidates (10%) are described for having an oxidoreductase activity (CG18547, CG3397, Cyp9b1, CG7675 and Cyp6d2). A change of gene expression within these proteins is indicative for an oxidative stress situation upon *kuk*-depletion. Furthermore, the anti-oxidative factor GstD1 was up regulated (log₂fold: + 6.02, group1). Additionally, methuselah-like 8 (log₂fold: - 11.25) and dawdle (log₂fold: + 5.12) were identified. Both proteins are linked to aging in *Drosophila*, suggesting a connection to genes involved in oxidative stress response.

Panther GO-Slim - Molecular Function
Total # Genes: 20 # Function Hits: 32

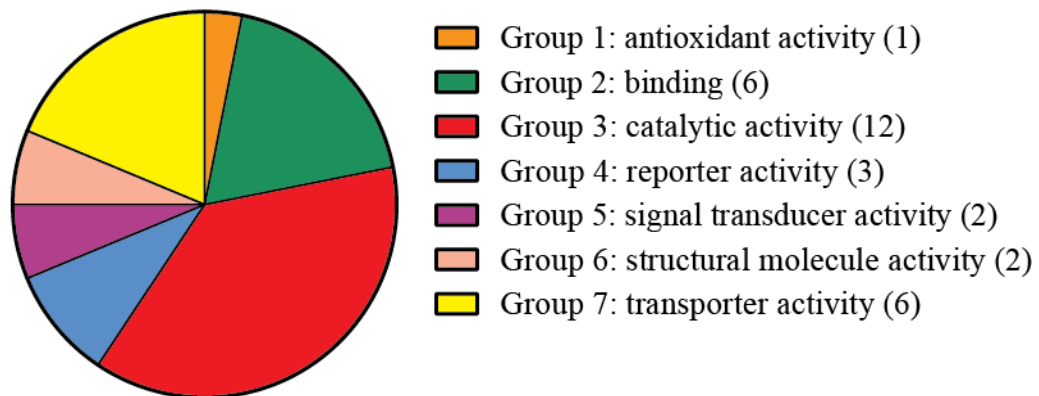


Figure 5: Differentially expressed genes in *kuk*-depleted embryos

Enrichment analysis based on the molecular function was performed using the PANTHER tool as a classification system. Seven groups have been described to contain at least one of the final 50 candidates. Unclassified genes are not considered in this schematic illustration and are referred as group “0” (Supplement Table: 1).

4.1.4 Survival rate is affected in *kuk*-depleted animals

In order to analyze if the observed gene expression changes for genes involved in stress response are associated with an accelerated aging effect, lifespan assays were performed (Figure 6 A). It was found that a loss of Kuk is only slightly affecting lifespan. However, the introduction of non-farnesylable mutant in a *kuk* deficient background decreased lifespan. KukC567S flies showed a 50% mortality at day 32, compared to wild type and $\Delta 15$ flies with a 50% mortality at day 42. The observed decrease in lifespan by the expression of a mutant Kuk allele might be due to the observed Kuk miss-localization (Figure 4 C). To analyze if gene expression changes are associated to a developmental phenotype in *kugelkern* deficient animals, survival rate analyses were performed. $\Delta 15$ animals showed a strong effect on embryonic viability as only approximately 25% of the larvae hatched (Figure 6 B). The introduction of a transgenic non-farnesylable Kuk protein (KukC567S) in *kuk*-depleted flies did not rescue the observed phenotype, even if survival during adult stage was increased up to 38% (Figure 6 B). However, survival rate analyses of animals which are only homozygous for a *kuk* depletion ($\Delta 15/Def$) did not show an effect on viability compared to wild type control animals, suggesting that the observed lethality in homozygous $\Delta 15$ embryos is *kuk* independent.

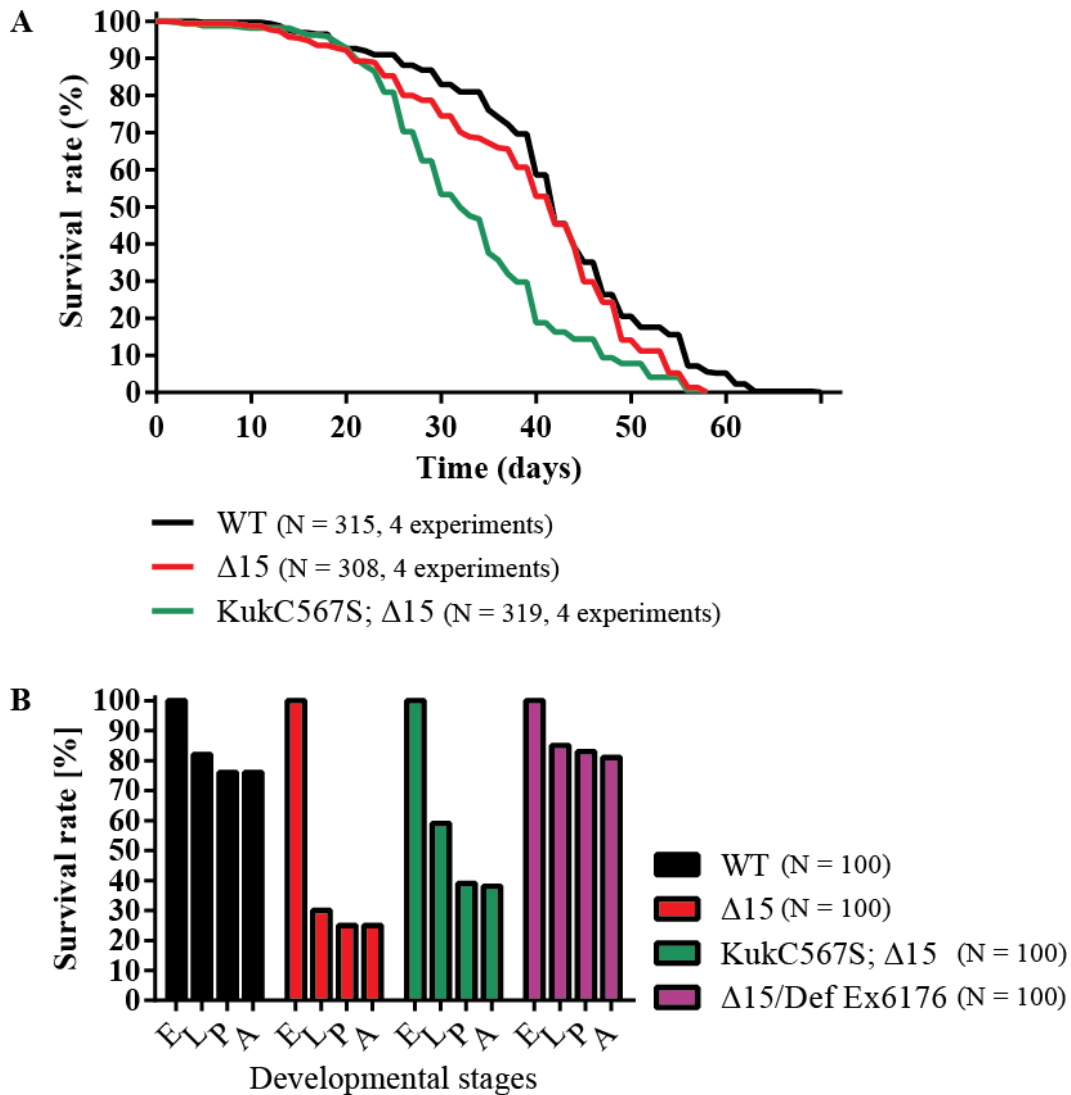


Figure 6: *kuk*-depleted animals show a decreased survival rate and lifespan

(A) Lifespan analyses showed that *kugelkern* depletion slightly affected viability during adulthood (log-rank test: WT vs. $\Delta 15$ $p = 0.0012$). The KukC567S expression in a $\Delta 15$ background instead caused a more severe shortening in lifespan (log-rank test: WT vs. KukC567S; $\Delta 15$ $p < 1.0 * 10^{-10}$; $\Delta 15$ vs. KukC567S; $\Delta 15$ $p < 1.0 * 10^{-10}$). Statistical analyses were performed by OASIS. (B) Survival rate analyses confirmed a high embryonic lethality of approximately 70% for $\Delta 15$ animals. The expression of a KukC567S transgene decreased the lethal effects during embryogenesis to approximately 40%. However, survival rate analyses of $\Delta 15$ animals which are kept over deficiency and by this only homozygous for a *kuk* depletion did not show an impairment of viability compared to wild type control animals.

4.2 Identification of biochemical interaction partners of Kuk

The aim of this study was the identification of farnesylation dependent interaction partners of Kuk. Therefore, a Co-IP approach with a modified GFP-nanobody (provided by Prof. Görlich, MPI for biophysical chemistry, Göttingen) was used. The Großhans laboratory established a GFP tagged UAS-Kuk construct, enabling promoter specific gene expression. By this, it was known that a GFP-Kuk expression through the *mat-Gal4* driver is able to rescue the *kuk* deficient phenotype. However, to create a situation, which is as close as possible to the native conditions, genomic GFP transgenes were generated, which are expressed under the endogenous Kuk promoter (Figure 3).

4.2.1 GFP-Kuk transgenes did not rescue the *kuk* loss of function phenotype

To determine if a GFP-tag is impairing Kuk function during cellularization, an embryo immunostaining was performed. As it was seen before in live imaging of early embryos (Figure 4 C) GFP-Kuk localizes to the nuclear envelope (Figure 7). A direct comparison of the nuclear envelope marker lamin Dm0 and GFP-Kuk showed the existence of a weak cytoplasmatic signal. GFP-KukC567S instead is predominantly nucleoplasmatic but also cytoplasmatic localized. However, the most important fact is that the expression of a GFP-tagged wild type allele is not able to rescue the cellularization phenotype, as it was seen with the UAS/Gal4 driven expression. These data showed that a GFP-tag is indeed affecting Kugelkern function, even if the majority of the protein is properly localized.

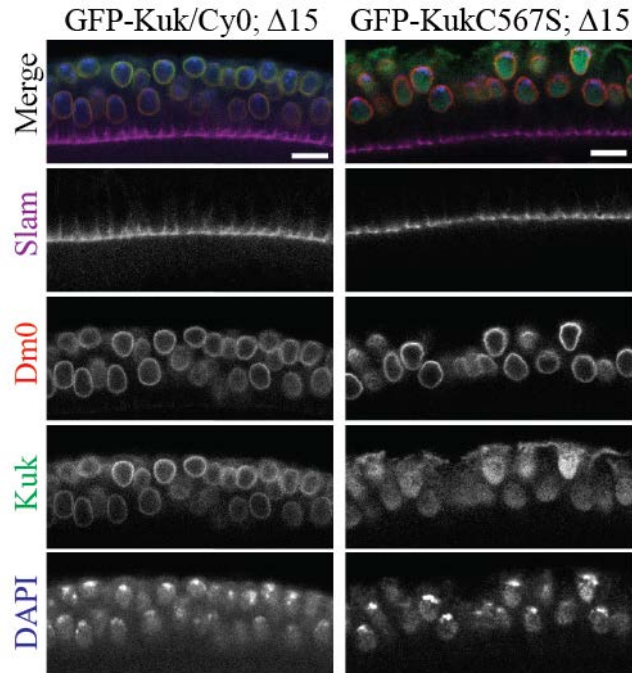


Figure 7: Genomic GFP-Kuk transgenes did not rescue the *kuk*-depleted phenotype

Immunofluorescence analyses for GFP-Kuk and GFP-KukC567S expressing flies in a $\Delta 15$ mutant background. Slam was used as a marker for cellularization. Dm0 and DAPI indicated the nucleus and Kuk was used to stain against the GFP-fusion proteins. In both cases a GFP-protein expression was not able to rescue the $\Delta 15$ mutant situation as the nuclei stayed roundish at the end of cellularization. A difference was observed comparing the localization of the two GFP-proteins. GFP-Kuk clearly localized to the nuclear envelope, whereas GFP-KukC567S was predominantly nucleoplasmatic but also cytoplasmatic localized. Scale bar: 10 μm .

4.2.2 Proteolytic cleavage of GFP-Kuk

To further investigate the reason for the failed complementation, western blot analysis of embryo extracts were performed and stained against Kuk and GFP (Figure 8 A). Both GFP-Kuk proteins differed in their migration behavior compared to wild type Kuk, due to their higher molecular weight. The loss of farnesylation for GFP-KukC567S was also visible in direct comparison to GFP-Kuk. However, native Kuk of wild type embryos showed only one dominant band, whereas up to three major bands were observed for the GFP-proteins. These data showed that the GFP-tag is promoting proteolytic cleavage. As the GFP-tag was fused to the N-terminal end (Figure 8 B), one can conclude that degradation occurs with the C-terminal half of Kuk, as the same bands can be detected for the GFP- and the Kuk-antibody. As I was interested in binding partner which are dependent on farnesylation, mediated by the C-terminal CaaX-motif, I decided to use the maternally

expressed GFP-Kuk protein (mat-Gal4, UAS-Kuk) for further experiments, as this was already shown to be functional and able to rescue the mutant situation.

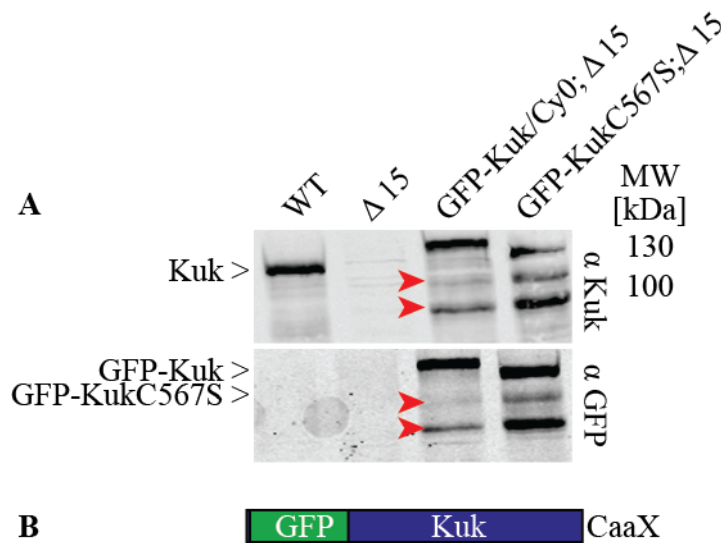


Figure 8: Protein degradation occurs at the C-terminal end of GFP-Kuk

(A) Western blot analysis of wild-type, $\Delta 15$ and GFP-Kuk(C567S); $\Delta 15$ embryo extract for Kuk (upper panel) and GFP (lower panel). The wild-type extract showed one dominant band for Kuk, but no signal for GFP. In Kugelkern deficient embryos ($\Delta 15$) neither a Kuk nor a GFP signal was detected. Extract of GFP-transgenic embryos showed several bands, which were similar between GFP-Kuk and GFP-KukC567S (arrowhead). An extract of 40 embryos was analyzed by SDS-PAGE. (B) Schematic illustration for the generated GFP-Kuk construct. The GFP was fused to the N-terminal site of Kugelkern. The farnesylable CaaX-motif instead is localized at the C-terminus.

Furthermore, I checked if a GFP-fusion in general is affecting protein stability and also leads to degradation within UAS/Gal4 expressed GFP-Kuk. For this purpose embryo extract of the wild type Kuk was compared to the GFP-proteins expressed under the native promoter and the maternal one (Figure 9 A). It is shown that degradation was present in all GFP-situations, which shared protein fragments of a similar size. Western blot analyses for the UAS/Gal4 expressed GFP-Kuk against GFP and Kuk confirmed that the cleavage products were still fused to GFP (Figure 9 B) An explanation for the rescue of the UAS/Gal4 expressed GFP-Kuk was given by its expression level, which was higher and thus probably able to compensate the occurring loss of functional Kuk (Figure 9 A). At this point it has to be mentioned, that the UAS/Gal4 driven GFP-Kuk was expressed in a heterozygous $\Delta 15$ situation, which was kept over a *kuk* deficiency ($\Delta 15 / dur^+, Df(3R)Ex6176$), also resulting in a protein null allele for Kugelkern (following termed as D15). As the vast majority of the

UAS/Gal4 expressed GFP-Kuk was not affected by proteolytic cleavage (Figure 9 A) and an embryo immunostaining re-confirmed its functionality (Figure 9 C) I used this fly strain for subsequent Co-IP analysis.

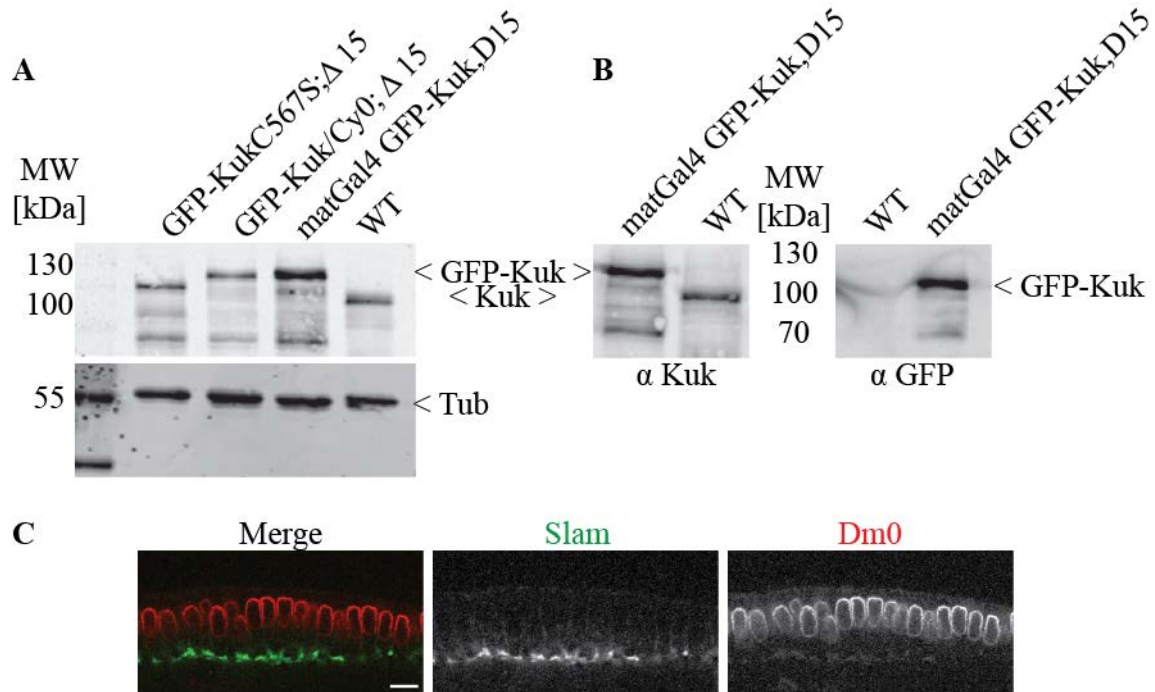


Figure 9: UAS/Gal4 expressed GFP-Kuk rescued the *kuk* depletion phenotype

(A) Western blot analysis of GFP-Kuk expressed under the native and the maternal promoter compared to extract of wild type embryos. Western blot analyses were performed against Kugelkern and α -tubulin, which was used as loading control. GFP-proteins under the native promoter were expressed in a homozygous $\Delta 15$ background ($\Delta 15$), whereas the maternal GFP-Kuk protein was expressed in a heterozygous $\Delta 15$ situation, kept over deficiency (D15). Comparisons of the GFP-Kuk bands showed a similar appearance, especially regarding the cleavage products. Wild type Kuk and natively expressed GFP-Kuk proteins had a similar band intensity. Maternal GFP-Kuk showed a higher intensity correlating with a stronger expression. (B) Western blot analysis of the maternally expressed GFP-Kuk stained against GFP and Kuk revealed that the Kuk cleavage products were still fused to GFP. An extract of 40 embryos was loaded for the analyses shown in A and B. (C) Side view of *Drosophila* embryos stained against Slam, a cellularization marker, and lamin Dm0 a marker for the nuclear envelope. Maternally expressed GFP-Kuk rescued the nuclear elongation phenotype in a *kuk* depleted background (D15).

4.2.3 Nuclei solubilization promoted further degradation

The identification of interaction partner by biochemical approaches is critically dependent on the experimental conditions. One of the crucial factors is the salt concentration, which will influence protein-protein interactions. It was shown before that Kuk can be extracted from the nuclear envelope by using 150 mM of NaCl (Brandt et al., 2006). Another important point which should be considered are unspecific background signals. In this approach a modified GFP-nanobody (provided by Prof. Görlich, MPI for biophysical chemistry, Göttingen) was used. The big advantage of this camelid derived single domain antibody is an intrinsically SUMO cleavage site, which enables an additional purification step and reduces unspecific binding. This is especially important for subsequent mass spectrometric analysis. To finally identify interaction partner, whose binding is determined by the farnesylation it was planned to compare isolated proteins of GFP-Kuk and GFP-KukC567S. Unspecific binding will be excluded by using the extract of *kuk* deficient embryos as control.

A nuclei fractionation experiment with subsequent co-immunoprecipitation is shown in Figure 10. Analyses of the total lysate of GFP-Kuk embryos again showed the full-length protein as well as its cleavage products, termed as GFP-Kuk Δ C-term. Enrichment of full length GFP Kuk was possible by fractionating embryonic nuclei (Figure 10, Nuclei). The input represents a protein sample after treating the isolated nuclei with 150 mM NaCl and 1% Triton X to extract the GFP-Kuk protein from the nuclear envelope. This solubilization step was essential for subsequent co-immunoprecipitation. However, nuclei solubilization severely affected GFP-Kuk protein stability and promoted degradation (Figure 10, red arrow). Consistent to this, a Kuk fragment with a molecular weight of around 55 kDa was enriched in the unbound sample after adding the GFP-input sample to the GFP-nanobody coupled beads. Elution was achieved by using the intrinsic SUMO cleavage site of the GFP-nanobody. Eluted GFP-Kuk protein was detected in the cleaved fraction (Figure 10, arrow). It was shown that GFP-Kuk can be efficiently isolated with this approach. However, as a GFP-Kuk fragment (Figure 10, red arrow head) was enriched due to occurring protein cleavage this approach had to be stopped. Thus, protein cleavage became a severe problem which prevented the identification of farnesylation dependent interaction partner of Kugelkern.

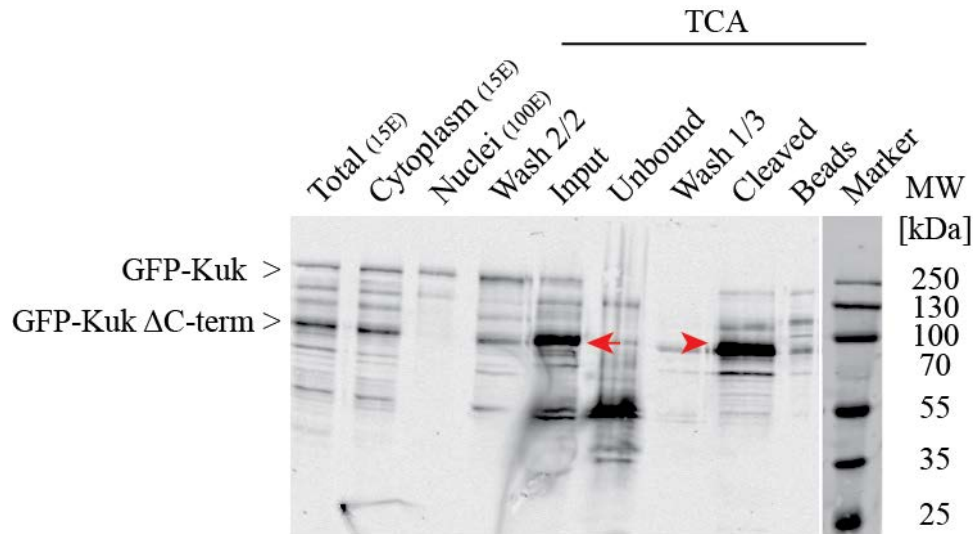


Figure 10: Solubilization promoted GFP-Kuk degradation

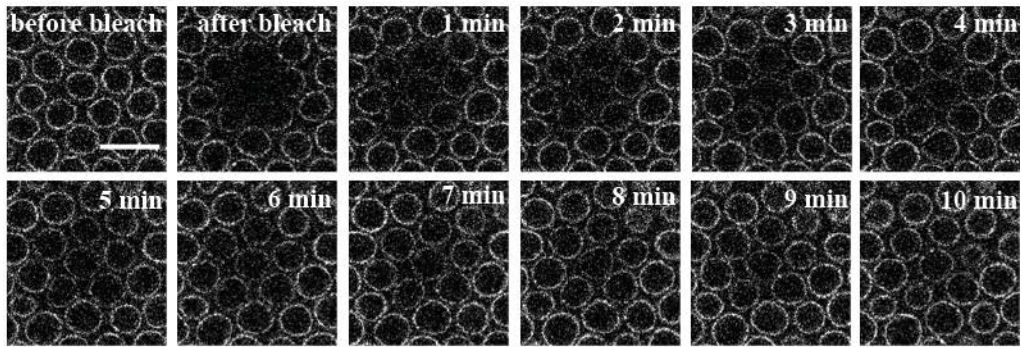
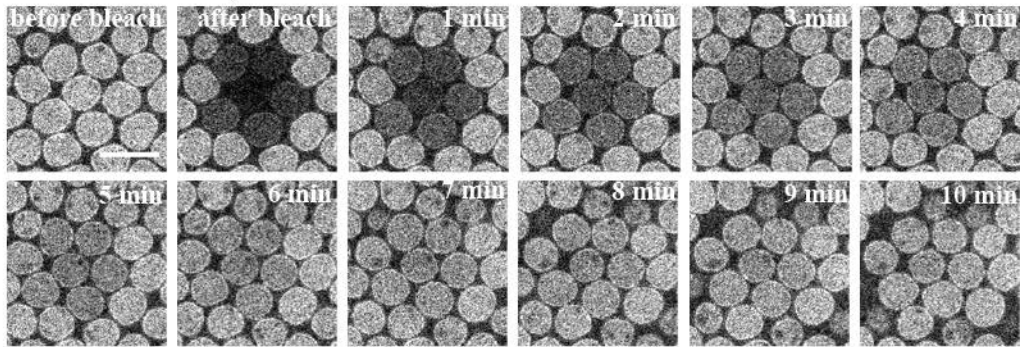
Western blot analysis of a nuclei fractionation experiment with subsequent co-immunoprecipitation using lysate of GFP-Kuk expressing embryos. GFP-Kuk was identified by Kuk antibody staining and detected in the nuclei fraction as well as in the cytoplasm, due to insufficient separation. Full length GFP-Kuk was enriched by nuclei fractionation. Solubilization was achieved using 150 mM NaCl and 1% TritonX 100 (input, 4.500 E). After solubilization the majority of the GFP-protein was proteolytic cleaved (red arrow). The input sample was further incubated to the GFP-nanobody coupled beads. The protein fraction which was not able to bind is shown in the unbound fraction. Three washing steps were performed and the first washing step is shown (wash 1/3). GFP-Kuk elution was achieved by SUMO cleavage (Cleaved, red arrow head). Protein which was not eluted is shown in the beads fraction. Trichloroacetic acid (TCA) was used for protein precipitation of the indicated protein fractions.

An alternative to the above mentioned approach is a co-immunoprecipitation of the native and mutant Kugelkern by a Kuk antibody coupled to Protein A dynabeads. In order to identify farnesylation dependent interaction partners, transgenic KukC567S flies without GFP were generated and crossed in the *kuk* deficient situation ($\Delta 15$). Solubilization analyses of the native Kuk revealed that this approach is promising as the majority of the Kuk protein stayed stable for even 4 hours after solubilization (Supplement Figure 2). First Co-IP experiments revealed that this system is working and I am confident to study Kugelkern protein isolates by mass spectrometric analysis in the near future.

4.2.4 Biochemical properties of GFP-Kuk (C567S)

Next, FRAP experiments were performed, using the established GFP transgenic lines for Kuk and KukC567S, to analyze the protein dynamics of Kugelkern. As the C567S mutation is changing the Kugelkern localization from the nuclear lamina to the nucleoplasm it was assumed that it also changes biochemical properties. In order to identify protein dynamics a circular area was bleached and the recovery rate was measured every 10 seconds over a time period of 10 minutes. To include the bleaching effect which was induced by image recording the fluorescence intensities of two control areas were measured and used for normalization.

The GFP signal of both GFP-proteins was efficiently bleached (Figure 11 A, B after bleach). After 10 minutes a signal recovery rate of ~ 25% for the wild type version and ~ 50% for the mutant version were observed. Thus, preventing a proper Kuk localization led to a more dynamic behavior. An interesting finding for the wild type allele is, that it recovers relative fast especially in direct comparison with lamins. For the GFP tagged *C.elegans* lamin (Ce-lamin) no recovery after more than 60 min have been observed (Wiesel et al., 2007). Similar results are published for the human lamins A ($t_{1/2} \sim 140$ min), B1 ($t_{1/2} > 180$ min) and the *Drosophila* lamin Dm0, indicating a large immobile fraction (Gilchrist et al., 2004, Moir et al., 2000, Zaremba-Czogalla et al., 2012).

A GFP-Kuk/Cy0; $\Delta 15$ B GFP-KukC567S; $\Delta 15$ 

C

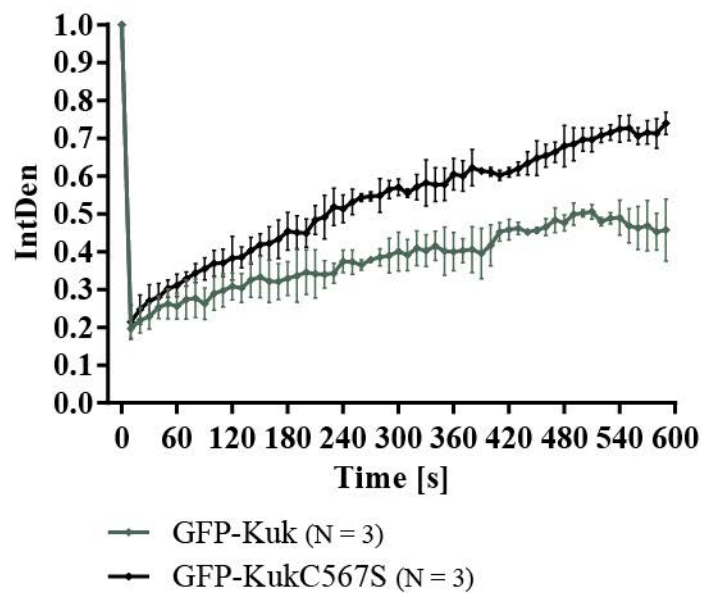


Figure 11: FRAP analysis of wild type and mutant GFP Kuk

FRAP experiment of early embryos expressing either genomic GFP-Kuk (A) or a non-farnesylable GFP-KukC567S mutant (B). Signal intensity was measured before and after photobleaching and subsequently every 10 s over a time period of 10 min. Fluorescence recovery rate was measured and analyzed using ImageJ. Schematic illustration was done with GraphPad Prism6 (C). Scale bar: 10 μ m.

4.3 Identification of genetic interaction partners of Kugelkern

An aim of this work was the identification of novel genes interacting with *kugelkern*. Tissue-specific overexpression of Kugelkern is known to induce morphological defects (Figure 12) (Brandt et. al., 2008). To identify *kugelkern* interacting genes a genetic screen for dominant suppressors in the wing as well as in the eye was performed. Tissue specific overexpression of Kuk was achieved using a UAS-Kuk driven by vestigial-Gal4, which was expressed in the dorso-ventral compartment border of larval wing discs. The GMR-Gal4 (glass multiple reporter) was used for expression within the larval eye imaginal discs. The hypothesis was that other downstream targets mediate the lobulations and infoldings which have been induced by Kuk overexpression (Brandt et. al., 2008). For this dominant screen, around 130 RNAi-lines (Supplement Figure 2) for genes concerning nuclear functions were employed. Two tissues were used due to the different gene functions of the tested RNAi-candidates, which could for example prevent the suppression of the induced phenotype in the wing, but could be observed in the eye. *Drosophila* is a relatively simple model organism and genetic analyses can be studied easily. The big advantages of this approach were first a fast screening of a high number of RNAi-lines and second the immediate identification of a candidate after suppressing the Kugelkern induced gain-of-function phenotype. The work flow of the performed RNAi-screen is depicted in Figure 12.

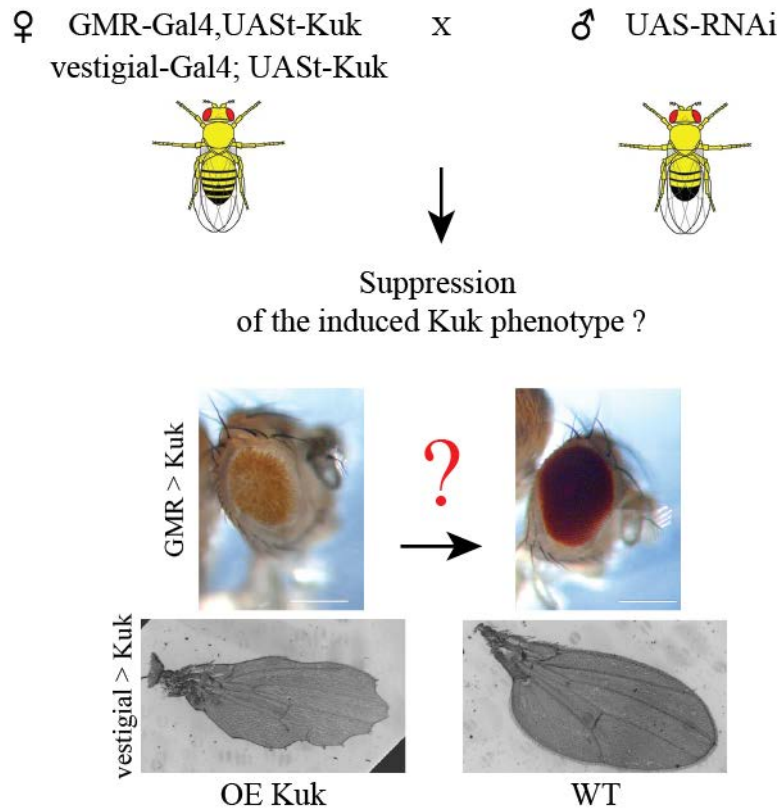


Figure 12: Scheme of the performed RNAi-screen

Virgins overexpressing Kugelkern controlled by vestigial-Gal4 or GMR-Gal4 were crossed to males containing a candidate specific RNAi construct. F1-progeny were checked for their genotype to contain the Gal4-driver, the UASSt-Kuk and the UAS-RNAi construct and screened for their tissue-specific phenotype. A genetic interactor of Kuk can be identified if the induced morphological defect is reverted. Fly clip art was taken from Kondo and Ueda, 2013.

4.3.1 Morphological defects upon Kugelkern overexpression were primary independent of apoptosis

A simple explanation for the observed gain-of function phenotypes could be that Kuk overexpression directly resulted in apoptotic processes, leading to morphological deformations. To rule this out, immunofluorescence analyses of wing- and eye-imaginal discs were performed. Apoptotic events were detected by Caspase-3 staining. Overexpression of Reaper, which has a central role in programmed cell death, was used as positive control. Wing-specific overexpression of Reaper led to an increase in Caspase-3 signal and finally caused adult wing deformations (Figure 13). Expression of DIAP, the *Drosophila* inhibitor of apoptosis, in combination with Reaper, resulted in a reduced Caspase-3 staining and wing formation occurred to be normal. Overexpression of Kuk also increased Caspase-3 staining in wing discs of stage 3 larvae. However, additional expression

of DIAP reduced but did not prevented Caspase-3 activation and still resulted in wing defects, suggesting that next to apoptosis also other processes were involved and mediated the observed phenotypes.

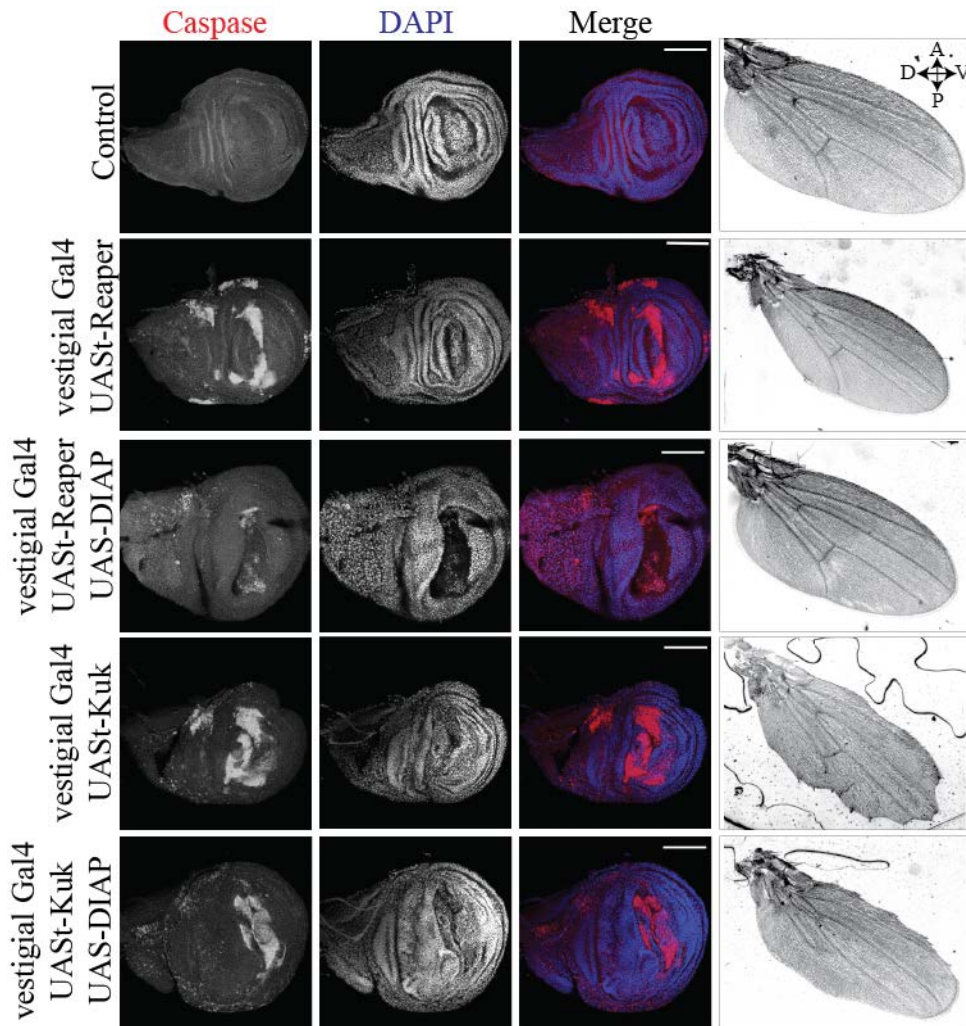


Figure 13: Kugelkern overexpression caused wing morphological defects

Immunofluorescence analyses of wing imaginal discs. L3 larvae of the depicted genotypes were stained against Caspase-3, as marker for apoptotic events, and DAPI was used as a DNA marker. Wild type discs were used as control and did not show a Caspase-3 activation. Wing specific expression of Reaper led to apoptosis and was used as positive control. Expression of an apoptotic inhibitor, DIAP, in combination with Reaper decreased Caspase-3 activation and resulted in a normal wing development. Kuk overexpression increased Caspase-3 intensity, which led to wing deformations, also in combination with DIAP.

The effect of Kuk overexpression referring to induction of apoptosis was also checked for eye-imaginal discs by Caspase-3 immunostaining. It was observed that the induction of the

eye phenotype was dose-dependent as a homozygous expression of GMR-Gal4, UASst-Kuk induced a stronger phenotype than the heterozygous situation (Figure 14). But, flies which were homozygous for GMR-Gal4, UASst-Kuk could be kept but not amplified for the RNAi-approach as they were strongly affected in viability. However, if the eye deformation is a result of directly induced apoptotic events, the effect for the Caspase-3 activation is expected to be stronger in the homozygous GMR-Gal4, UASst-Kuk situation than the heterozygous one. Due to this eye-imaginal discs of homozygous animals were analyzed. Ubiquitous GFP-cadherin expressing animals were used as control (Figure 14 B) and stained in the same tube together with Kuk overexpressing ones (Figure 14 C). As there was no induction of apoptotic events during larval development (Supplement Figure 3), eye imaginal discs of prepupae were tested. Immunofluorescence analysis showed a weak signal for Caspase-3 in control discs, which was slightly increased in the Kuk overexpressed situation. However, these events occurred only in a dot like manner and were not as strong as in the wing imaginal discs before (Figure 13). These results indicated that Kuk overexpression indeed partially resulted in apoptosis but it seemed that this was a consequence and not the primary reason of the observed morphological defects.

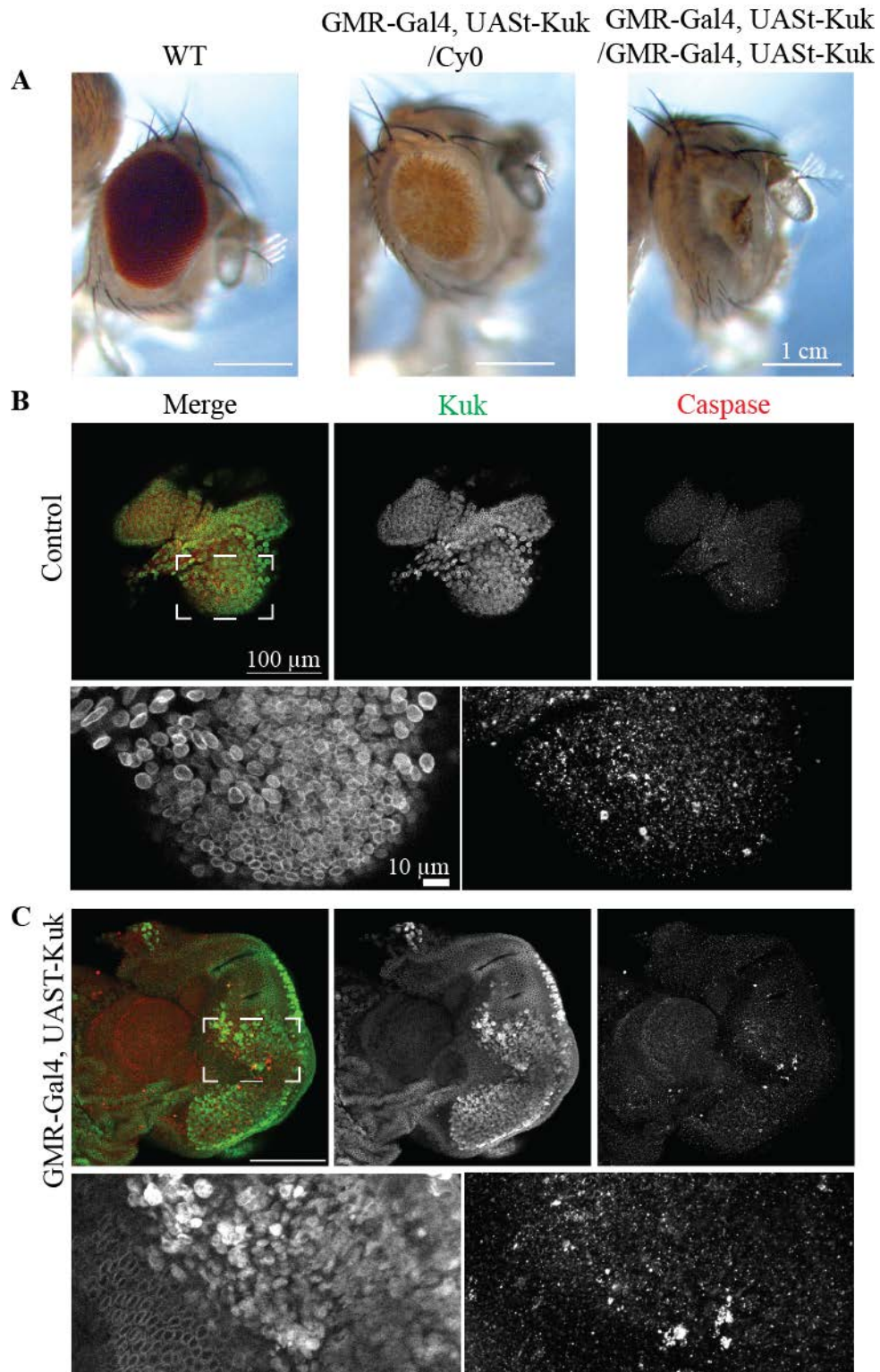


Figure 14: Kuk overexpression induced eye-defects primary independent of apoptosis

Eye morphological defects were induced by Kuk overexpression in a dose-dependent manner. (A) Eye phenotypes of wild type flies and flies overexpressing Kuk in a homozygous and heterozygous situation controlled by the GMR promoter. (B-C) Eye imaginal discs of a ubiquitous GFP expressing control situation (B) and an eye specific Kuk overexpressing situation (C). Immunofluorescence analyses were performed

against Kuk and Caspase-3. Caspase-3 activation was detected on a very low level for the control as well as the Kuk overexpressing situation.

4.3.2 Genetic interaction partners of Kuk remain undiscovered

To finally search for genetic interaction partners of *kuk* the RNAi-screen was performed (Figure 12). Therefore, flies overexpressing Kuk were crossed with around 130 candidates for genes concerning nuclear functions, which were available in the RNAi-library of the Großhans laboratory (Supplement Figure 2). The females of the parental generation were heterozygous (vestigial-Gal4/CyO, UAS_t-Kuk/UAS_t-Kuk or GMR-Gal4, UAS_t-Kuk/CyO), meaning only half of the progeny were screened as the other half contained the balancer chromosome and did not overexpress Kuk. The big advantage of this situation was that an internal control for each candidate was directly provided. However, within all tested candidates, no genetic interaction partner was found for Kuk, neither in the wing nor in the eye. For all screened wings at least the proximal posterior region was affected (Figure 15 a-j). Only the knockdown of Kuk itself, which was used as control, rescued the gain-of-function phenotype (Figure 15 e-f). The same effect was seen for the performed screen in the eye (Figure 15 k-p). These results showed first, that the number of tested candidates was too small and second, that the principle of the RNAi-screen in general worked.

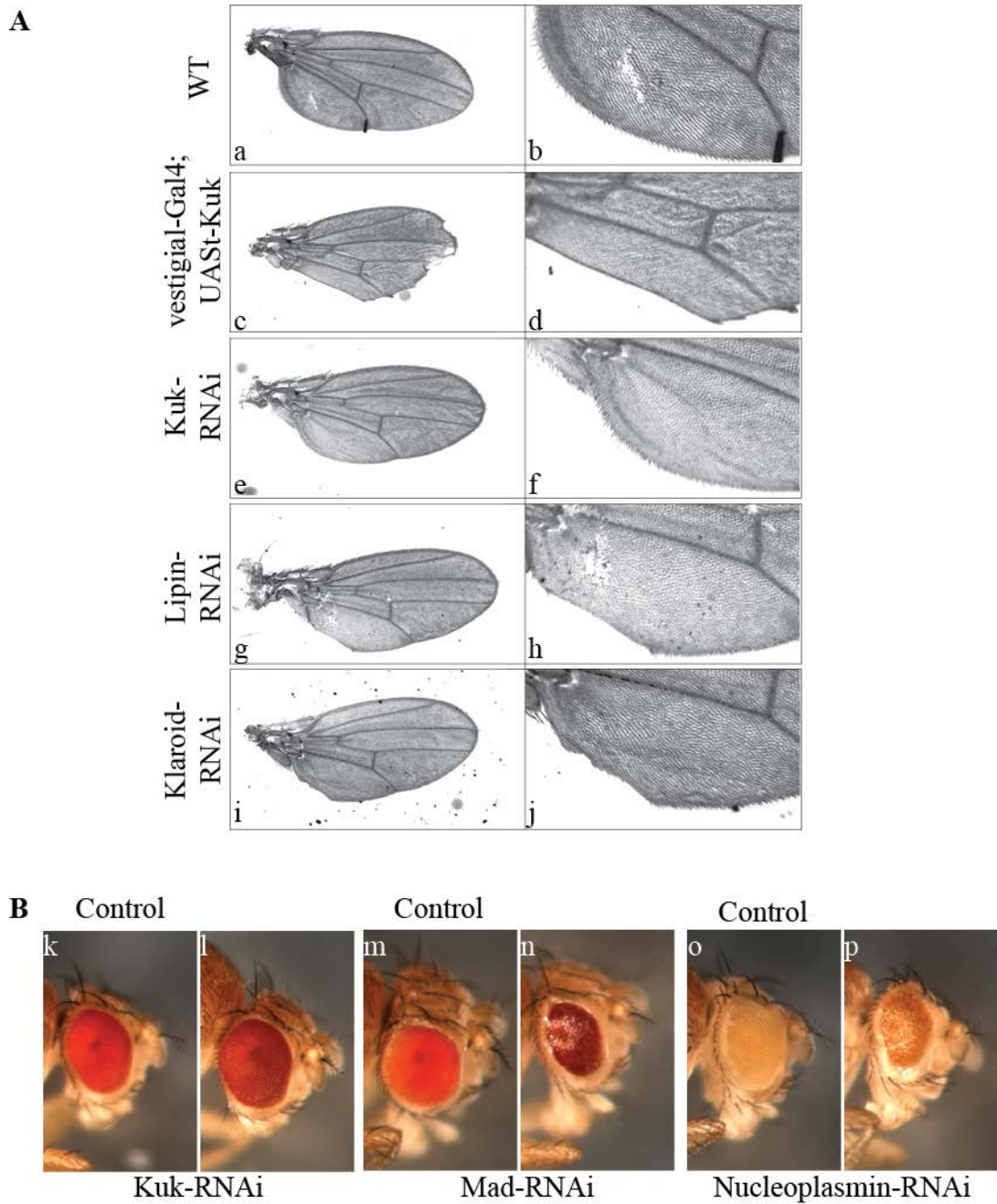


Figure 15: Genetic interaction partners of *kuk* remain unidentified

(A) Genetic screen performed for the wing. (a) Wings of wild type flies were used as control. (c) Wing specific overexpression of Kugelkern induced morphological defects, which were reverted by a knockdown of Kuk (e). (g-j) Wing pictures of Lipin- and Klaroid RNAi expressing flies in the background of Kuk overexpression. (b, d, f, h, j) Representative pictures of the magnified wing area which was affected in all tested candidates. (B) Genetic screen performed for the eye. Representative pictures of the eye-phenotypes of flies expressing an RNAi construct for Kuk, Mad or Nucleoplasmin in the background of Kuk overexpression (l, n, o). Kuk-RNAi (l) was used as positive control and restored the gain of function phenotype. Knockdown of other candidates concerning nuclear function had no effect e.g. Mad (n) or GD22623 (p). The internal control of each situation was used as direct comparison (k, m, o).

4.4 The role of Narf in nuclear morphogenesis and aging

Narf was identified as a farnesylation dependent binding partner of human Prelamin-A (Barton and Worman 1999). Recently Prof. Wollnik and coworkers revealed that a dominant *de novo* mutation of human Narf causes clinical symptoms that share similarities to HGPS a human premature aging syndrome. In this study I tested the hypothesis that Narf is an interactor of farnesylated Kugelkern and Lamin and established a Narf disease model.

4.4.1 Generation of a Narf specific antibody

The *Drosophila* homologue of Narf is CG17683, hereinafter referred as Narf. Experiments based on antibodies are indispensable for understanding protein functions. Due to this I generated a Narf specific antibody. The cDNA clone RE37350 was used as the template for PCR and the coding sequence of Narf was inserted into QE80N60 vector. The recombinant protein was expressed in bacteria for four hours at 37 °C induced by 1 mM IPTG. *E. coli* cells were lysated by a combination of freeze and thaw, enzymatical lysis by lysozym and mechanical homogenization using the microfluidizer (Figure 16 A). As the majority of the protein stayed in the insoluble pellet fraction (P) a denatured protein purification using His-tag and 8 M urea was performed (Figure 16 B). Immunization was subsequently done by BioScience into guinea pig and rabbit and the final sera were tested in western blot analyses for their specificity (Figure 17 A). Three of the four final sera showed a number of unspecific bands, which were even visible in a high antibody dilution (sera of gp 02 and rabbit 1634, 1635). One serum, the gp 01, showed a predominant band at the expected size of ~ 55 kDa. To further verify the Narf specificity for this antibody a clonal analysis using the flip out system was performed. The basic principle behind that assay is a temperature dependent expression of a clonal marker and a flippase. The flippase enables specific expression of a desired UAS gene sequence by inducing a recombinatory flip out (Jiang et al., 2009). This systems was used for a clonal overexpression of Narf in the *Drosophila* gut. GFP was used as clonal marker and indicates Narf overexpressing cells. The big advantage of this approach is a direct comparison of Narf overexpressing and control cells, which locate next to each other in the same tissue and could be stained and imaged under same conditions. It is shown in Figure 17 B that the generated Narf antibody indeed recognized an elevated protein level in a Narf overexpressed situation, which is overlapping with the GFP control signal. This result strongly indicates a Narf specificity of the new antibody.

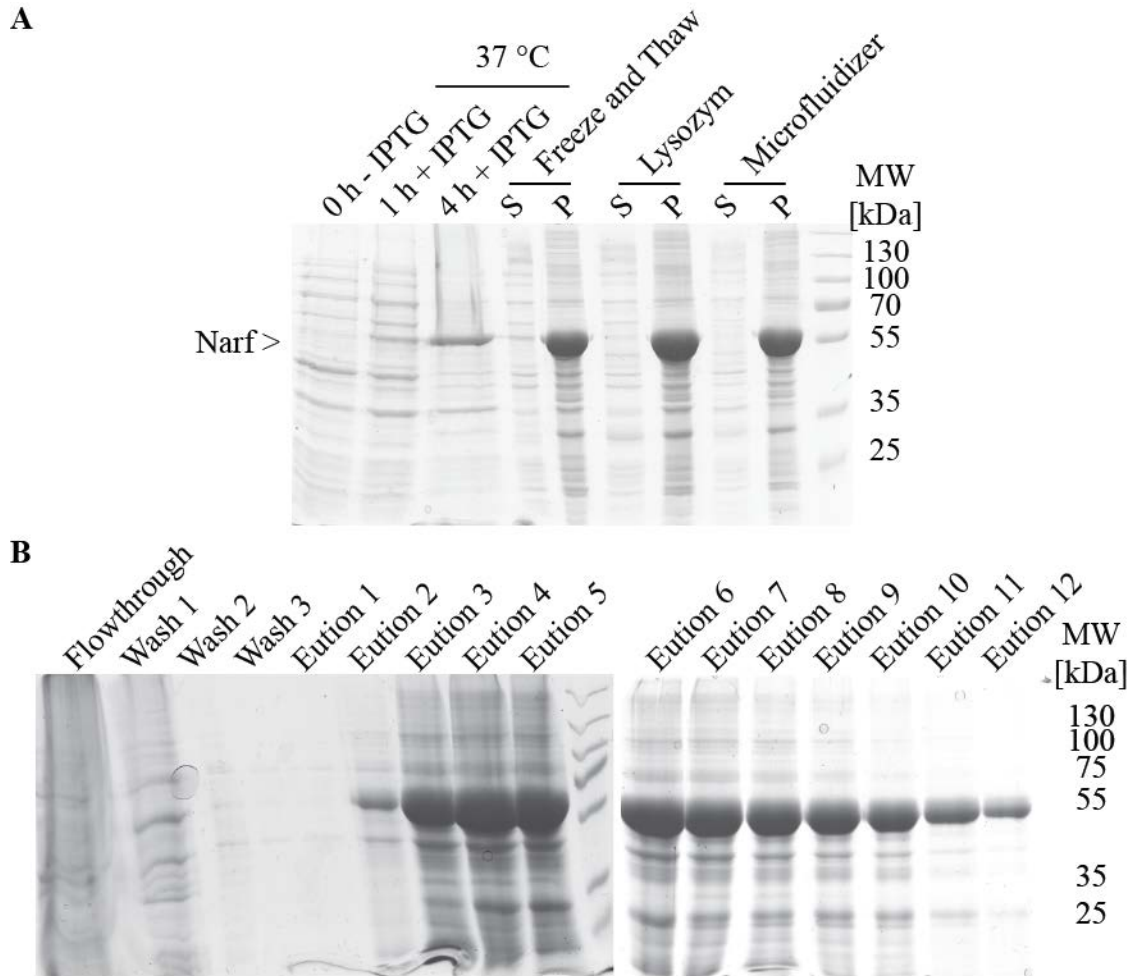


Figure 16: Protein expression and purification of QE80N60-Narf

(A, B) SDS-PAGE analysis of Narf expression and purification. (A) Narf expression was performed for 4 hours at 37 °C induced by 1 mM IPTG. Cell lysis was done by freeze and thaw, enzymatical lysis using lysozyme and mechanical homogenization using the microfluidizer. Comparison of the soluble supernatant fraction (S) and the insoluble pellet fraction (P) showed a high insoluble protein amount. According to this protein purification was performed under denatured conditions using His-Tag (B). Elution was achieved by a change in pH-value. Narf protein containing fractions were collected and used for immunization.

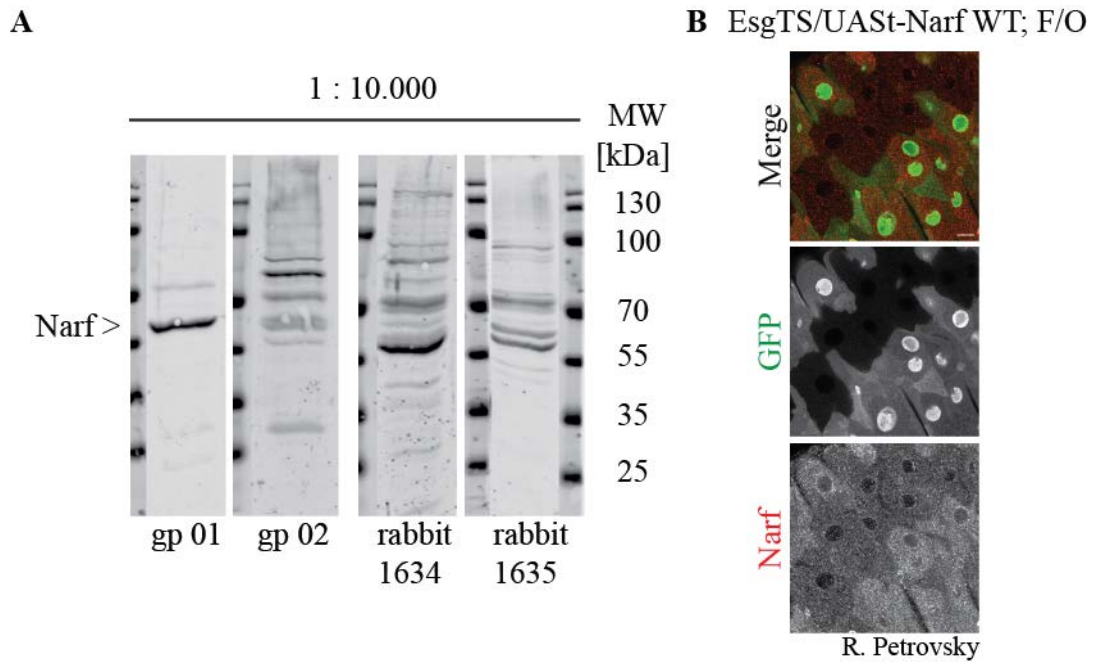


Figure 17: The antibody stained specific for Narf

(A) Western blot analysis of embryo extract stained for Narf using the different sera with the indicated dilution and batches name. Besides gp 01 all sera show a high amount of unspecific binding. (B) Immunofluorescence analysis of a clonal, Narf overexpressing gut stained for Narf using the sera gp 01. Scale bar: 10 μ m. The clonal analysis was conducted by R. Petrovsky.

4.4.2 Narf localized to the nuclear envelope

In order to identify Narf localization immunofluorescence analyses using the generated antibody were performed. S2 cells as well as early *Drosophila* embryos were studied. Co-stainings for nuclear envelope markers such as lamin Dm0 or Nup153 showed that Narf clearly localized to the nuclear envelope (Figure 18 A-D). Another evidence that the antibody stains specifically for Narf was given by the observation that the signals, of the Narf antibody and a mCherry tagged Narf protein expressed in S2 cells, show similar results (Figure 18 A). Airy Scan microscopy of fractionated embryonic nuclei and embryonic amnioserosa cells showed that Narf localization resembles the lamin Dm0 localization pattern and both proteins are partially overlapping in their local distribution (Figure 18 C-D). Since Narf and Dm0/Kuk are locating within the same nuclear area, it is possible that they are also interacting with each other. However, unlike initially described for human Narf (Barton and Worman, 1999), the *Drosophila* homologue is not restricted to the nuclear envelope but can be also found within the cytoplasm. This observation was given by immunofluorescence analyses and confirmed by fractionation experiments of embryo

extract (Figure 18 E). Western blot analysis showed that the majority of Narf is cytoplasmatic but a distinct proportion can be also found in the nuclear fraction, together with lamin Dm0, which was used as nuclear fraction marker.

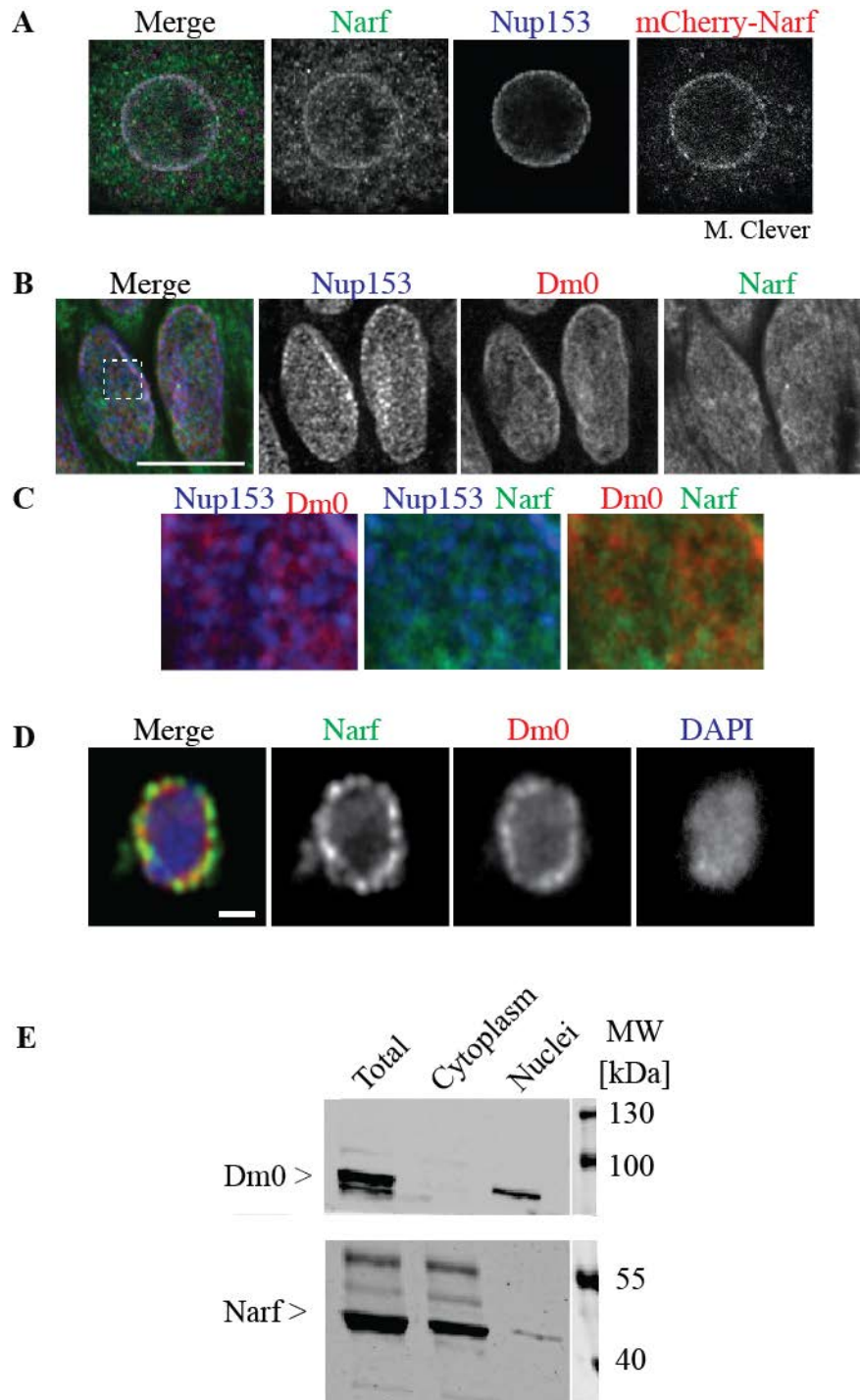


Figure 18: Narf localized to the nuclear envelope

Immunofluorescence analyses of S2 cells (A), embryonic amnioserosa cells (B, Scale bar: 10 μm , magnification depicted in C) and fractionated embryonic nuclei (D, Scale bar: 1 μm) show that Narf localizes to the nuclear envelope. Airy Scan microscopy of fractionated nuclei (D) revealed that Narf distribution partially overlapped with Dm0 and is different from Nup153 localization. Immunofluorescence analyses were confirmed by a fractionation experiment performed with wild type embryo extract (E). Western blot analysis showed a predominant signal within the cytoplasmic fraction. Nevertheless, a distinct signal was also observed within the nuclear fraction. Success of fractionation was given by Dm0 detection. The lysate of 25 embryos was loaded for each fraction. Generation of a mCherry-tagged Narf version and subsequent immunofluorescence analysis of S2 cells were performed by M. Clever.

4.4.3 Narf has a function during *Drosophila* development

Narf is known to possess an essential function for viability in *Drosophila*, since four different lethal alleles (NC37, NC38, NC70 and NC109) have been already identified (Coulthard et al., 2010). However, only NC38 and NC109 are further described and known to contain mutations within the third exon. In the allele NC109 two nucleotide substitutions cause amino acid exchanges from valine (V) to aspartic acid (D) at position 152 and serine (S) to alanine (A) at position 154. NC38 possesses a nonsense mutation as it introduces a stop codon (*) at position 166 (Figure 19 A). To study Narf function during development I used flies containing these lethal alleles, which are available at the Bloomington Stock Center. In order to document the potential mutant Narf region in NC37 and NC70 genomic DNA containing Narf was sequenced. Even if it was possible to reproduce the previous described data for NC38 and NC109, I did not find any mutation within the coding region of the uncharacterized alleles NC37 and NC70 (Figure 19 B).

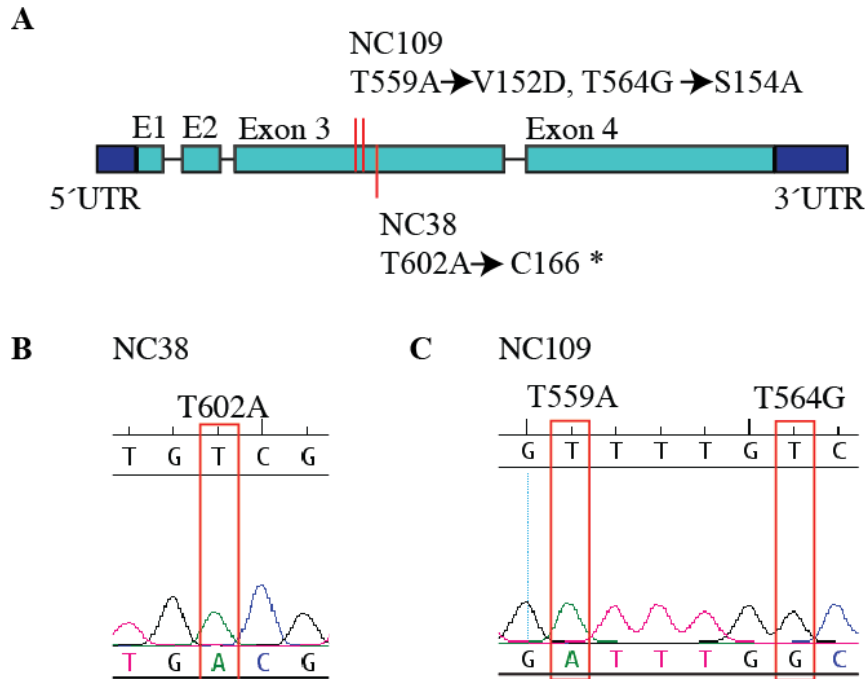


Figure 19: The lethal alleles NC38 and NC109 contained the described mutations

(A) Schematic illustration of the Narf gene structure and the genomic position of the characterized lethality causing mutations. Sequencing analyses of NC38 (B) and NC109 (C) revealed the presence of the described mutations according to Coulthard et al., 2010.

Survival rate assays were performed to address the lethal phase. To be able to distinguish between a homo- and a heterozygous situation, I established fly stocks in which the lethal alleles are kept over GFP-tagged balancer chromosomes (GFP, CyO). As GFP expression was controlled by the twist promoter, the selection according to fluorescence was already possible at embryonic stage and became more striking during larval stage (Figure 20 A). Around 100 embryos of each genotype were collected and scored for their survival during development. As control wild type embryos were used, which reach adulthood with a probability of ~ 75%. Animals expressing the lethal alleles in a heterozygous manner already show a decrease of ~ 50% in survival rate from embryonic to larval stage. At this point it has to be mentioned that it is not possible to distinguish between homozygous (GFP, CyO/GFP, CyO) or heterozygous GFP expressing embryos (NC/GFP, CyO) and that the homozygous expression for a balancer chromosome is lethal at embryonic stage (e.g. Meneely, 2014). Thus, the survival rate of heterozygous situations can be considered to be in the same range like wild type. However, homozygous situations showed a clear decrease

in survival rate and differed in their severeness during development. Hence, the strongest lethal allele was NC37 as it already showed an embryonic lethality. The alleles NC38 and NC109 were larval lethal and animals homozygous for NC70 were even able to survive until adult hood with a probability of 25%.

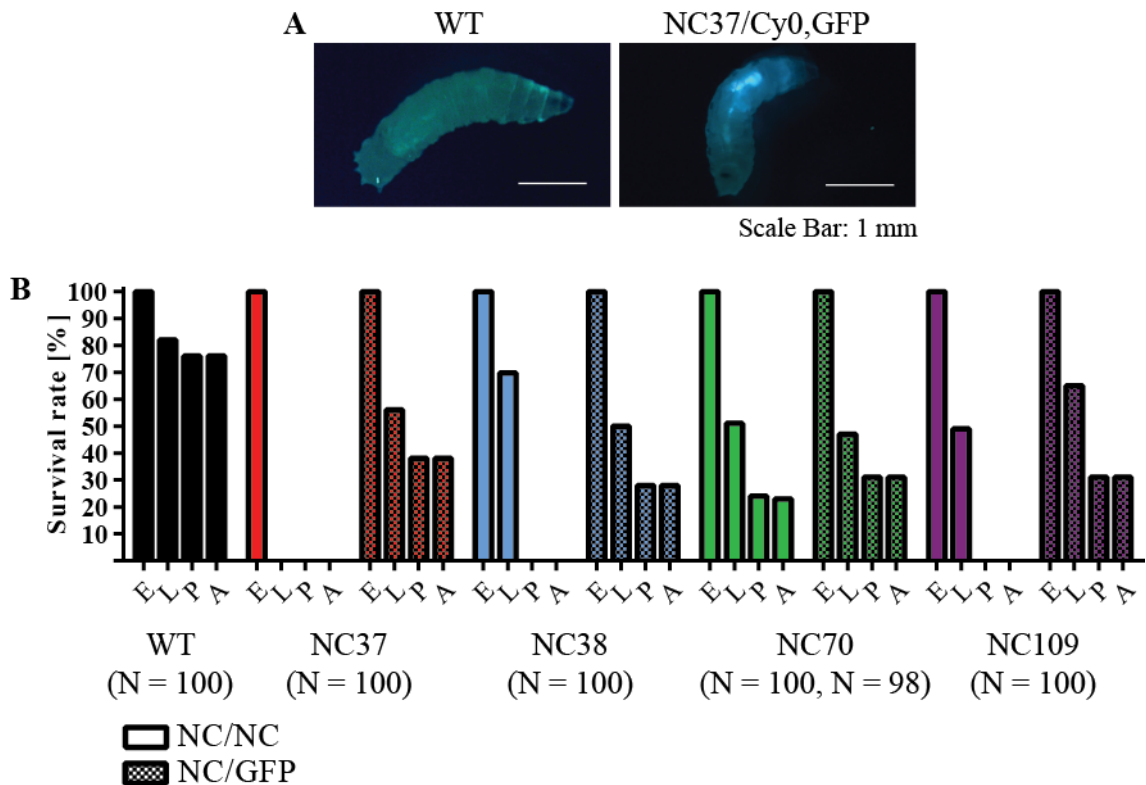


Figure 20: Characterization of different Narf lethal alleles

(A) Fluorescence analysis of wild type and GFP expressing larvae. Wild type larvae showed auto-fluorescence. However, larvae expressing GFP under the control of the twist-promoter were clearly distinguished. (B) Survival rate assays of animals being homozygous or heterozygous for the indicated lethal alleles. Genotype selection was initially based on fluorescence analysis during embryonic stage and survival rate was determined over time.

4.4.4 The lethal allele NC 38 probably resulted in nonsense-mediated decay

It was observed that homozygous NC38 animals were able to hatch. However, they died soon during larval stage. In order to characterize the reason of lethality, embryo- and larvae extract were analyzed for Narf protein expression. During embryonic development no differences in protein levels between homo- and heterozygous situations were observed (Figure 21). However, reaching the larval stage was accompanied by a clear decrease in Narf

protein level. As there was also a protein band shift observable, it was assumed that the detected protein bands represented different isoforms. Thereby, the embryonic expressed Narf might be the isoform PD with a molecular weight of 49.3 kDa (<http://flybase.org/reports/FBgn0262115>) and maternally provided, whereas the larval protein might be zygotically expressed and refers to isoform PA (54.5 kDa) or PC (54.1 kDa). The premature stop codon in NC38 might led to the nonsense-mediated mRNA decay, thereby causing the reduction of Narf protein, which can be considered as a quasi-null allele.

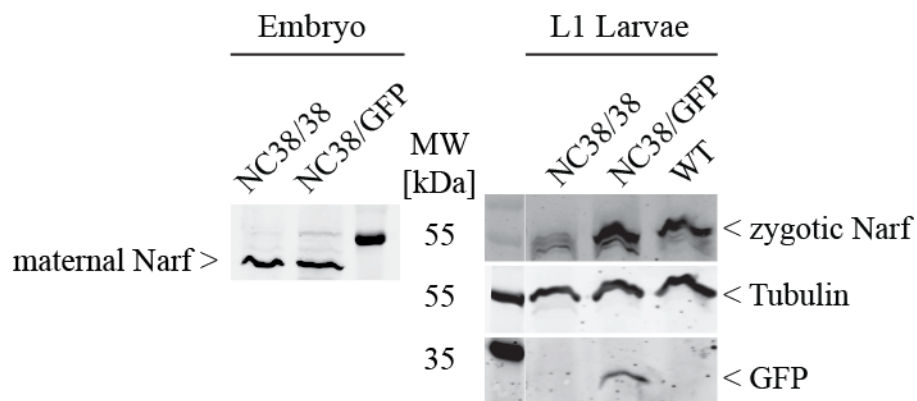


Figure 21: Narf protein level is decreased dramatically in NC38 homozygous larvae.

Western blot analysis of embryo and larvae extract from homozygous or heterozygous situations of the Narf lethal allele NC38. Embryo extract of late embryos did not show a difference in protein level. But, in early L1 stage a decrease in protein level of the homozygous situation was observed in direct comparison to the heterozygous situation and wild type larvae. Furthermore a change in running behavior for Narf was detected in larvae extract, indicating a new zygotically expressed isoform. Tubulin staining was used as loading control and GFP staining was used as a proof for successful genotype selection.

4.4.5 Genomic transgenes mimicing the human patient situation

With the aim to identify the organismal effect of the human Narf mutation, I generated genomic constructs of the wild type *Drosophila* Narf as well as a mutant allele containing an amino acid exchange homologues to the human patient (Narf H/R) (Figure 22). To mimic the heterozygous mutant patient situation it was planned to express the genomic Narf H/R transgenes in NC38 heterozygous flies as it was shown before that this allele comes close to a null allele. Flies that express instead the native Narf in the same genetic background were planned to be used as control.

```

Narf_human   367 H F V E V L A C 374 Patient allele: H367R
CG17683_Dm  388 H F V E V M A C 395           H388R
              * * * * * * *

```

(modified to <http://www.uniprot.org/align>)

Figure 22: Position of the human patient situation is conserved in *Drosophila*.

Partial amino acid alignment of the human Narf, referring to the sequence region which contains the human mutation, in comparison to *Drosophila* Narf. Fully conserved amino acids are marked with an asterisk (*).

In order to establish genomic alleles a touchdown PCR using the oligonucleotides MK44/MK45 was performed on genomic DNA of wild type flies. The PCR product spanning a gene region of 3.992 nucleotides was digested by NheI and BglII and subsequently cloned into the linearized pAttB vector. To introduce the mutation the genomic wild type allele was digested by XhoI and NdeI and the 667 bp fragment was replaced by a synthesized fragment containing the desired mutation. Gene fragment synthesis was done by eurofins including a nucleotide exchange of CAC at position 1323 - 1325 (nucleotides downstream of ATG) against AGA coding for arginine (R) instead of histidine (H). Both constructs were finally site specific integrated into the *Drosophila* genome using a genomic attP site (25C6) containing fly line. Transgenic flies expressing the genomic Narf wild type allele in wild type background were successfully established. However, it was not possible to establish transgenic flies carrying the mutant allele. Injections of the genomic constructs by Genetivision, using different genomic attP sites (59D3, 68A4), led to similar results showing that the observed lethality of the mutant Narf allele is independent of the integration site.

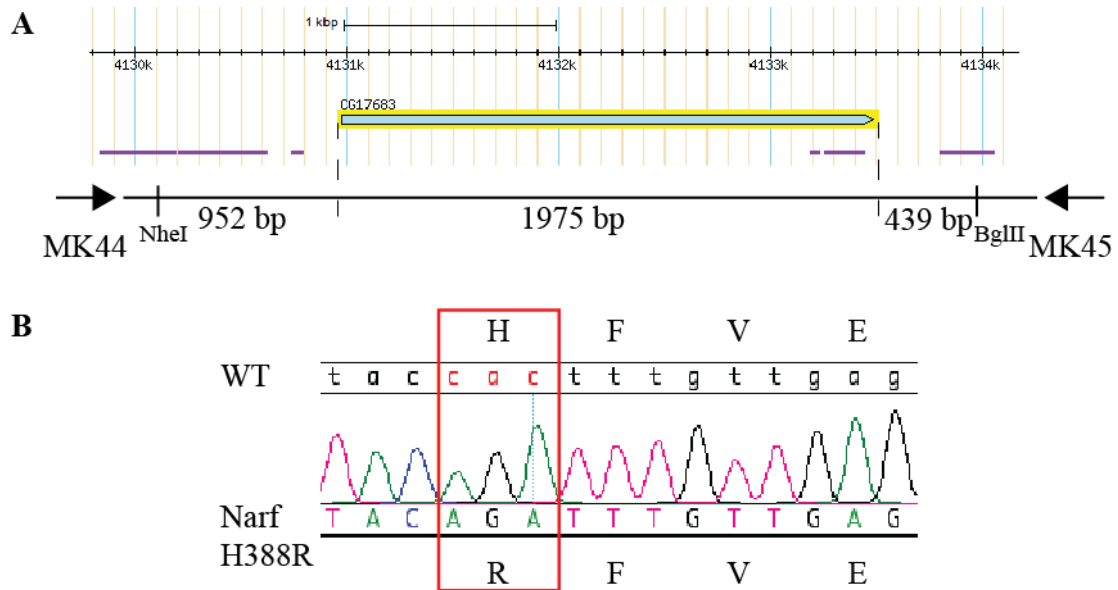


Figure 23: Generation of genomic Narf alleles

(A) Amplified area of the genomic locus used for the generation of genomic Narf alleles. PCR amplification was performed using the oligonucleotides MK44/45 on genomic DNA of wild type flies. Restriction digest by NheI and BglIII enabled the cloning into the final donor vector. Schematic illustration was modified according to <http://flybase.org/reports/FBgn0262115> (B) Sequencing analysis performed with Seqman confirmed the introduction of the desired mutation by gene synthesis.

4.4.6 Increase of genomic copies of Narf might positively affect viability

Since it was not possible to establish a genomic Narf H/R allele, the question arose if expression of an increased number of genomic Narf copies affects viability. Three differently inserted transgenic lines for the Narf wild type allele were established (25C6-2L, 59D3-2R, 68A4-3L), in none of them an effect on viability and fertility has been observed. To study this in more detail survival assays and lifespan analysis have been performed using one transgenic line which was integrated on the second chromosome. To be able to distinguish between homo- and heterozygous flies, expressing three or four genomic copies of Narf, the transgenic flies were kept over a GFP-tagged balancer chromosome (GFP, CyO). Survival rate analysis during development showed, that the expression of an increased number of genomic copies is not negatively affecting viability (Figure 24 A). However, compared to wild type embryos Narf overexpressing animals even show a higher survival rate. As it is not possible to distinguish between homozygous (GFP, CyO/GFP, CyO) or heterozygous GFP expressing embryos (genomic Narf/GFP, CyO) around ~ 25% of the 3x

genomic Narf expressing embryos (Figure 24 A, green) will die before reaching larval stage, due to a homozygous expression of the balancer chromosome. Thus, the survival rate of both overexpressing situations seems to be increased compared to wild type embryos.

Furthermore no decrease on lifespan was detected compared to wild type flies (Figure 24 B). Thereby, it also seems that Narf overexpressing flies show an increase in lifespan dependent on Narf copy number. At this point it has to be mentioned that the used control, which was the originally injection strain (BL#25709-25C6), had the most similar genetic background but already showed a shortening on lifespan compared to wild type flies. Thus it was not clear if the difference in lifespan might be an inbreeding effect within control flies and a hybrid effect on Narf expressing flies or dependent of Narf.

In order to verify the effect of gene dose on life span, flies containing genomic transgenes on different chromosomes were crossed with each other. However, the upper limit was the expression of four genomic copies, since genomic Narf integrated on the third chromosome was homozygous lethal perhaps due to integration site.

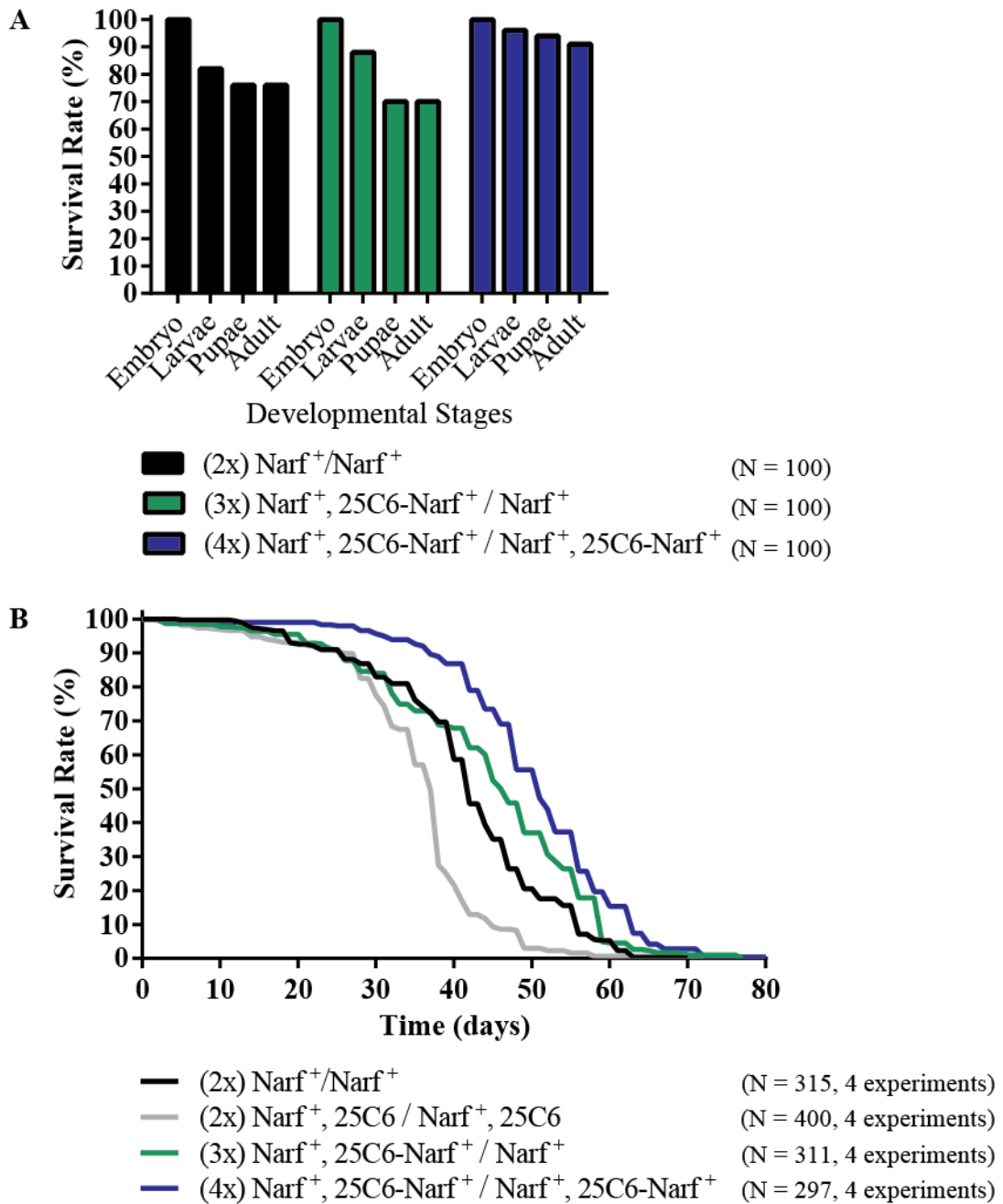


Figure 24: Overexpression of genomic Narf increased survival rate

(A) Survival rate assay of animals expressing three (3x) or four (4x) copies of genomic Narf compared to wild type embryos with naturally two genomic Narf copies (2x). Narf overexpression had no negative effects on survival rate during development. (B) Survival rate analyses during adulthood showed that an overexpression of genomic Narf alleles prolonged lifespan (log-rank test: Ctrl vs. WT $p < 1.0 \times 10^{-10}$, WT vs. 3x Narf $p = 1.6 \times 10^{-5}$, WT vs. 4x Narf $p < 1.0 \times 10^{-10}$, 3x Narf vs. 4x Narf $p = 8.1 \times 10^{-6}$). Statistical analyses were performed by OASIS, illustration was done using GraphPad Prism6.

4.4.7 Ubiquitous overexpression of Narf had beneficial effects on lifespan

It was observed that an increase of the genomic copy numbers of Narf prolonged lifespan (Figure 24). Furthermore, it was shown that a higher improvement of survival rate can be achieved by expressing four instead of three genomic copies. To further validate these data a Narf overexpressing situations was accomplished using the UAS/GAL4 system. As lifespan seemed to be dependent on Narf expression strength, different ubiquitous drivelines (actin- (GS), armadillo and tubulin-Gal4) were tested for their effect on Narf protein expression level in adult males (Supplement Figure 4). A control experiment was performed with a transgenic UAS-GFP fly line. It is shown that highest GFP expression was achieved using the actin GS or tubulin driver line. However, highest Narf expression was detected in case of tubulin-Gal4. Thus, lifespan analyses were performed overexpressing both Narf alleles (wild type and H/R mutant) controlled by tubulin-Gal4. To prevent differences in lifespan due to hybrid effects and to provide a control situation with the most similar genetic background, the originally used injection strain (BL#25709-25C6) was crossed against the driver line. Consistent to the before mentioned data a prolongation in lifespan was observed. Furthermore, comparable lifespan curves were detected for both Narf alleles. To summarize, it was shown that Narf overexpression, starting during early development, had beneficial effects on organismal level, reasoning a role of Narf in aging.

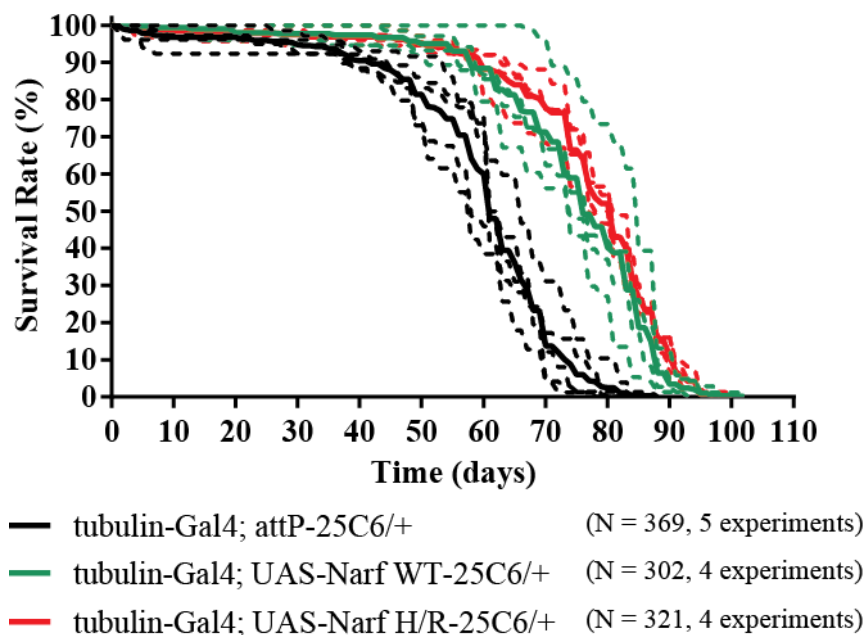


Figure 25: Ubiquitous overexpression of Narf prolonged *Drosophila* lifespan

Lifespan analyses of Narf overexpressing flies (green: wild type allele, red: mutant H/R allele) compared to control flies (black). Overexpression was controlled by tubulin-Gal4 a ubiquitous driver line. Survival rate

analyses were performed with a minimum of four replicates (dashed lines) each with ~ 75 males. The mean value was taken (solid lines) and used for statistical analyses. A ubiquitous up regulation of Narf significantly increased lifespan (log rank test: Ctrl vs. OE Narf WT $p < 1 * 10^{-10}$, Ctrl vs. OE Narf H/R $p < 1 * 10^{-10}$, OE Narf WT vs. OE Narf H/R $p = 0.0033$).

4.4.8 Using the CRISPR approach for generating a Narf null allele

In order to study Narf function in a clear genomic background it was planned to generate a Narf null allele using the CRISPR/Cas9 approach. Thereby targeted chromosomal double strand breaks (DSB) are induced using the microbial Cas9 nuclease protein. Site directed specificity is achieved by locating the Cas9 protein via single guided RNAs (sgRNA) which consist of 20 nucleotides excluding the protospacer-adjacent motif (PAM) (Jinek et al 2012). DNA cleavage results in activation of the DSB repair machinery which will remove DNA damage by the non-homologous end joining (NHEJ) pathway or the homology-directed repair (HDR) pathway (reviewed in Lieber et al., 2010). The second repair mechanism is based on the insertion of a homology DNA template, enabling gene deletions by replacing the gene locus with exogenous sequences. In this study the pHD-DsRed-attP vector was used as a tool to deplete the genomic locus of Narf in exchange with a dsRed selection marker, loxP sites and an attP site, allowing site specific recombination after introduction within the gene locus (Gratz et al., 2014). A germ-line specific expression of the Cas-9 protein is furthermore preventing lethality in case of essential genes. Narf specific sgRNAs were identified by the CRISPR Optimal Target Finder (<http://flycrispr.molbio.wisc.edu>), generated by oligonucleotides annealing and cloned into the BbsI linearized pBFvU6.2 and U6.2B vectors. To enable HDR two homology arms of around ~ 1 kb (Beumer et al., 2013, Gratz et al., 2014) were amplified and successively cloned into the linearized pHD-DsRed-attP vector. Thereby adjacent areas to the genomic locus of Narf were chosen which lied outside of repetitive sequences (Figure 26 A, purple lines). Subsequent injection in Cas9 expressing embryos was performed by BestGene Inc. However, out of 55 GO adults no RFP positive G1 fly was established. A fail in null allele generation might be reasoned to the heterochromatic position of Narf next to the centromere or the large gene spanning region of ~5.3 kb, decreasing efficiency in repair mechanism. In order to still get a null allele of Narf, the all-inclusive service from inDrosophila was used. In this case an attP site will be introduced by replacing the gene area from the 5'UTR till 368 nucleotides after the 3'UTR (position 4130968 to 4133852). Once a conditional null allele is established a tool is generated which enables the study of a multitude of Narf situations

(e.g. knock-out situation, GFP-transgenes or analyses of a genomic and mutant Narf H/R allele in a clonal flip-out system (Figure 26 B)).

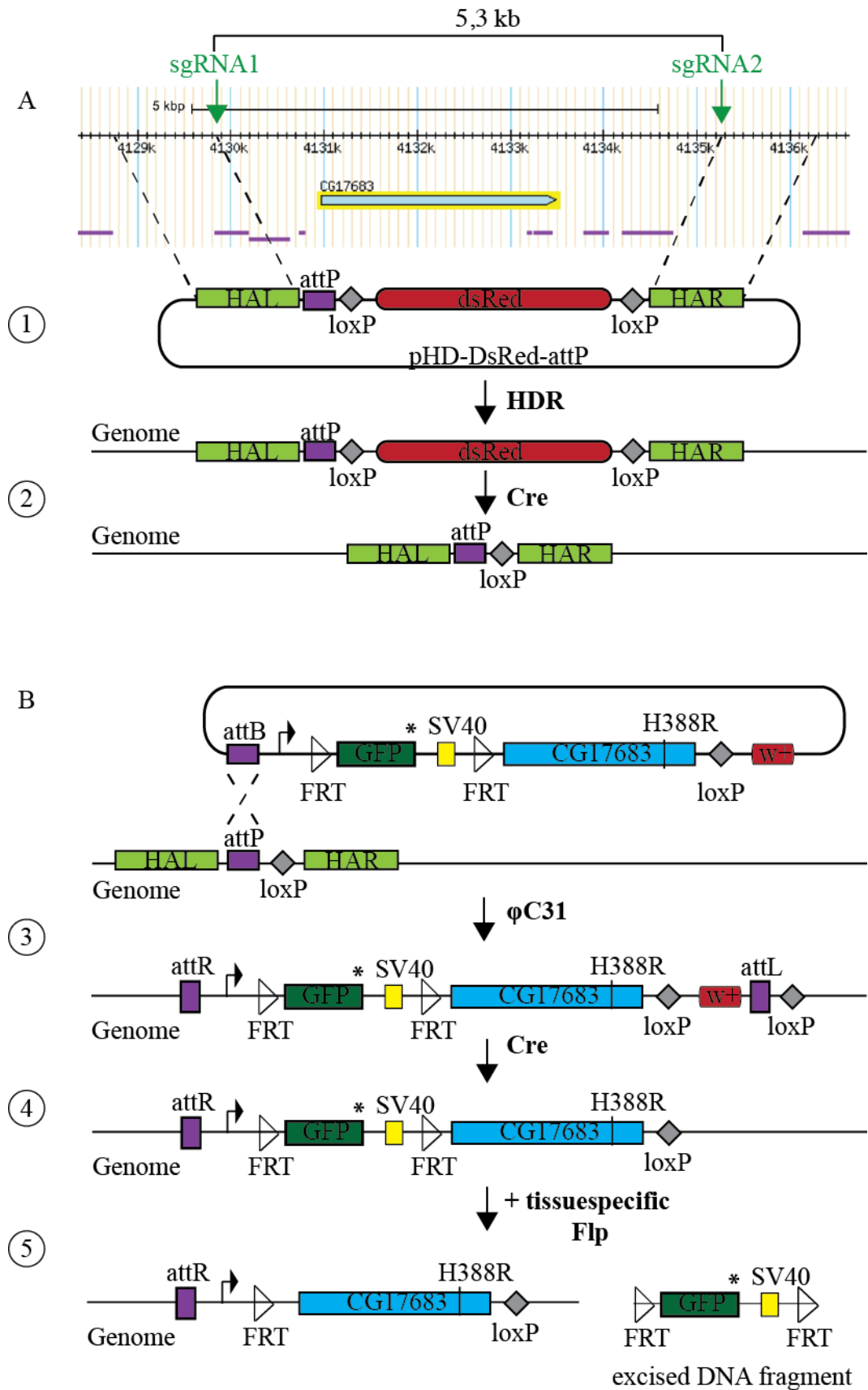


Figure 26: Generation of a conditional Narf null allele by CRISPR/Cas9

(A) Single guided RNAs (sgRNAs) are used to target the Cas9 nuclease protein and induce site specific chromosomal double strand breaks (DSBs). Upon DNA damage the DSB repair machinery will be activated. By providing an exogenous vector sequence, including two 1 kb homologous gene regions (HAL-homology arm left, HAR-homology arm right), homology directed repair (HDR) will take place (1). Thus, a null allele is generated by replacement of the genomic locus. Successful generation of transgenic flies can be detected by the introduced selection marker *dsRed*, which can be later removed by Cre-loxP recombination (2). (B) The introduction of a genomic attP site enables site specific integration by using the ϕ C31 integrase and makes the null allele conditional. To mimic the heterozygous human patient situation it is planned to express a genomic Narf (H/R) allele in a clonal and negatively GFP-marked manner. Potential lethal effects will be prevented by a tissue specific expression. In order to do this an attB vector will be site specifically integrated (3) carrying the coding sequences for GFP and the desired Narf allele. A successful integration will destroy the attP site which will be detected by the expression of the mini white (w^+) selection marker. Excessive vector sequences will be removed by Cre-loxP recombination, enabled by the introduction of a second loxP site and recognized by the loss of the mini white (w^+) selection marker (4). Thus, the genomic Narf promoter will control GFP expression up to the stop codon (*) and followed by a SV40 terminator signal. As these sequences will be flanked by two FRT (flippase recognition target) -sites the expression of a flippase recombinase (FLP) will be able to remove this cassette in a tissue specific manner (5). This approach will allow the heterozygous expression of a genomic and mutant Narf H/R allele. Narf expressing cells will be negatively marked by the loss of GFP expression.

4.4.9 The GeneSwitch Gal4 system was used to muscle specifically express GFP in a dose dependent manner

Another possibility to study protein function is the usage of the GeneSwitch-Gal4 system. This approach enables a spatial and temporal specific expression of transgenes within *Drosophila*. The basic principle behind is that the GeneSwitch-Gal4 protein becomes only active in the presence of the mifepristone (RU 486, hereinafter referred to shortly as RU) activator. Spatial expression is given by a tissue specific enhancer, which drives Gal4 gene expression (Figure 27 A). The big advantage of this system is the same genetic background of induced and non-induced flies, thereby providing a better control.

In order to know the right working concentration range of RU, I checked the effect of target gene expression under different RU concentrations. Therefore, an UAS-GFP transgene was muscle specifically expressed using the MHC-GS Gal4 (myosin heavy chain) driver line. The GFP level was then used as readout for gene expression level. Immunofluorescence analyses and western blot analyses showed that the GFP protein was expressed within thoracic muscle tissue after 10 days of induction (Figure 27 B, C). Furthermore it was shown

that this expression occurs in a dose dependent manner, controlled by distinct RU-concentrations (Figure 27 B). A dose-response relationship, based on the measured mean grey value of the detected GFP-signal and a control-signal, is shown in Figure 27 D. The half maximal effective concentration (EC₅₀) within a range of 2 – 200 µM of RU was found to be at 50 µM.

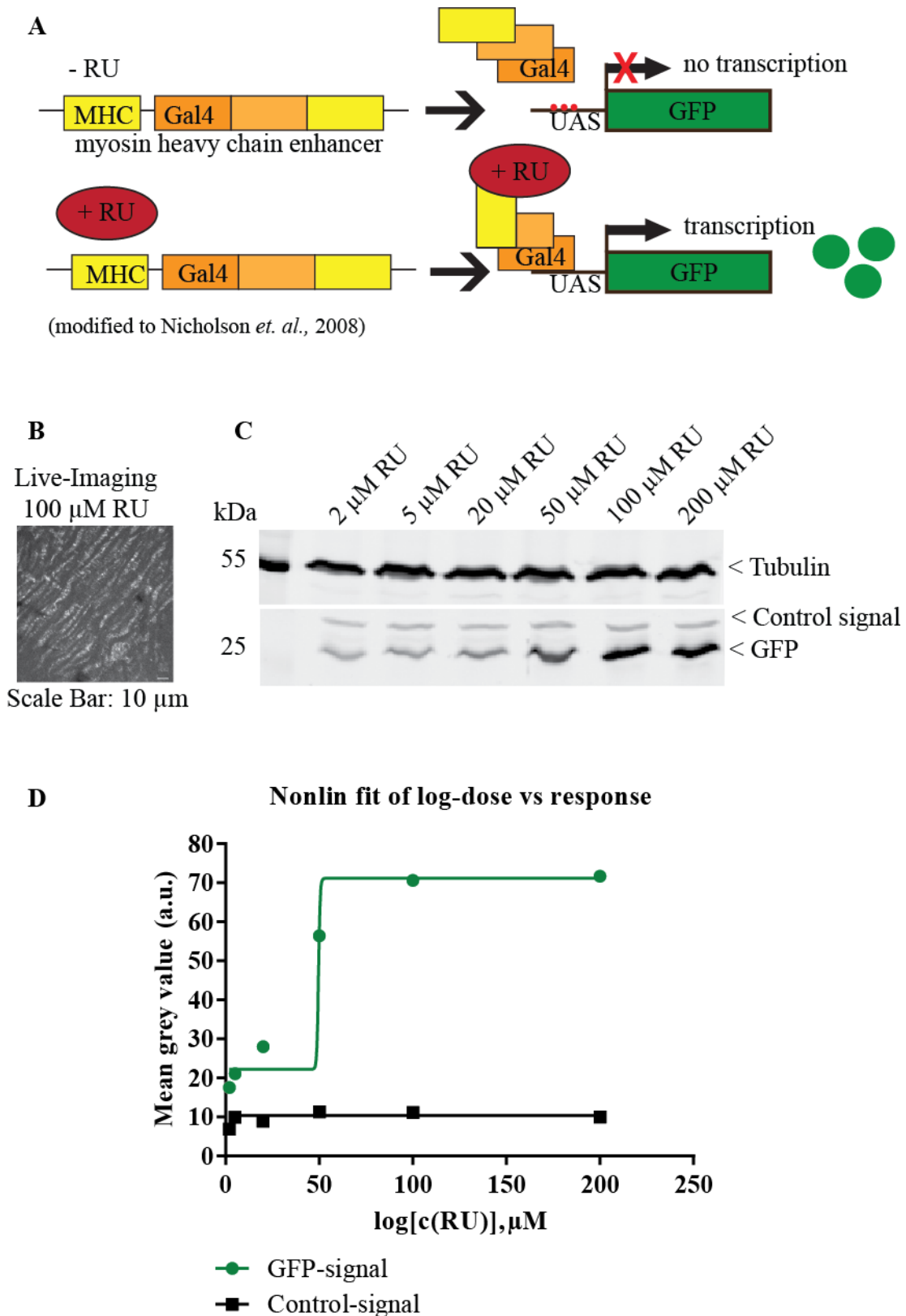


Figure 27: The GeneSwitch system enables spatial and dose-dependent gene expression

(A) Schematic illustration of the basic mechanism of the GeneSwitch system. Spatial and temporal gene expression is controlled by a tissue specific driver (e.g. MHC) which control Gal-4 protein expression. Transcriptional activation of the Gal-4 protein is achieved in the presence of the activator mifepristone (RU486)

which enables expression of an UAS-transgene (e.g. UAS-GFP). (B) Live-imaging of thoracic expressed GFP controlled by the MHC driver line. Induction was performed with 100 μM of RU for 10 days. (C) Western blot analyses of thorax samples of GFP expressing flies controlled by the MHC enhancer. Induction was done as indicated with different concentrations of RU for 10 days. Antibody staining was performed against GFP and α -tubulin as control. An unspecific signal generated by the GFP antibody was used as an additional control-signal for subsequent mean grey value quantification. (D) Logarithmic dose-response relationship, based on the measured mean grey value of the detected GFP-signal and the control-signal. The EC_{50} concentration was calculated to be at 50 μM within a range of 2 – 200 μM of RU.

4.4.10 The GeneSwitch system was used to muscle specifically overexpress Narf

In order to use the GeneSwitch system to study Narf-protein function, I generated transgenic flies containing the wild type Narf and the mutant version driven by UAS. Therefore, the cDNA clone RE37350, provided by the Berkeley *Drosophila* Genome Project (BDGP), was used. To study the effect of the mutant Narf allele, the H388R mutation was introduced via site directed mutagenesis. Subsequent sequencing analysis confirmed the success. The cDNA fragments of the wild type and the mutant situation were subsequently cloned into the pUAS-attB vector via NotI/BamHI restriction followed by a blunt end ligation into the NotI/XhoI linearized donor vector. Both constructs were finally site specifically integrated using embryos containing a genomic attP site and transgenic flies were successfully established.

Next, I checked if it was possible to overexpress Narf in the muscle using the GeneSwitch system with two different concentrations of RU (20 μM , 200 μM). Western blot analysis of thorax samples confirmed that Narf was indeed overexpressed after 10 days of induction compared to non-induced flies (Figure 28). However, a dose dependency was not as clear as it was seen for GFP overexpression (Figure 27 C).

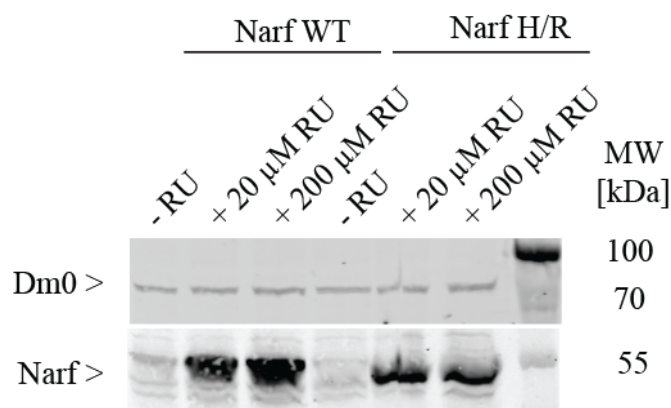


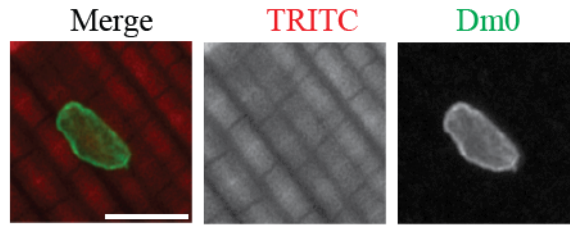
Figure 28: The GeneSwitch Gal4 system enabled Narf overexpression

Western blot analysis of thorax samples of Narf overexpressing flies controlled by the MHC enhancer. Induction was done with 20 μ M and 200 μ M of RU for 10 days. Non-induced flies were used as control. Antibody staining was performed against Narf and lamin Dm0 as control. Both RU concentrations induced a Narf overexpression. However a dose dependent difference in gene expression was not detected.

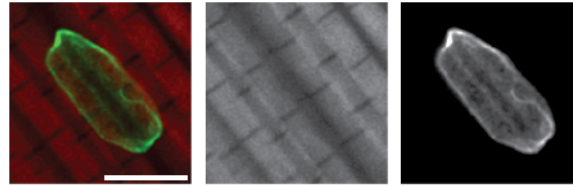
4.4.11 Overexpression of Narf increased nuclear size in muscle cells

One of the hallmarks of progeria patient cells is an abnormal nuclear structure. Next, I examined the effect of Narf overexpression on nuclear morphology. An immunofluorescence analysis of thorax samples, using an antibody staining for lamin Dm0 as nuclear marker, was performed. After 10 days of induction an increase in nuclear size has been observed in Narf overexpressing flies compared to non-induced control flies (Figure 29). Furthermore, quantification of the nuclei area showed that the overexpression of the mutant Narf allele seems to be more severe (Figure 29 D). However, changes in nuclear positioning or muscle structure have not been observed. To further validate if RU alone is inducing nuclear size changes, wild type flies crossed with the MHC-Gal4 driver line were treated with 200 μ M RU. As the quantification shows RU alone is indeed affecting nuclear size. However, nuclei in a Narf overexpressed situation are still significantly larger, suggesting an additive effect of Narf and RU in these situations.

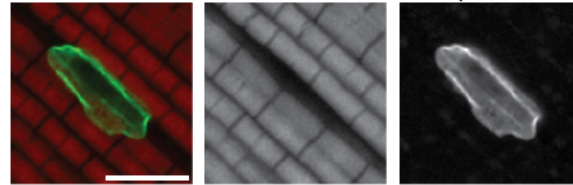
A MHC-GS Gal4 Narf WT - RU (Control)



B MHC-GS Gal4 Narf WT + 200 μ M RU



C MHC-GS Gal4 Narf H/R + 200 μ M RU



Scale Bar: 5 μ m

D

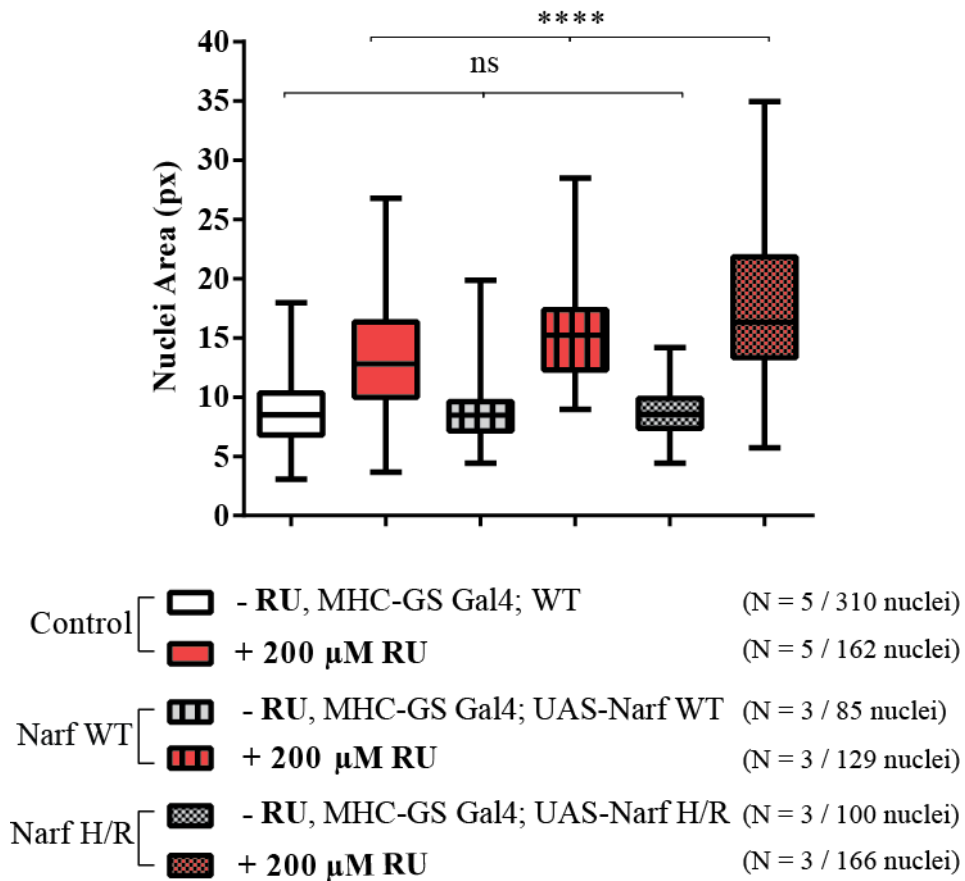


Figure 29: Narf overexpression affected nuclear size

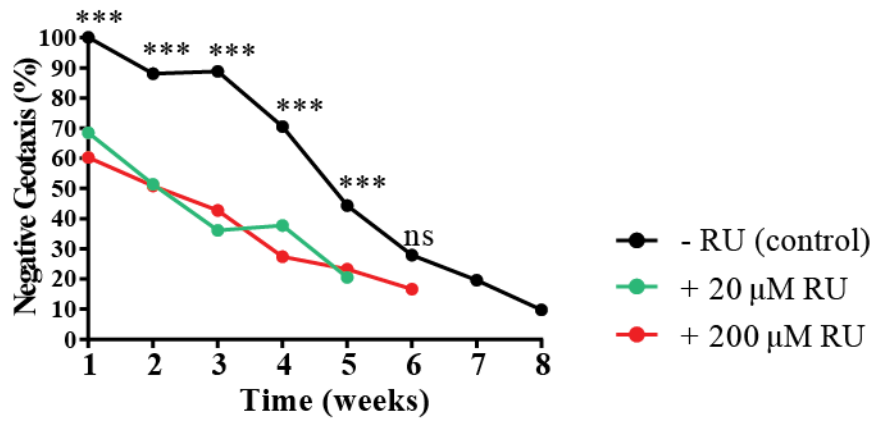
(A-C) Immunofluorescence analyses of thorax samples. Overexpression of the wild type (B) or the mutant Narf allele (C) was induced using 200 μ M of RU for 10 days. Non-induced flies were used as control (A). Nuclei were stained with lamin Dm0 and muscle tissue was marked using TRITC phalloidin. (D) Quantification of the nuclei area. Wild type flies crossed with the MHC enhancer and treated with 200 μ M of RU showed an increase in nuclear size verifying that RU alone has an effect on nuclear size compared to non-induced situations (Ctrl^{-RU} vs. Ctrl^{+RU} $p = 3.19 \cdot 10^{-21}$). Overexpression of the Narf alleles induced by 200 μ M of RU significantly increased nuclear size compared to RU treated control flies (Ctrl^{+RU} vs. Narf WT^{+RU}; $p = 9.66 \cdot 10^{-6}$, Ctrl^{+RU} vs. Narf H/R^{+RU}; $p = 4.74 \cdot 10^{-16}$). Overexpression of the mutant Narf allele had stronger effects on nuclear size than overexpression of the wild type allele (Narf WT vs. Narf H/R; $p = 1.15 \cdot 10^{-6}$). Quantification was done manually using ImageJ and statistical significance was calculated using unpaired t -test (**** $p < 0.0001$).

4.4.12 Muscle specific overexpression of Narf affected negative geotaxis behavior

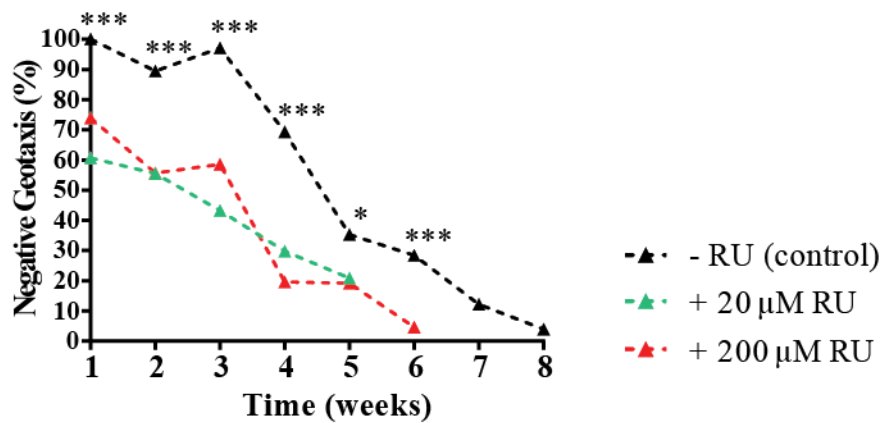
After finding that Narf overexpression is inducing nuclear shape changes, I wondered if this might be associated with muscle weakness. In order to study this a negative geotaxis experiment was performed. Negative geotaxis is a natural and age dependent climbing behavior of *Drosophila* characterized by a negative response to gravity. It was already shown that a muscle specific overexpressing of Kuk or Lamin B results in an early decline in this climbing ability (Brandt et al., 2008). To validate if a muscle specific overexpression of the wild type and the mutant Narf allele leads to a similar phenotype negative geotaxis assays with a maximal duration of eight weeks were performed. Non-induced flies with the same genetic background were used as controls. RU induction was done for one week before measurements of the climbing high were started. The mean climbing high of the first measurements was set to 100%. In both control situations a very similar age dependent decline in mobility was visible. Induced flies showed a clear decrease in negative geotaxis compared to control flies independent of the overexpressed Narf alleles (wild type or H/R) and the used RU concentration (Figure 30 A, B). An explanation that the observed effect is not becoming more severe with an increased RU concentration can be given by the very similar protein expression of Narf using 20 μ M or 200 μ M of RU (Figure 28). However, as it was seen before that RU alone is indeed affecting nuclear size this experiment has to be complemented by an additional control to rule out that RU alone is sufficient to induce the observed effects. This experiment was also started but could not be finished due to seasonal temperature differences which caused a change in *Drosophila* behavior. However, it was

shown that nuclear shape changes are dependent on Narf expression, suggesting that this will be also true for negative geotaxis behavior.

A MHC GS Gal4; UAS-Narf WT



B MHC GS Gal4; UAS-Narf H/R



C MHC GS Gal4; UAS-Narf
WT vs. H/R

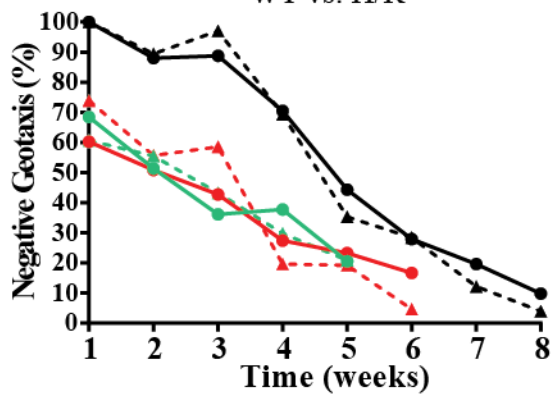


Figure 30: Narf overexpression might affect negative geotaxis behavior

(A-B) Negative geotaxis experiments of Narf overexpressing flies induced by either 20 μM (green) or 200 μM of RU (red). Measurements were started after one week of induction and performed with at least 10 and maximum 25 males dependent on survival rate over time. Mean climbing high of one week old non-induced control flies was set to 100%. For both situations a clear decrease in climbing high is observed independent of the used RU concentration. (C) Direct comparison of the mean climbing high in flies overexpressing the wild type and the mutant Narf allele. No significant changes between the wild type and the mutant allele were detected using 20 μM of RU (green circle/triangle). Low significant changes were detected for 200 μM (red circle/triangle) after week 3 and 6 (week 3: WT⁺²⁰⁰ vs. H/R⁺²⁰⁰ $p = 0.0279$, week 6: $p = 0.0389$). Statistical significance was calculated using unpaired t -test (ns $p > 0.05$, * $p < 0.05$, ** $p < 0.01$, *** $p < 0.001$).

4.4.13 Muscle specific overexpression of Narf affected *Drosophila* lifespan

Negative geotaxis experiments were performed over a maximal time period of 8 weeks. But, the analyses of induced flies had to be stopped 2-3 weeks earlier compared to control flies due to a lower survival rate. This observation led me hypothesize that an overexpression of Narf leads to a shortening in lifespan. However, to exclude that RU induction itself is responsible for a decrease in survival rate a control experiment using wild type flies and 200 μM of RU was performed. The analyses were done in four replicates each with around 75 male due to a high level of intraspecific variations in *Drosophila* lifespan. It is shown in Figure 31 that RU alone is not affecting lifespan, suggesting that Narf overexpression might be associated with a decrease in lifespan.

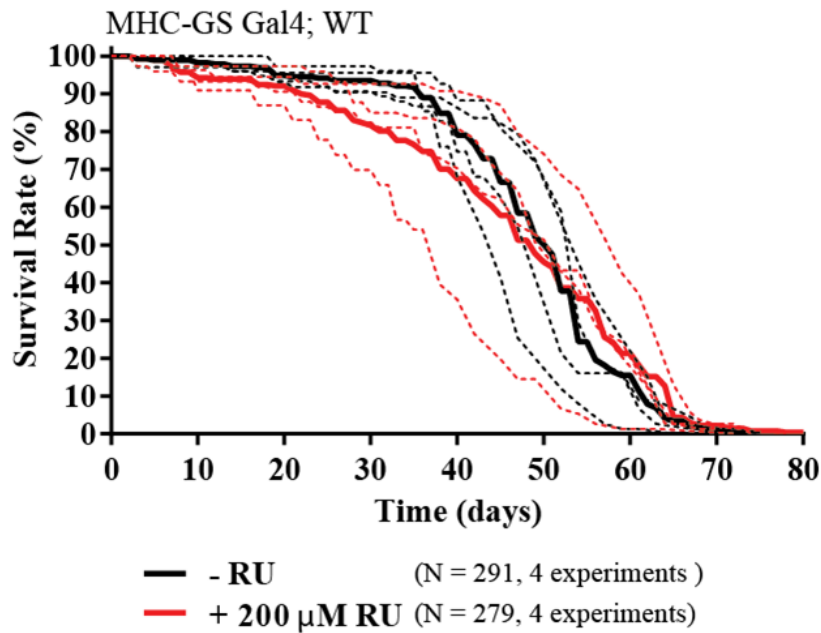
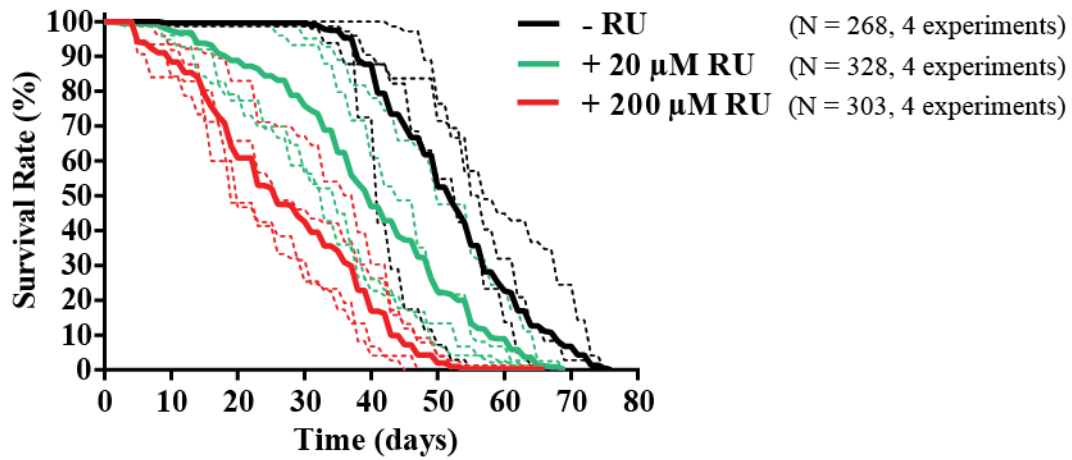


Figure 31: RU468 treatment did not affect *Drosophila* lifespan

Lifespan analyses of wild type flies treated with 200 μ M of RU (red) compared to non-induced control flies (black). Survival rate analyses were performed in four replicates (dashed line) each with ~ 70 males. The mean value was taken (solid line) and used for statistical analyses which was performed using OASIS an online application tool for lifespan analysis, log-rank test $p = 0.2265$ ($p > 0.05$, not significant).

In order to provide a proof that Narf overexpression affects survival rate during adulthood lifespan analyses with Narf overexpressing flies were performed. To analyze if an overexpression of the mutant Narf allele might further affect lifespan both alleles were tested in parallel. For both alleles a clear decrease in lifespan upon Narf overexpression compared to non-induced control flies was observed (Figure 32). This effect seems to be dose-dependent as lifespan shortening correlates with the RU concentration. A quite interesting observation was that the lifespans of the wild type and the mutant Narf allele behaved quite similar if induced with 20 μ M of RU. An induction with 200 μ M instead seems to cause more severe effects for the mutant Narf H/R allele, indicating a gain-of function for the mutant allele.

A MHC-GS Gal4; UAS-Narf WT



B MHC-GS Gal4; UAS-Narf H/R

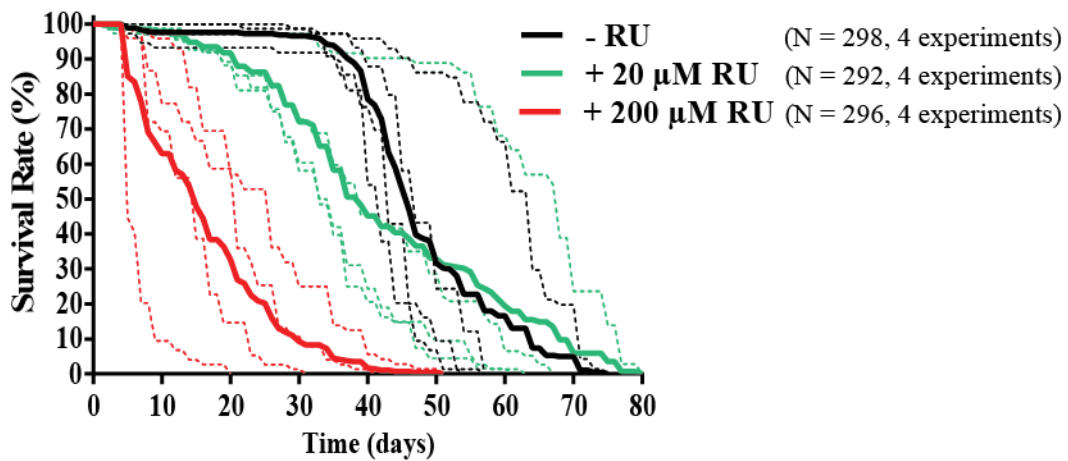
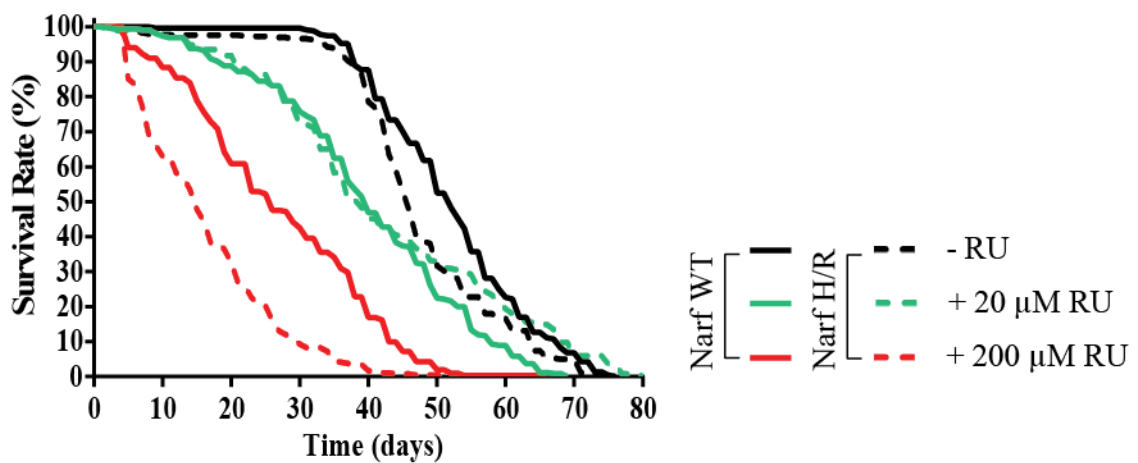
C MHC-GS Gal4; UAS-Narf
WT vs. H/R

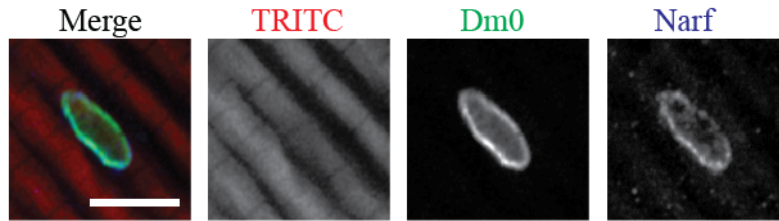
Figure 32: Narf overexpression during adulthood affected *Drosophila* lifespan

(A-B) Lifespan analyses of Narf overexpressing flies (A - wild type allele, B - mutant H/R allele) treated with 20 μ M (green) and 200 μ M of RU (red) compared to non-induced control flies (black). Survival rate analyses were performed in four replicates (thin lines) each with \sim 75 males. The mean value was taken (thick lines) and used for statistical analyses. For both Narf overexpressing situations dose-dependent decrease in survival rate was detected compared to non-induced control flies (log-rank test: WT^{-RU} vs. WT^{+20/+200} $p < 1 * 10^{-10}$, H/R^{-RU} vs. H/R⁺²⁰ $p = 0.4238$, H/R^{-RU} vs. H/R⁺²⁰⁰ $p < 1 * 10^{-10}$). (C) Direct comparison of the mean lifespans in flies overexpressing the wild type and the mutant Narf allele. An induction with 200 μ M of RU (red) is affecting survival rate in a higher magnitude than induction with 20 μ M of RU (green). Overexpression of the mutant Narf H/R allele induced by 200 μ M of RU is more severe than the wild type allele under the same conditions (log-rank test: WT⁺²⁰⁰ vs. H/R⁺²⁰⁰ $p < 1 * 10^{-10}$) Significant differences can be also detected without induction (log-rank test: WT^{-RU} vs. H/R^{-RU} $p < 1 * 10^{-10}$) and using 20 μ M of RU (log-rank test: WT⁺²⁰ vs. H/R⁺²⁰ $p = 4.6 * 10^{-5}$). Statistical analyses were performed by OASIS, illustration was done using GraphPad Prism6.

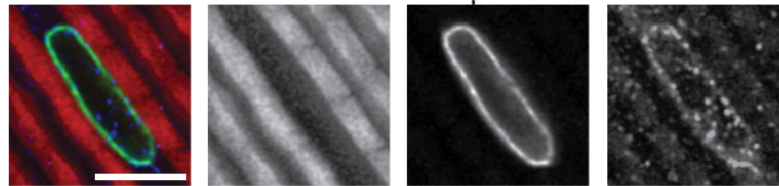
4.4.14 Knock-down of Narf did not significantly increase nuclear size in muscle cells

Until now it is not clear if the dominant human patient mutation represents a gain-of-function or loss-of-function allele. In order to check for cellular effects in a knockdown situation a long hairpin structure specific for the fourth exon of Narf, available at VDRC, was muscle specifically expressed and a thorax staining against Dm0, Narf and TRITC phalloidin was performed after 15 days of RU induction. Muscle nuclei of non-induced control flies were quite similar in appearance compared to previous experiments (Figure 29), showing a reproducible robustness for this approach. The knockdown of Narf resulted in a high variance in nuclear size and led to the observation of enlarged muscle nuclei (Figure 33 B, C). However, a subsequent quantification revealed that there is no statistical relevance for the observed effects. In order to control the efficiency of the Narf knockdown an immunofluorescence analysis was performed. However, the Narf antibody staining is associated with unspecific background preventing a following quantification. But, using 200 μ M of RU seems to affect Narf protein localization in a higher extend than a weaker induction with 20 μ M of RU, suggesting a proper expression of the hairpin structure.

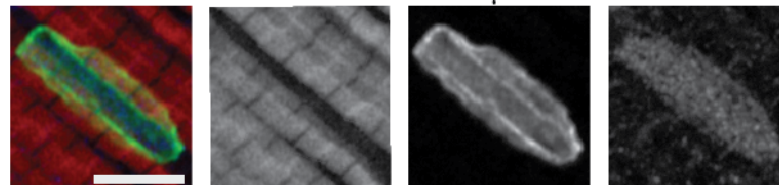
A MHC-GS Gal4 Narf-RNAi - RU (Control)



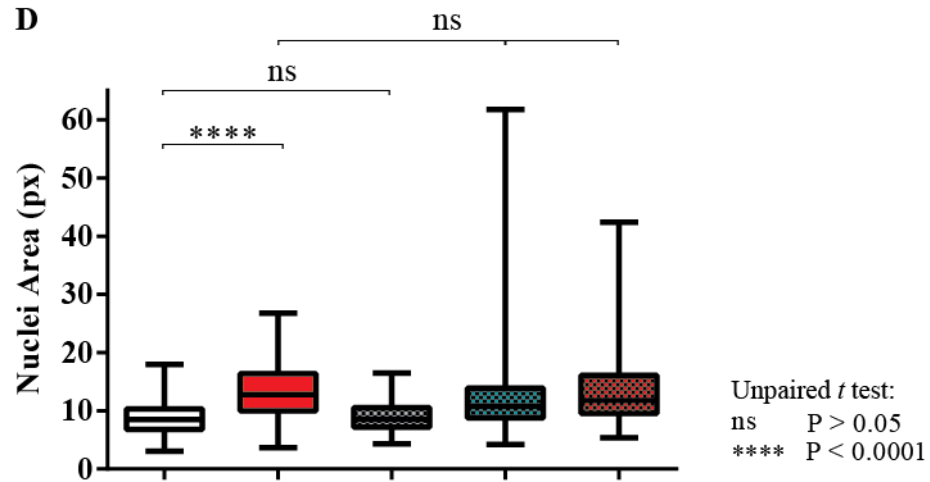
B MHC-GS Gal4 Narf-RNAi + 20 μ M RU



C MHC-GS Gal4 Narf-RNAi + 200 μ M RU



D



Control	[□ - RU, MHC-GS Gal4; WT	(N = 5 / 310 nuclei)
		■ + 200 μ M RU	(N = 5 / 162 nuclei)
Narf-RNAi	[▨ - RU, MHC-GS Gal4; UAS-Narf RNAi	(N = 3 / 89 nuclei)
		▩ + 20 μ M RU	(N = 4 / 67 nuclei)
		▪ + 200 μ M RU	(N = 4 / 82 nuclei)

Figure 33: Narf knock-down did not affect nuclear size

(A-C) Immunofluorescence analyses of thorax samples. Knock-down situation using 20 μ M (B) and 200 μ M of RU (C) after 15 days of induction. Non-induced flies were used as control (A). Immunostaining was performed with Narf, lamin Dm0 as an indicator for nuclear envelopes and TRITC phalloidin was used as a marker for muscle tissue. In both knock-down situations a higher variance in nuclear size was observed which was not seen in RU treated wild type flies. Representing pictures are shown in B and C. Scale bar: 5 μ m. (D) Quantification of the nuclei area. Wild type flies crossed with the MHC enhancer and treated with 200 μ M of RU showed an increase in nuclear size verifying that RU alone has an effect on nuclear size compared to non-induced situations (Ctrl^{RU} vs. Ctrl^{RU} p=3.19*10⁻²¹, compare Figure 29). Narf knock-down in muscle cells induced by 20 μ M or 200 μ M of RU had no significant effect on nuclear size (Ctrl⁺²⁰⁰ vs. Narf RNAi⁺²⁰: p = 0.2393, Ctrl⁺²⁰⁰ vs. Narf RNAi⁺²⁰⁰: p = 0.0802). Quantification was done manually using ImageJ and statistical significance was calculated using unpaired *t*-test.

4.4.15 Muscle specific knock-down of Narf during adulthood affected lifespan

Since changes in nuclear size were detected after Narf RNAi expression in muscle cells, lifespan analyses were performed to verify if this phenotype might affect viability during adulthood. Indeed a muscle specific knock down of Narf significantly decreased survival rate of ~ 24%. Induced flies showed a 50% mortality rate at day 44 compared to control flies which had a 50% mortality at day 58. That this effect is independent of RU induction was shown before using a ten times higher RU concentration (Figure 31). Next, western blot analyses were performed to verify that the expression of a Narf specific hairpin structure mediates a decrease in Narf protein level (Figure 34 B). Thorax samples of induced and non-induced flies were tested at different time points during adulthood. However, a reduction was not observed as a Narf signal was only hardly detectable. An explanation can be given by a very weak thoracal expression which is consistent to tissue expression profile data available at <http://flybase.org/reports/FBgn0262115>. Furthermore, it is described that Narf is moderately expressed in imaginal discs. Due to this it was tested if a wing disc specific Narf knockdown controlled by the MS1096 driver is inducing morphology effects in adult wings (Supplement Figure 5). Down regulation of Narf in the wing blade caused wing phenotypes. However, a wing specific overexpression of Narf had no effects, suggesting the functionality of the hairpin mediated knock down. RNA sequencing analysis finally revealed an exon based down regulation of Narf and confirmed the previous data (Supplement Table: 5).

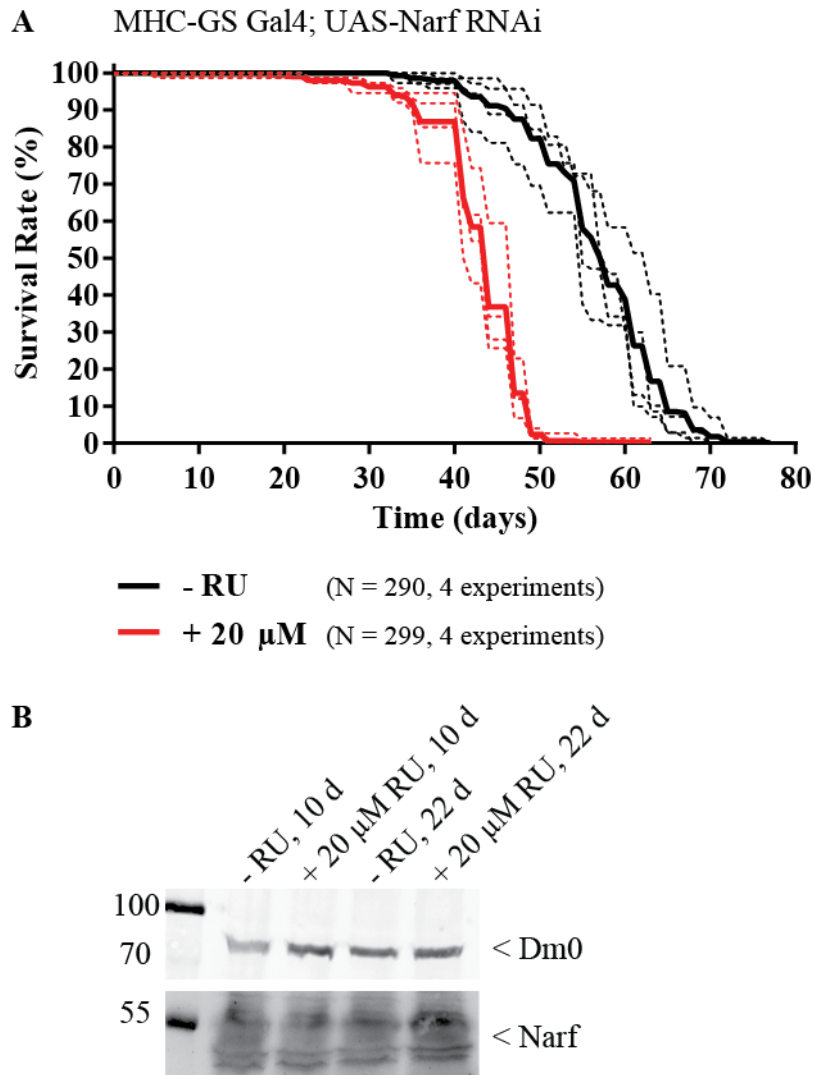


Figure 34: Muscle specific knockdown of Narf decreased lifespan

(A) Lifespan analyses of Narf-RNAi expressing flies treated with 20 μ M of RU (red) compared to non-induced control flies (black). Survival rate analyses were performed in four replicates (dashed lines) each with \sim 75 males. The mean value was taken (solid lines) and used for statistical analyses. A muscle specific down regulation of Narf significantly decreased lifespan (log rank test: Narf RNAi^{-RU} vs. Narf RNAi⁺²⁰ $p < 1 * 10^{-10}$). (B) Western blot analyses of thorax samples at different time points after induction with 20 μ M of RU. Non-induced flies were used as control. The lysate of 2.5 thoraces was loaded and an antibody staining was performed against Narf and lamin Dm0 as loading control. A decrease in protein level after Narf RNAi expression was not observed since Narf is only weakly expressed within the thorax.

4.4.16 Narf is essential during adult stage

It had been observed that a ubiquitous Narf knockdown controlled by α -tubulin Gal4 resulted in a 100% lethality before flies reached adulthood. Western blot analyses of larvae extract revealed an efficient decrease in protein level (Supplement Figure 6). To study the effect of a ubiquitous Narf knockdown in adult flies and to circumvent the problem of lethality lifespan analyses were performed using the inducible actin GeneSwitch Gal4 driver line. Narf is essential during adulthood as induced flies showed a decrease in survival rate already in week one. An interesting observation was that a subpopulation of flies of approximately 5% was able to survive and showed a longer lifespan compared to control flies. In order to investigate the reason western blot analyses were performed using fly extract at different time points after induction. An astonishing observation was that contrary to the assumption an increase in protein level was observed after 11 days and became more dominant over time. As 90% of the flies are still alive at this time point it seems that Narf was actively up regulated in the majority of induced flies, suggesting a specific function. An up-regulation of Narf might be associated with an organismal stress response as induced flies show a high lethality rate.

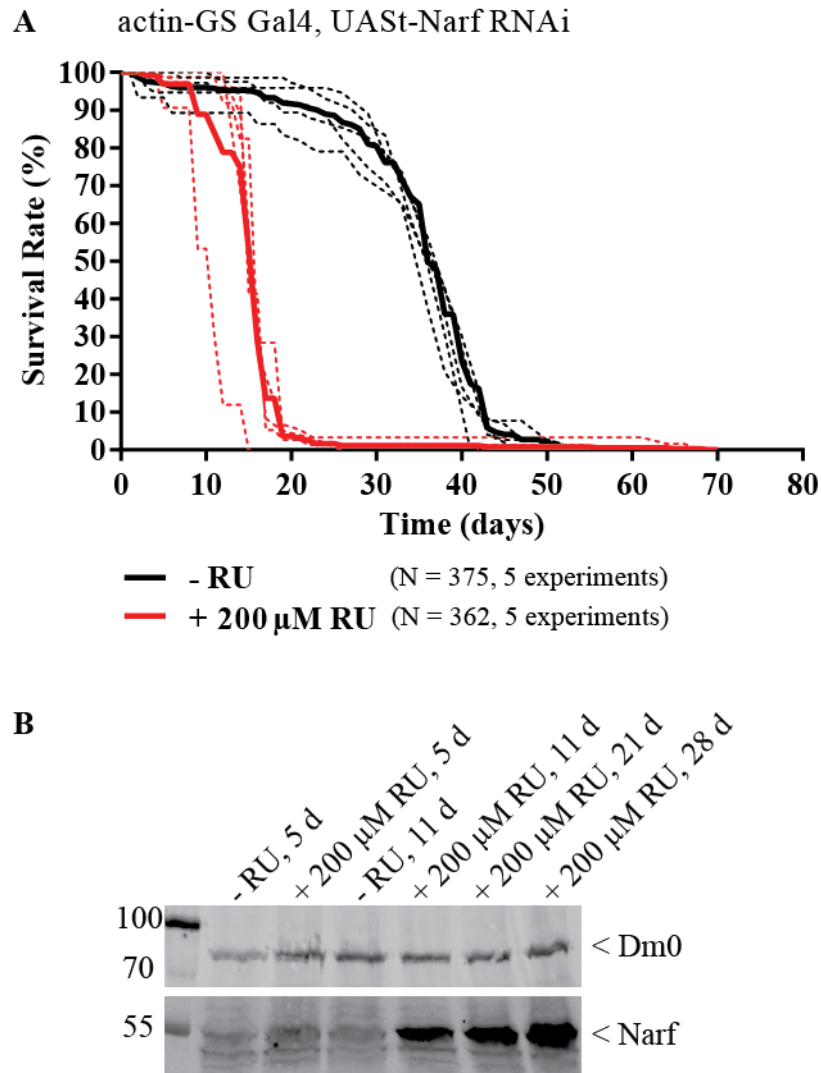


Figure 35: Ubiquitous down regulation of Narf during adulthood severely affected survival rate

(A) Lifespan analyses of Narf-RNAi expressing flies treated with 200 μ M of RU (red) compared to non-induced control flies (black). RNAi expression was controlled by actin GS Gal4 a ubiquitous driver line. Survival rate analyses were performed in five replicates (dashed lines) each with \sim 75 males. The mean value was taken (solid lines) and used for statistical analyses. A ubiquitous down regulation of Narf severely decreased lifespan (log rank test: Narf RNAi^{RU} vs. Narf RNAi⁺²⁰⁰ $p < 1 * 10^{-10}$). (B) Western blot analyses of fly samples at different time points after induction with 200 μ M of RU. Non-induced flies were used as control. The lysate of 2.5 males was loaded and an antibody staining was performed against Narf and lamin Dm0 as loading control. Contrary to the assumption an increase in protein level was observed after eleven days and became more dominant over time.

4.4.17 Gene expression is changed in Narf overexpressing or down regulating situations

The change in Narf protein expression is affecting *Drosophila* on organismal level. To gain more insights about cellular changes upon muscle specific overexpression or down regulation of Narf and to get an idea of its role in biological mechanisms the transcriptom of coding genes from thorax samples was analyzed. RNA was extracted from ten thoraces in four biological replicates for each genotype (OE Narf WT, OE Narf H/R, Narf-RNAi). Narf down regulating flies, mediated by RNAi, were treated with 20 μ M of RU, whereas an overexpression was induced by 200 μ M of RU. Induction was performed for 10 days. Subsequent RNA sequencing analyses were performed at the Microarray and Deep-Sequencing Facility in Göttingen. It was shown before that RU induction itself had effects on nuclear size (Figure 29), suggesting that it might also influence gene expression level. Previous RNA sequencing experiments of the Großhans laboratory performed by R. Petrovsky confirmed that the gene expression profile is altered between thorax samples of induced and non-induced MHC-GS Gal4 flies. In order to enable the identification of Narf specific candidates independent of RU treatment, induced MHC-GS Gal4 thoraces were used as control. At that time the experiment was performed in triplets and induction was done with 200 μ M of RU for 5 days.

After analysis of the gene expression profiles, candidate lists for Narf overexpressing situations were aligned against the candidate list of the RU treated control situation. This led to an identification of 177 candidates for the overexpressed Narf wild type allele and 266 candidates for the mutant Narf H/R allele (Figure 36 A). A comparison of these candidates showed that 139 can be found in both lists. The identification of the top 50 candidates, dependent on the 25 highest and lowest log₂fold changes, revealed a high amount of similarity as 30 candidates were found in both lists (Supplement Table 3, 4). This indicates that the Narf H/R allele behaves almost like the wild type Narf. Genotype specific genes are referred as group “0, red”. The identification of Narf (CG17683) for being the highest up regulated candidate showed that induction as well as RNA sequencing analysis worked. An interesting observation is that especially genes involved in cellular detoxification (e.g. Cyp4p3, GstE14, Ugt36Bb), DNA/chromosome metabolism (e.g. phr, GATAe) and proteolysis (e.g. CG33159, CG18636) are detected in both Narf overexpressing situations. A down regulation of Narf led to the identification of 465 candidates, by which 97 were also found upon Narf(H/R) overexpression. Within the top 50 candidates 14 can be also found in

the top 50 lists of the Narf overexpressing situations (Figure 36 B). The remaining 36 candidates can be divided in to two subgroups. The first subgroup contains 16 candidates which can be found within the total lists for Narf overexpression. The second subgroup contains 20 candidates, which are specific for a down regulation of Narf (Supplement Table: 5, Group 0). The most interesting candidates are Cyp12d1-d and mthl8. Cyp12d1-d is also involved in cellular detoxification and mthl8 (methuselah-like 8) is annotated to be involved in aging in *Drosophila* due to its homology with mth (methuselah) which caused a lifespan extension upon mutation (Lin et al., 1998). The similarity of gene expression response by overexpression and depletion of Narf suggests that both situations represent a loss-of-function situation.

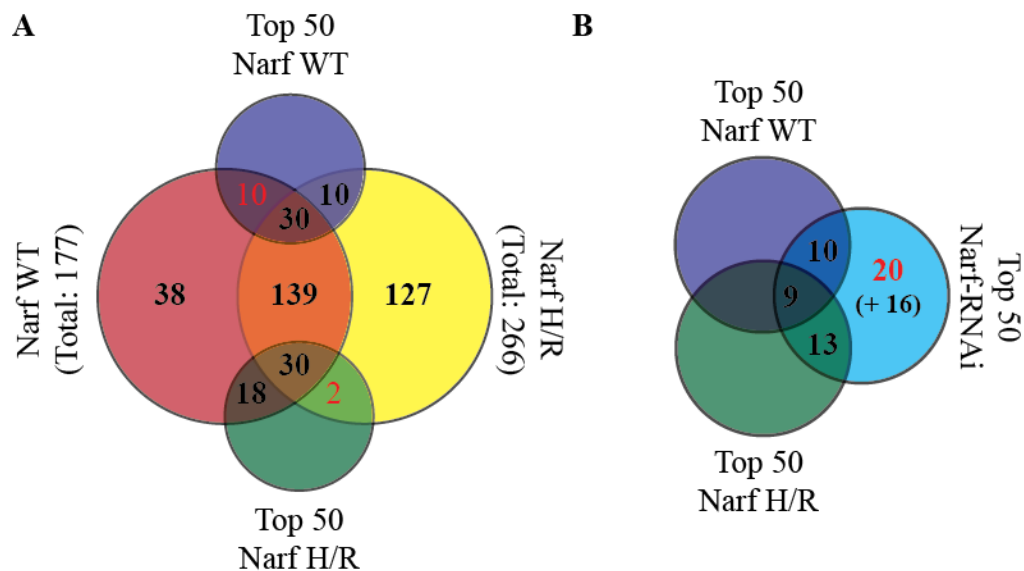


Figure 36: Gene expression is changed in altered Narf expressing situations

(A) Venn-diagram of gene expression changes comparing the overexpression of the wild type and the mutant Narf allele. The total lists of identified candidates are set in relation to the top 50 candidates. Red numbered candidates are gene type specific. (B) Venn-diagram of top 50 candidates for Narf down regulation in relation to Narf overexpression. Narf-RNAi specific genes are marked in red. Candidates which can be found within Narf OE total list but are not included within top 50 lists are set in clamps.

4.4.18 Klp68D is a Narf interaction partner

In order to identify new protein interaction partner of Narf, a yeast- two hybrid assay was performed using the screening service from hybrigenics. The basic principle behind that assay is the restoration of an active transcription factor by direct interaction of two proteins fused with a DNA binding domain (DBD) or a Gal4 activation domain (AD). Protein interaction brings DBD and AD in a close proximity and allows transcriptional activation of a reporter gene. Reporter gene expression enables yeast cell growth on a selective medium and positive clones are later sequenced to identify new interaction partners (Brent et al., 1985, Fields et. al., 1989). In order to identify novel interaction partners a Lexa DNA binding domain was N-terminally fused to the full length Narf protein, based on the cDNA clone RE37350 (BDGP), and screened against a *Drosophila* embryo library. In total 116 million interactions were tested and 43 positive clones were identified. Final sequencing analyses lead to the identification of seven genes (BtbVII, CG5807, Klp68D, prd, Rpl22, RpS18 and troll). All steps were performed by the company. A high confidence in interaction was only given for Klp68D. All the other genes were categorized as technical artefacts or in case of Rpl22 described for being most likely an unspecific interaction. Klp68D belongs to the family of kinesin-like motor proteins, is primary expressed in the nervous system and described to be involved in the axonal transport of the choline acetyltransferase (Pesavento et al., 1994, Ray et al., 1999)

4.5 Is Narf involved in aging in *C. elegans*?

Caenorhabditis elegans is an excellent and established model system in aging research. The *C. elegans* genome contains a single lamin gene (*lmn-1*). It is known that Ce-lamin is critical for a normal lifecycle and is involved in aging as the reduction of the lamin levels during postembryonic development shortens lifespan. Furthermore, age-dependent changes in nuclear morphology such as an increased abnormal shape, extensive nuclear stretching and fragmentation have been described (Haithcock et al., 2005). It was demonstrated that the treatment with farnesyl transferase inhibitors (FTI) can reverse these age dependent changes in nuclear morphology, showing a dependency on farnesylation. However, lifespan was not affected (Bar et al., 2009, Bar and Gruenbaum 2010).

The Narf homologue in *C. elegans* is Oxy-4. Oxy-4 was identified in a screen for mutants with an increased sensitivity to oxidative stress. Importantly this study also reported that *oxy-4* mutants had a shortened lifespan of about 20% (Fujii et al., 2009). Interestingly, the identified mutant strain has a single point mutation at the homologues position of the human patient mutation. However, the molecular mechanism remains unclear and a connection to the nuclear lamina and lamin farnesylation was not made. The aim of this study was to analyze the functional relationship between Oxy-4 and Ce-lamin and to investigate how they contribute to aging.

4.5.1 Oxygen sensitivity of *oxy-4* mutants

For my analyses, the *oxy-4* (qa5001) worms strain was used, which was identified by Fuji et al., in 2009. I therefore rechecked the strain and tried to reproduce the previously described results. One of the hallmarks for this strain is an increased sensitivity to oxidative stress. To test this phenotype, an oxygen sensitivity assay was performed by culturing eggs in the presence of 75% of oxygen. My analysis confirmed the oxygen-sensitivity of the *oxy-4* mutant worms, as they show a delay in development compared to *oxy-4* mutant worms grown at normoxic conditions (21% of oxygen) (Figure 37 A). However, I did not observe the described arrest in L1–L2 stage with 90% of oxygen (Fujii et al., 2009). Furthermore, *oxy-4* mutant worms were developmentally delayed even when grown at normal conditions compared to wild type (Figure 38 A). Sequencing of the *oxy-4* genomic locus confirmed the point mutation in the *oxy-4* gene that led to a change from aspartic acid (D) to asparagine (N) at codon 373 in the worm strain (Figure 37 B).

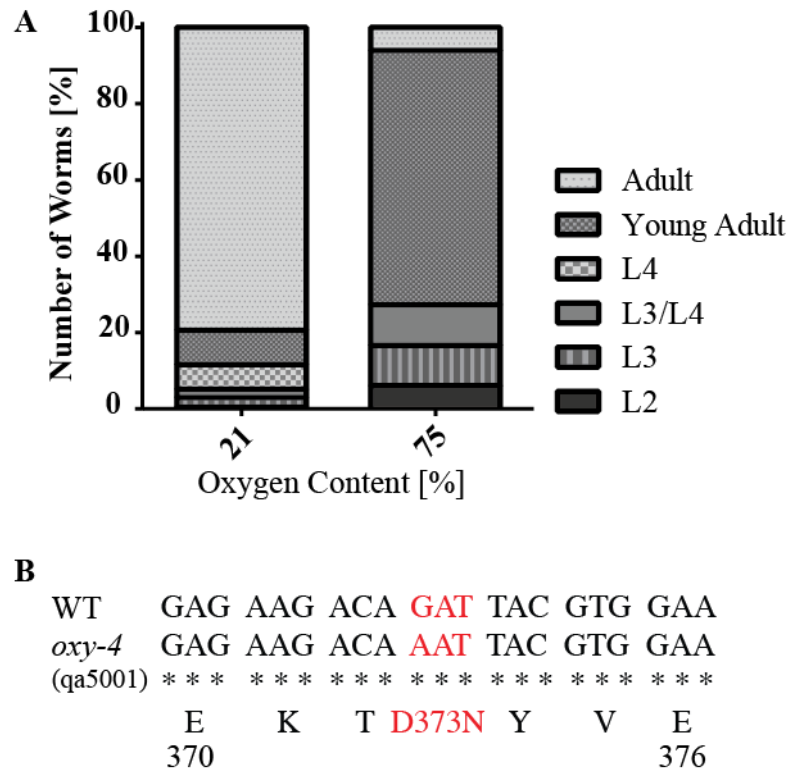


Figure 37: *oxy-4* mutants were sensitive to oxidative stress

(A) Nematode embryos were incubated in the presence of 21% and 7% percent of oxygen and the developmental stages were determined after 5 days. Mutant worms incubated with 75% of oxygen showed a delay in development. Statistical analyses were performed with N = 233 for *oxy-4* mutant worms under normoxic and N = 66 under hyperoxic conditions. Developmental larval stages are referred as L2 to L4. (B) Sequencing results revealed that a point mutation leads to an amino acid exchange from aspartic acid (D) to asparagine (N).

4.5.2 *oxy-4* mutants showed a developmental delay under normal conditions

To further analyze the observed developmental delay under normal conditions, a time course analysis of *oxy-4* mutant worms, wild type worms and *oxy-4* RNAi worms was performed. For this purpose, worms were synchronized at L1 stage and then grown at 20 °C for three days (Figure 38 A). The length of the worms was measured manually in ImageJ and data analyses was performed with GraphPad Prism6 (Figure 38 B). After 50 hours, wild type and *oxy-4* RNAi worms reached adulthood and their final length, whereas *oxy-4* mutant worms still grew after 71 hours. These results are consistent with the previous report (Fujii *et. al.*, 2009), in which the authors described a delay in development of *oxy-4* mutant worms

of 1–1.5 days compared to wild type at 20 °C. The difference in phenotype between RNAi treated and mutant worms can be explained by an inefficient down-regulation of Oxy-4 via RNAi. Quantitative real-time PCR-analyses of *oxy-4* RNAi treated wild-type worms revealed a remaining gene expression of 45% compared to wild-type worms treated with an empty vector control (EV-RNAi) (Figure 44 B).

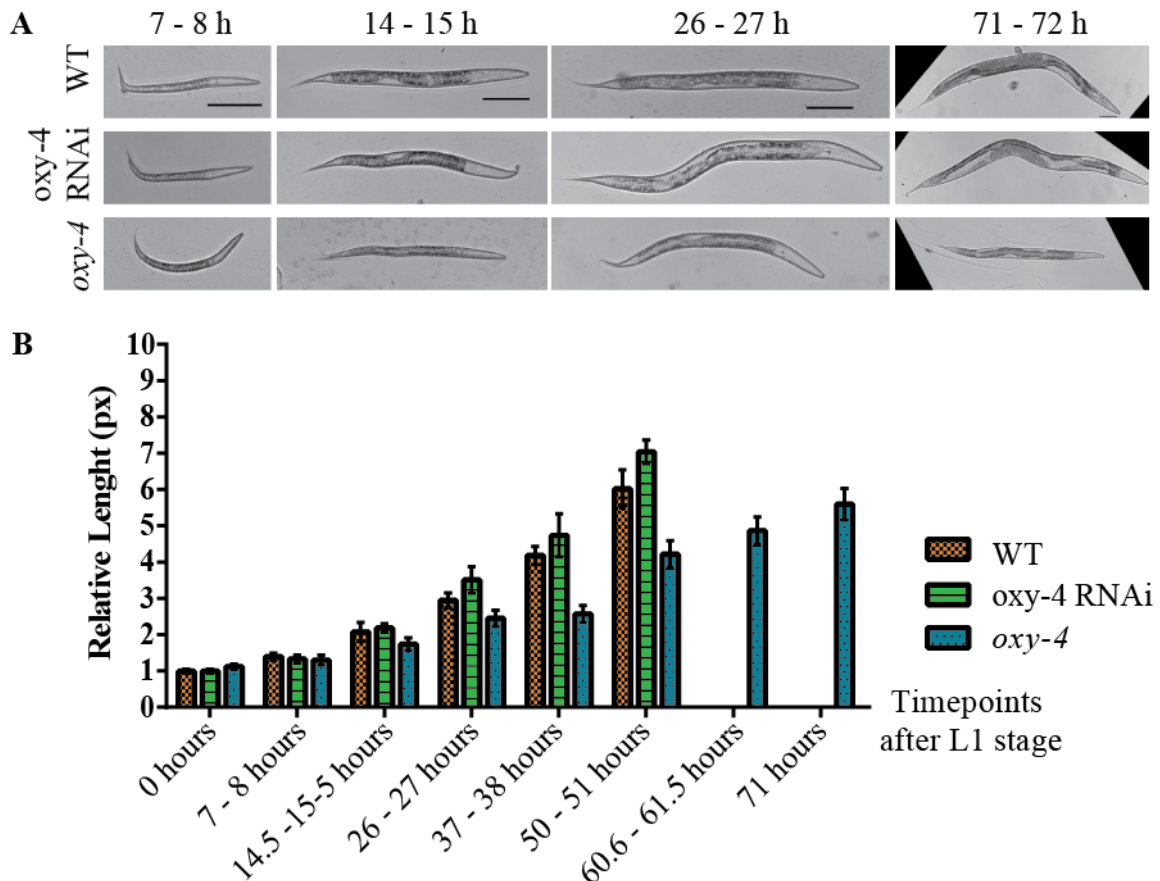


Figure 38: Developmental delay of *oxy-4* mutants under normoxic conditions

Time course analysis of wild type, *oxy-4* RNAi treated wild type and *oxy-4* mutant worms. All genotypes were synchronized to L1 stage and body lengths were analyzed at distinct time-points. Representative pictures are shown in A. Quantification of worm lengths at different time points is presented in B. *oxy-4* RNAi treated worms showed a similar growth as wild type worms, whereas the development of *oxy-4* mutant worms is delayed.

4.5.3 Unchanged muscle structure in *oxy-4* mutants

In *C. elegans* two main types of muscles can be found: the striated and the non-striated muscles. Previous studies have demonstrated that a specific lamin mutation in *C.*

elegans, which reflects the HGPS situation, leads to disorganization of sarcomeric actin filaments in striated body-wall muscle already at L4 stage (Bank et al., 2012). Furthermore, the human patient with the dominant *de novo* mutation in Narf showed an effect on muscle structure. I next examined whether *oxy-4* mutant worms are also affected in their muscle structure. Worms at different time points during development were collected and the striated muscle structure of the body wall was analyzed by phalloidin staining. Compared to wild type worms, no morphological changes in muscle structure were visible in *oxy-4* mutant worms even after 5 days of adulthood (Figure 39).

In addition, I checked the effect on the non-striated muscles in *C. elegans*. For this purpose, the pharynx was analyzed. As the food intake correlates with growth in *C. elegans*, and a developmental delay in *oxy-4* mutant worms was observed, I wondered if a connection to a malfunctioning pharynx can be found. To check the muscle function a pumping experiment was performed, counting the grinding movement during pumping. Indeed, a statistical significant difference in pumping behavior between wild type and *oxy-4* mutant worms was detected (Figure 40). Next I examined if this effect was due to morphological reasons. Therefore, the pharynx structure was analyzed by phalloidin staining. However, no aberrations in pharynx morphology were detected (Figure 41).

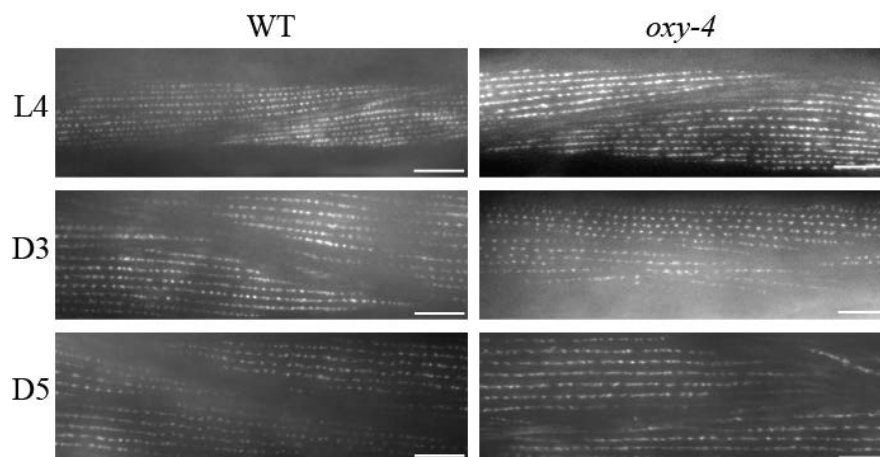


Figure 39: Striated muscle structure was normal in *oxy-4* mutant worms

Wild type and *oxy-4* mutant worms were stained against phalloidin at three distinct time points during development (L4-larval stage 4, D3- three days of adulthood, D5- five days of adulthood). Even after five days of adulthood no effects in body wall muscle structure were observed in *oxy-4* mutant worms compared to wild type. Scale bar: 10 μm

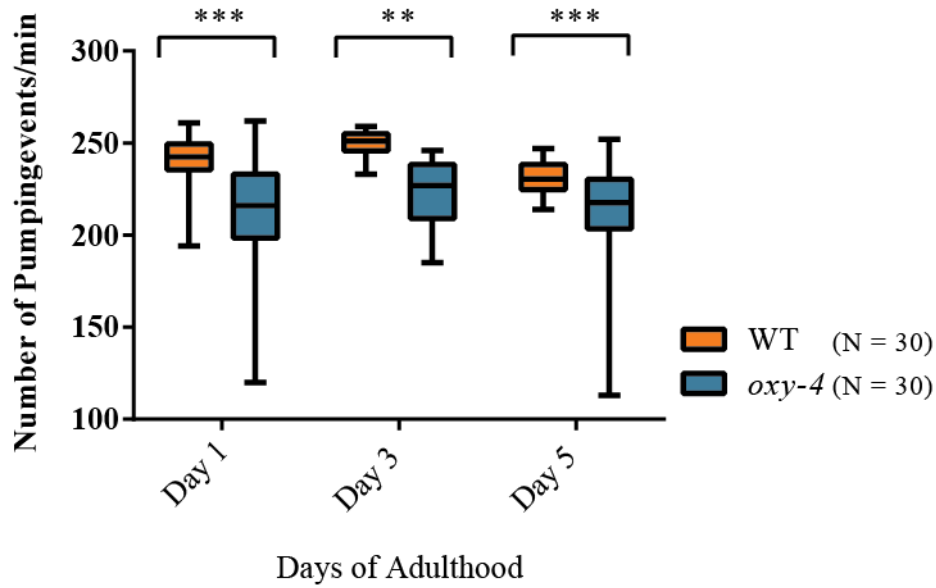


Figure 40: *oxy-4* mutants showed a decline in pharyngeal pumping

Statistical analyses of the pumping behavior of wild type and *oxy-4* mutant worms at different time points after reaching adulthood. The error bars show min to max values. The difference in pharyngeal movement was statistically significant (** $p \leq 0,004$; *** $p \leq 0,001$, unpaired *t*-test). Illustration was done by GraphPad Prism 6.

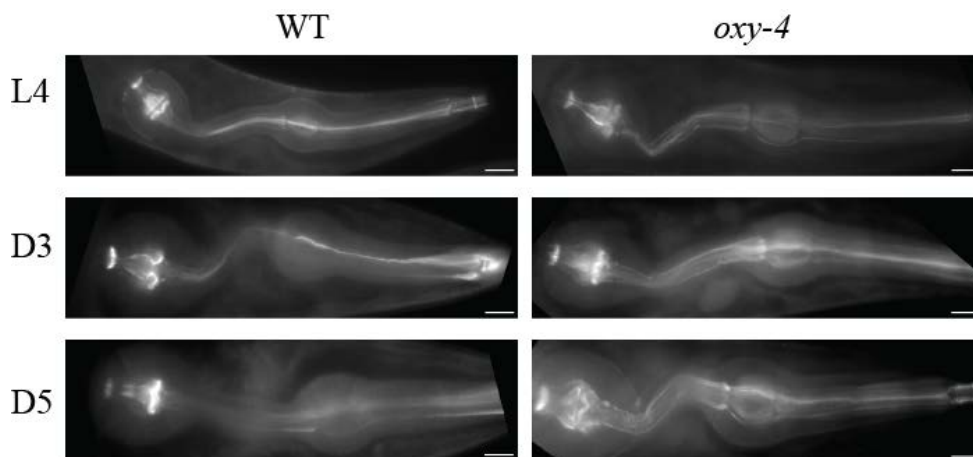


Figure 41: *oxy-4* mutant worms were normal in non-striated muscle structure

Morphological pharynx analysis of wild type compared to *oxy-4* mutants was carried out by phalloidin staining at different time points during development (L4-larval stage 4, D3- day three of adulthood, D5- day five of adulthood). Even after five days of adulthood no effects in non-striated muscle structure can be observed in *oxy-4* mutant worms. Scale bar: 10 μm

4.5.4 Nuclei morphology and Ce-lamin farnesylation were not affected in *oxy-4* mutants

Ce-lamin and Oxy-4 are involved in aging, as a shorter lifespan was observed in their mutant situations (Fujii *et. al.*, 2009, Haithcock *et. al.*, 2005). A link to the nuclear lamina and the Ce-lamin farnesylation state was still unrevealed. To investigate the effect to the nuclear lamina, a Ce-lamin antibody staining of L4 larvae of the wild type strain and *oxy-4* mutants was performed. I examined the appearance of muscle and hypodermis nuclei. In *oxy-4* mutants a small number of nuclei showed an aberrant phenotype (Figure 42 B, E). However, this effect was also observed in the control situation, suggesting that a distinct amount of nuclei naturally showed this lobulations and infoldings. Statistical analyses confirmed that the observed effect on nuclei morphology is not significant (n.s.) (Figure 42 C, F). As it is supposed that the effect on the nuclear envelope disruption becomes more severe with age, it is possible that an effect can be detected in older worms.

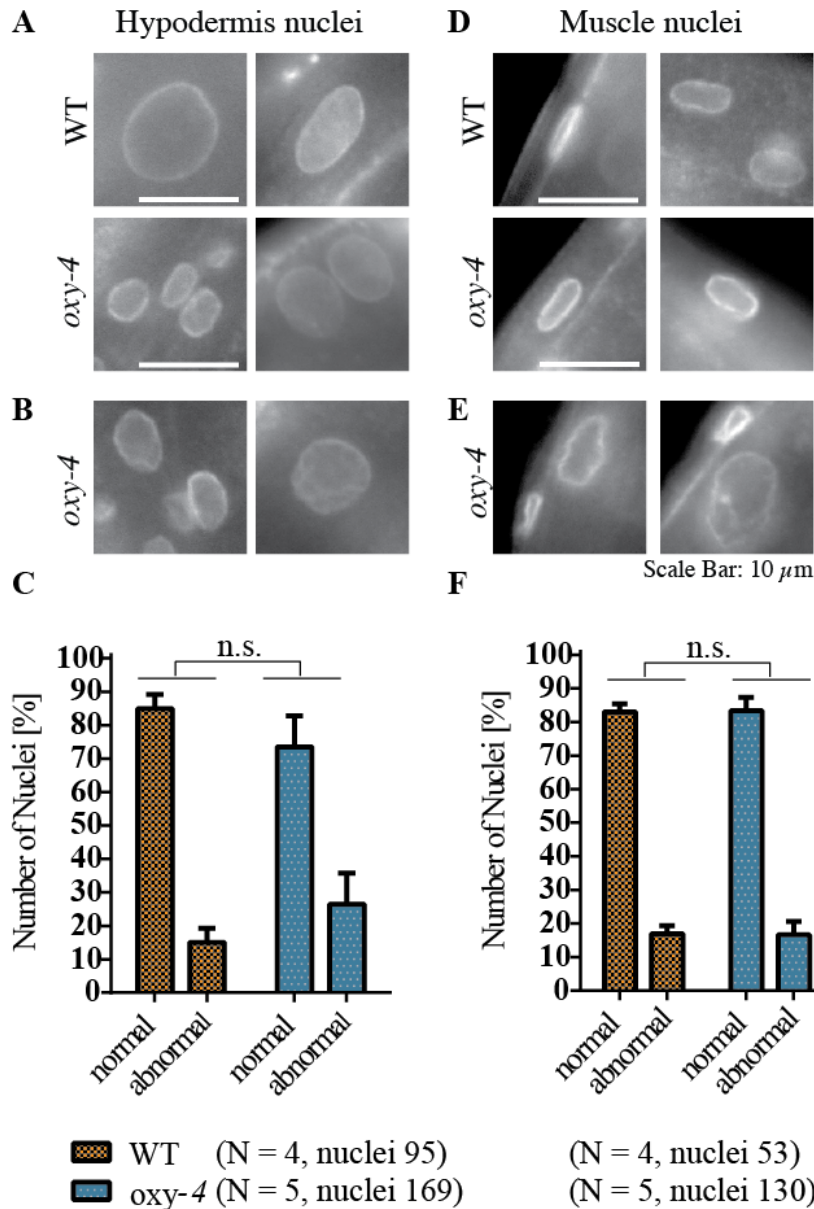


Figure 42: Nuclear morphology was not affected in *oxy-4* mutant worms at larval stage

Nuclei morphology in wild-type and *oxy-4* mutant worms was analyzed by Ce-lamin immunostaining. The nuclei appearance of two different tissues was studied: (A-C) hypodermis nuclei and (D-F) muscle nuclei. Nuclei which were referred as abnormally shaped are shown in B and E. Statistical analyses showed that these deformations occurred in the same ratio also in wild-type worms and the number of misshaped nuclei is not significantly (n.s) higher in *oxy-4* mutant worms. Statistical analyses were performed with at least four different worms of each genotype. Nuclei were counted, the appearance was studied and grouped to normal or abnormal shaped. As this approach is subjective, this analysis was performed thrice. The number of nuclei shown in C and F demonstrates the mean number of analyzed nuclei.

To investigate the effect on the farnesylation state of Ce-lamin in *oxy-4* mutants, a band shift assay was performed. Therefore, protein extracts of L4 larvae of wild type and *oxy-4* mutant worms were separated via a SDS-PAGE and analyzed by Western-Blot experiment for a difference in Ce-lamin size (Figure 43). As positive control, L4 staged wild type worms were treated with *fdpsi-1* RNAi until 5 days of adulthood to downregulate polyprenyl synthetase, which directly inhibits the production of farnesyl-PP (Bar and Gruenbaum in 2010). However, it was not possible to detect a band shift between wild type and the positive control (wild type + *fdpsi* RNAi). Thus, it remains an open question, if the farnesylation of Ce-lamin is affected in *oxy-4* mutants. The fact that the Ce-lamin immunostaining of wild type worms and *oxy-4* mutants looked quite similar (Figure 42 A), suggests an unaffected farnesylation state of Ce-lamin.

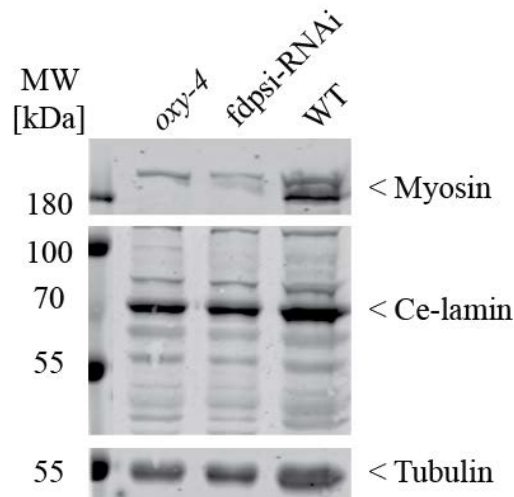


Figure 43: A lack of farnesylation in Ce-lamin did not result in a protein shift.

Western blot analysis of *oxy-4* mutants, wild type worms treated with *fdpsi*-RNAi and non-treated control worms. Ce-lamin was detected at ~ 70 kDa. Downregulation of polyprenyl synthetase was used as positive control but did not lead to a change in Ce-lamin protein size. According to this, no effects on Ce-lamin in an *oxy-4* mutant background were observed. Myosin and tubulin staining were used as loading controls.

4.5.5 Do Oxy-4 and Ce-lamin act via the same pathway?

The advantage of *C. elegans* in aging research is its short lifespan of three weeks. Thus, aging experiments can be conducted within weeks. In addition, the genetic background which is a big and cumbersome problem in *Drosophila* plays no role, as the animals are hermaphrodites. Due to this, I conducted lifespan assays to reveal the functional relationship between Ce-lamin and Oxy-4. Therefore, I first performed lifespan experiments by using *oxy-4* RNAi. However, no difference to control worms was detected (Figure 44 A). To

examine if this effect was due to an insufficient down-regulation of Oxy-4, a qPCR-analyses were performed (Figure 44 B). The result confirmed that RNAi treatment was insufficient and a gene expression of 45% remained. Gene expression of *lmn-1* instead was efficiently reduced, which was comparable to previous published data (Zuela et al., 2016).

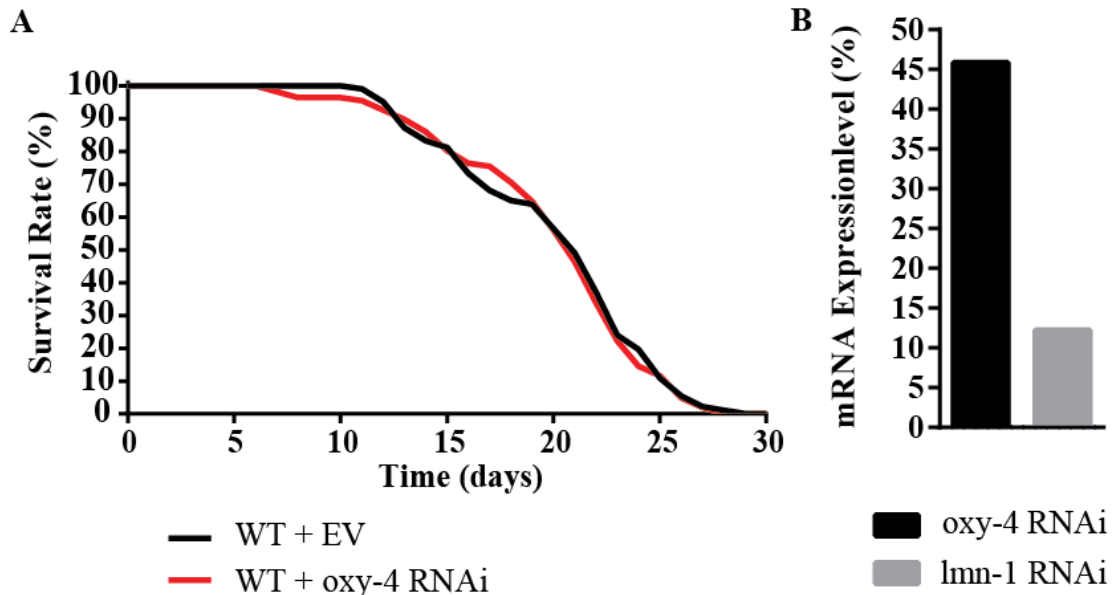
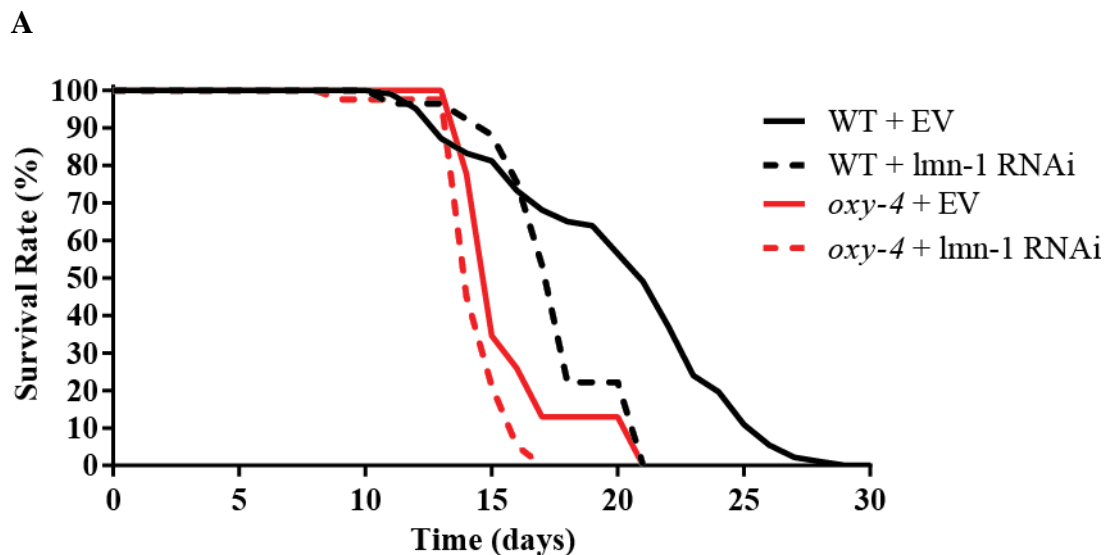


Figure 44: Inefficient knockdown of oxy-4

(A) Lifespan analyses of wild type worms treated with *oxy-4* RNAi or an empty vector control RNAi L4440 (EV). For each condition 100 L4 larvae were separated with ongoing RNAi treatment and the survival rate was determined. The assay was performed at 20°C. Statistical analysis was performed with OASIS, log-rank test = 0.7169. (B) qPCR-analyses of wild type embryos grown on either *oxy-4* or *lmn-1* RNAi plates at 20°C. L4 staged worms were used for mRNA extraction with subsequent cDNA preparation. Wild type worms treated with an empty vector (L4440) were used as control to determine the reduction in gene expression. Knockdown of Ce-lamin was used as positive control, as this RNAi construct was verified (Zuela et al., 2016). Lifespan and qPCR-analysis of *oxy-4* RNAi revealed that the down-regulation of oxy-4 was not sufficient and had no effect on organismal aging.

Finally, I tested if Oxy-4 and Ce-lamin contribute to aging via the same pathway. Therefore, wild type and *oxy-4* mutant worms were treated with either an empty vector (EV) or *lmn-1* RNAi. As it is already described that down-regulation of Ce-lamin in wild type background leads to a decrease in lifespan (Figure 45 A) (Haithcock et al., 2005). The same effect was observed for *oxy-4* mutant worms, consistent to already published data (Fujii et al., 2009). To study a functional relationship between Oxy-4 and Ce-lamin, lifespan analysis of *oxy-4* mutant worms with *lmn-1* RNAi treatment were carried out. There are two potential

mechanisms. 1) If Oxy-4 and Ce-lamin contribute independently to aging, an additive effect is expected. 2) If Oxy-4 acts via Ce-lamin, single mutants will behave similar as the double mutant. In Figure 45 B the results of the log-rank test analyses are depicted. Based on this, Oxy-4 and Ce-lamin would act independently, as lifespan curves of *oxy-4* mutants with and without *lmn-1* RNAi were significantly different ($p = 0.0126$). It needs to be mentioned at this point that the number of worms for *oxy-4* mutant situations was limited and this experiment was, due to experimental reasons, performed only once. Summarizing, it remains an open question if Oxy-4 and Ce-lamin act within the same pathway. To make a conclusion it will be necessary to repeat this approach.



B

vs	WT + <i>lmn-1</i> RNAi	<i>oxy-4</i> + EV RNAi	<i>oxy-4</i> + <i>lmn-1</i> RNAi
WT + EV RNAi	$p = 0.0064$	$p = 0.0082$	$p = 1 * 10^{-10}$
WT + <i>lmn-1</i> RNAi		$p = 0.0101$	$p = 1 * 10^{-10}$
<i>oxy-4</i> + EV RNAi			$p = 0.0126$

Figure 45: Lifespan analyses of *oxy-4* mutants with additional *lmn-1* RNAi treatment

(A) Lifespan analyses of wild type and *oxy-4* mutant worms. Embryos were grown on either empty vector RNAi L4440 (EV) plates or treated with *lmn-1* RNAi. 100 L4 larvae for each wild type condition and 50 L4 larvae for *oxy-4* mutant situations were separated with ongoing RNAi treatment and the survival rate was determined. Lifespan analyses were performed at 20 °C. (B) Statistical analyses were performed by OASIS (log-rank test). Illustration was accomplished by GraphPad Prism6.

5 Discussion

5.1 Kugelkern and its role in aging

5.1.1 The *kuk* deficient fly line $\Delta 15$ might still contain recessive mutation(s)

Kugelkern is connected to accelerated aging-related phenotypes in *Drosophila* as an overexpression caused nuclear morphological changes, a reduction in heterochromatin and shortened the mean lifespan of adult flies (Brandt et al., 2008). In order to investigate a loss-of-function situation in a more detail an established fly strain, homozygous for a *kugelkern* deletion ($\Delta 15$), was used in this study and further analyzed for its gene expression profile. RNA sequencing analyses revealed alterations in gene expression especially for genes involved in stress response (Figure 5, Supplement Table: 1). In order to analyze if this might be connected to accelerated aging phenotypes in *kuk* depleted flies, lifespan analyses were performed. $\Delta 15$ and wild type control flies had the same 50% mortality rate and showed only on a low significant level differences in lifespan (Figure 6 A). Since no connection between alterations in gene expression and mean lifespan was found the question arose if lifespan analyses have been performed with representative males even if the fly strain was easy to keep, which is indicative for a good viability and fertility. Furthermore, it has to be mentioned that the chromosome harboring the $\Delta 15$ deletion was cleaned as secondary lethality causing mutations had to be removed in order to establish a homozygous $\Delta 15$ fly strain (M. Clever). However, it might be that recessive mutations retained after chromosomal cleaning. In order to analyze this aspect survival rate analyses during development were performed. Indeed, homozygous $\Delta 15$ animals showed a decrease of approximately 70% in embryonic survival compared to wild type animals. Survival rate analyses of animals which were only homozygous for a *kuk* depletion ($\Delta 15/Def$) showed a wild type like viability, suggesting that the observed lethality is independent of *kuk* (Figure 6 B). As RNA sequencing analyses were done with 6-8 hours staged embryos it might be reasonable that the embryos, which are about to die, are causative for the observed alterations in gene expression. This would be consistent to the identified candidate genes which are especially involved in stress response. Thus, it remains unclear if *kuk* depletion by itself affects gene expression.

5.1.2 Proteolytic cleavage might be mediated by PEST-sequences

Besides the lamins, Kugelkern is the only known nuclear protein which also contains a CaaX-motif for farnesylation. The hypothesis is that the morphological phenotypes in the wing and the eye observed upon tissue specific overexpression are mediated by farnesylation dependent protein complexes. In order to identify these farnesylation dependent interaction partners of Kugelkern I planned to perform Co-immunoprecipitation experiments using a modified GFP-nanobody followed by mass spectrometric analyses. Accordingly, genomic and GFP-tagged alleles of the wild type Kuk and a non-farnesylable mutant (KukC567S) were established and expressed in a *kuk* depleted background. However, subsequent rescue experiments showed that the GFP-tagged wild type Kuk was not able to rescue the nuclear elongation phenotype in *kuk* depleted embryos (Figure 7). Following analyses confirmed that the expressed GFP-Kuk is only partially functional as proteolytic cleavage is interrupting protein function (Figure 8 A). As similar proteolytic cleavage products were detected in a UAS/Gal4 expressed situation which is rescuing the nuclear elongation phenotype, it is reasonable that this might be a dose dependent effect (Figure 9). Interestingly, proteolytic cleavage occurred especially at the C-terminal half of Kuk whereas GFP-fusion was directed to the N-terminal site (Figure 8 B). All GFP-Kuk transgenes were affected and Kuk-fragments already occurred within the total extract directly after embryo lysis, which suggest that proteolytic cleavage was a general problem and independent of the transgenes, the used Co-IP conditions or the genetic background. Furthermore, it was shown in immunofluorescence analyses that GFP-Kuk partially miss-localized to the cytoplasm, suggesting a loss or disturbance of required localization elements like the nuclear localization signal (NLS).

Furthermore, it was observed that the proteolytic cleavage of GFP-Kuk seemed to affect preferentially two sites as two major cleavage products were detected with a molecular mass of approximately 70 and 100 kDa (Figure 8 A). *In silico* analyses revealed that Kugelkern contains two PEST motifs between the amino acid positions 268 – 299 and 487 – 524 (Supplement Figure 8), which were identified by the software epestfind (emboss.bioinformatics.nl/cgi-bin/emboss/epestfind). PEST motifs are proline (P), glutamic acid (E), serine (S) and threonine (T) rich amino acid sequences and have been found in the majority of fast degrading proteins (Rogers et al., 1986). Sequence analyses of nuclear proteins revealed this relationship that proteins with a structural function such as Histones and lamins which are supposed to be stable, do not contain PEST-sequences; whereas

nuclear proteins with regulatory functions at least have one motif (Chevaillier et al., 1993). Consistent to this, no potential PEST motif was found for lamin Dm0 in *Drosophila* (Supplement Figure 9). However, it remains unclear why the N-terminal GFP-fusion of Kuk led to an activation of the cleavage signal. PEST-signals are described for being conditional and induced by different conditions such as light or phosphorylation (Rechsteiner and Rogers, 1996). So it might be also reasonable that the GFP-fusion led to protein fold changes which either made the PEST-motifs directly accessible or activated them indirectly by exposing regulatory amino acids. However, western blot analysis of solubilized endogenous Kuk confirmed that these cleavage products also appear within the native situations as two additional protein bands with a molecular weight of approximately 55 and 75 kDa were detected (Supplement Figure 2). Nevertheless, the majority of the Kuk protein stayed stable even after four hours of solubilization. By this, the requirement for an alternative Co-IP approach by a Kugelkern specific antibody coupled to protein A dynabeads is given. Farnesylation dependent interaction partners will be revealed by a comparison of wild type and non-farnesylable Kuk lysates. Transgenic KukC567S flies were successfully generated in this study and need to be crossed in a cleaned *kuk* deficient situation. However, the disadvantage of this approach is a missing elution step of Kuk-binding proteins from the beads, which will lead to a higher background. This problem will be minimized by a control experiment with the lysate of *kuk* depleted embryos.

5.2 Narf is involved in aging in *Drosophila*

The group of Prof. Wollnik (Institute for Human Genetics, Göttingen) recently identified a dominant *de novo* mutation in Narf in a human patient which shared clinical features to HGPS patients like reduced subcutaneous fat, mild osteoporosis and nuclear morphology defects (personal communication). Phenotypic similarities of the human patients, its initial identification by binding to farnesylated Prelamin A and the exclusive nuclear rim localization in HeLa cells (Barton and Worman, 1999) led to the hypothesis that Narf might represent a new progeria gene related to laminA. How Narf might contribute to aging or if the characterized human mutation represents a gain of function or a loss of function allele are not known yet. A first step to understand the underlying molecular mechanisms was to establish *Drosophila* as model system and to study the effect of Narf. In this study it was shown that the *Drosophila* homologue CG17683 indeed is involved in regulating aging processes. Even if this study just provides a starting point of Narf and its

role in aging one criteria of being a member of “aging genes” was already fulfilled by showing that a loss-of function leads to a decrease in lifespan (Figure 34) whereas a gain-of function is prolonging *Drosophila* lifespan (Figure 24, Figure 25).

5.2.1 Narf might have an essential role in Fe-S protein maturation

Narf is known to possess an essential function for development in *Drosophila*, since four different lethal alleles (NC37, NC38, NC70 and NC109) are already identified (Coulthard et al., 2010). However, the time point of lethality was not further studied yet. Survival rate analyses of the two characterized lethal alleles (NC38 and NC109) showed a lethality during larval stage (Figure 20). Reasoning to this the lethal allele NC38 was proven to contain a premature stop codon (Figure 19) which might lead the nonsense-mediated mRNA decay, showing that a ubiquitous loss-of function results in lethality. Western blot analyses showed that Narf is probably maternally provided and a zygotic expression starts at the switch from embryonic to larval stage (Figure 21) which goes along with the observed larval lethality. Consistently, a tubulin driven down regulation by Narf-RNAi caused a pre-adult lethality phenotype of 100 percent penetrance.

In order to analyze a Narf loss of function effect during adulthood, the GeneSwitch system was used and ubiquitous down regulation of Narf was driven by actin upon induction with mifepristone (RU468). Thereby it was observed that the majority of the flies died within approximately three weeks, suggesting an essential function of Narf also during adulthood (Figure 35).

An explanation for the observed lethality might be given by an essential role of the *Drosophila* homologue in Fe-S protein biogenesis, as it was described for the yeast homologue Nar1 as well as for the mammalian homologue IOP1 (Narf-like) (Balk et al., 2004, Song and Lee, 2008). The maturation of Fe-S proteins is a quite conserved mechanism and can be simplified in four steps in yeast. Initially, a Fe-S cluster is assembled on a mitochondrial scaffold enzyme. Subsequently the cluster is released and transferred to a targeted apo-protein where it is finally integrated. Mitochondrial Fe-S proteins are solely dependent on the iron-sulphur-cluster (ISC) assembly machinery, whereas cytosolic and nuclear Fe-S proteins also requires the cytosolic iron-sulphur protein assembly (CIA) machinery (reviewed in Lill, 2009). Nar1 was described for being one of the CIA proteins and for this reason, Nar1 is essentially required for maturation of cytosolic and nuclear Fe-S proteins. Nar1 depleted yeast cells are lethal, which was explained by the need of Nar1 for

the biogenesis of the cytosolic Fe-S protein Rlip. Depletion of Rlip led to a nuclear export defect of both ribosomal subunits and finally caused translational arrest (Balk et al., 2004, Don et al., 2004, Kispal et al., 2005, Yarunin et al., 2005).

That also the mammalian ortholog IOP1 is involved in maturation of cytosolic Fe-S proteins was shown in HeLa cells and MEFs (mouse embrionic fibroblasts) as knockdown of IOP1 is affecting the activity of different cytosolic Fe-S proteins but has no effect of tested mitochondrial Fe-S proteins or non Fe-S proteins (Song et al., 2009; Song and Lee, 2008, 2011). The described effects were shown to be specific for IOP1 as a knockdown for IOP2/Narf did not affect Fe-S protein maturation (Song and Lee, 2008). An IOP1 depletion in mice was shown to be lethal during early embryogenesis as well as in adults if the knock-out was performed in an inducible way (Song and Lee, 2011). A functional explanation was given by the observation that an IOP1 knockdown in HeLa cells led to a global decrease in protein synthesis which finally caused growth impairment and a decreased cell viability as it was similarly seen in yeast before (Song and Lee, 2008).

Nothing is known about the *Drosophila* homologue and its putative role in Fe-S protein maturation yet. However, the mechanism is quite conserved and it might explain the observed lethality effects during development and adulthood as it was seen in yeast and mice before.

5.2.2 Lifespan analyses as a tool to study aging

Lifespan analyses are a central physiological test to study the effect of a distinct gene referring to aging. However, one of the most challenging task using lifespan analyses is to provide suitable controls. It is known that *Drosophila* lifespan can vary a lot dependent on genetic as well as on environmental conditions such as diet, infection, gender, mating status, temperature, humidity and circadian rhythm (reviewed in He and Jasper, 2014). To provide comparable situations all lifespan analyses were performed using synchronized males which were kept at 25 °C with 70 percent humidity and a day night shift of 12 hours. Furthermore a sample size of ~ 200-300 flies was used, the fly density was limited to ~ 70-80 flies per cage and lifespan analyses were performed in three to four replicates. A critical problem of a different genetic background was partially circumvented by using the GeneSwitch system. There the offspring of the same crossing are analyzed and gene expression is controlled by addition of the activator mifepristone (RU486) in a dose-dependent manner (Figure 27). The concentration of RU suggested for lifespan analyses is quite broad with a range from

25 – 500 μM (e.g. Copeland et al., 2009, Bahadorani et al., 2010, Biteau et al., 2010). However, the RU effect itself has to be considered carefully as it is supposed to influence *Drosophila*'s food uptake probably to its bad palatability. Thus, changes in lifespan could be due to a dietary restriction effect. However, this kind of effect was observed for low-nutrient food in most instances (Yamada et al., 2017).

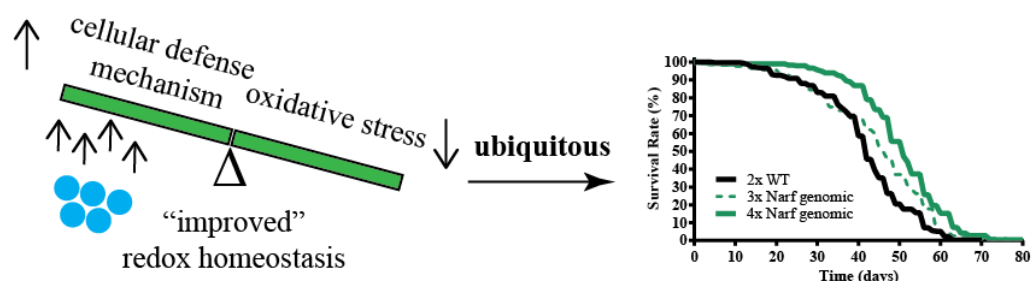
In this study, high nutrition food was used and gene expression was induced with a maximal concentration of 200 μM of RU. In order to validate if RU might affect life time under these conditions, lifespan analyses of wild type flies in the absence and the presence of 200 μM of RU were analyzed. It was shown that RU had no effects on *Drosophila* lifespan (Figure 31), allowing the usage of the GeneSwitch system for survival analyses.

5.2.3 Narf overexpression might increase intracellular stress defense mechanisms

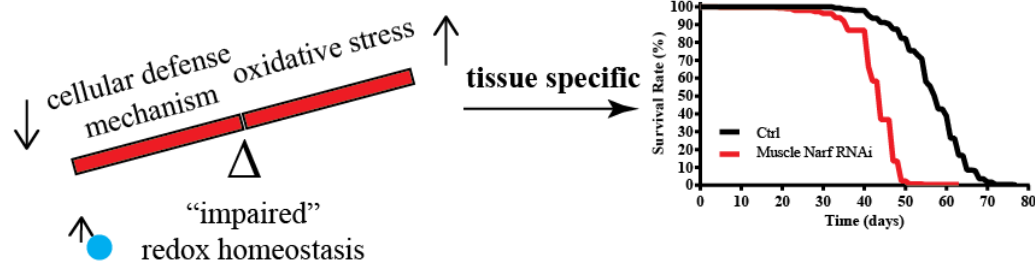
A lot of genes are described for shortening lifespan in *Drosophila*. However, talking about “aging genes” implicate the consideration of genes which have a beneficial effect on organismal aging. I showed in this study that Narf could be a new member of these genes as a loss-of function led to a decrease in lifespan (Figure 34) whereas a gain-of function prolonged *Drosophila*'s lifespan (Figure 24, Figure 25). RNAi experiments were performed in a muscle specific manner as it was shown that a ubiquitous downregulation caused lethality. Overexpression was achieved by an increase of the genomic copy numbers of Narf or by the tubulin-Gal4 controlled expression of a UAS-Narf transgene (Figure 24, Figure 25). Both gain-of functions situations were characterized by an overexpression starting already during embryogenesis. Western blot analyses confirmed an elevation in Narf protein level under the control of tubulin-Gal4 in larval stage (Supplement Figure 6) as well as during adulthood (Supplement Figure 4). How Narf might improve organismal aging on the molecular level still needs to be studied. However, a hint that an up-regulation of Narf might improve the stress response in aged flies and by this contribute to a delay in the aging process was given by Corbin et al., which identified the human IOP1 (Narf-like) as a key factor for hyperoxia protection in HeLa cells. They showed that the mRNA as well as the protein levels are increased for IOP1 in hyperoxia resistant cells and that the achieved overexpression was required for protection of cytosolic and nuclear Fe-S proteins in situations of hyperoxia-induced oxidative stress (Corbin et al., 2015). Fe-S proteins contain iron which makes them fragile especially in the presence of oxidative stress as they are easily oxidized. An

efficient protection of Fe-S proteins under these conditions is necessary as they are involved in a variety of different processes and essential for life (Johnson et al., 2005).

A Gain-of function situation



B Loss-of function situation



● Narf protein

Figure 46: Model for the role of Narf and its contribution to aging in *Drosophila*

It was shown in this study that a ubiquitous overexpression of Narf led to a prolongation in lifespan, whereas a tissuespecific down regulation caused a shortening in lifespan. I am hypothesizing that Narf is involved in balancing the cellular redox homeostasis which is mediated by its gene expression levels. High Narf protein levels might activate cellular defense mechanisms or might improve the protection of essential Fe-S proteins in the presence of oxidative stress as it was described for the human IOP1 (Narf-like) (Corbin et al., 20015). As Narf overexpression is beneficial for organismal aging, it is conceivable that Narf leads to an amelioration of oxidative stress occurring during normal aging. A loss of function instead might decrease the ability of cellular detoxification mechanisms or might cause an enhanced fragility of Fe-S proteins against oxidative stress which goes along with a decrease in lifespan. However, the molecular mechanisms are not known yet and still needs to be studied.

An unexpected observation was made by the ubiquitous downregulation of Narf during adulthood. As discussed before, the majority of the flies died within three weeks upon Narf downregulation, probably due to an essential role in Fe-S protein maturation. However, a subpopulation of approximately 5% showed even a prolongation in lifespan, which was correlating with an increased Narf protein expression (Figure 35). Even if lifespan extension was not a general effect as the majority of the flies died, the effect of a Narf overexpression

was indeed a general phenomenon. Western blot analyses showed an increase in Narf protein level starting at the second week correlating to a time point where approximately 75% of the RNAi expressing flies are still alive. Sample preparation was furthermore performed with the extract of ten flies, supporting the idea of a common effect.

However, the simplest explanation would be that an efficient down regulation of Narf was not induced. Knock down studies were performed using a long hairpin structure specific for the fourth exon of Narf. To analyze the general function of the Narf-RNAi construct different driver lines were used and Narf protein level were validated. In order to do this also thorax samples were checked for Narf protein expression after a muscle specific Narf knockdown (Figure 34 B). A decrease in protein level after Narf RNAi expression was not observed by western blot analyses. Time points of 10 d, 22 d and 30 d after induction were tested. However, a Narf signal was not detectable neither in control nor in RNAi samples, showing that Narf is only weakly expressed within the thorax. These data are consistent to tissue expression profile data (<http://flybase.org/reports/FBgn0262115#expression>). To further test if Narf protein level is decreased immunofluorescence analyses of muscle nuclei were performed. However, after induction with 20 μ M still a staining of the nuclear rim was observed. Using 200 μ M of RU led to a more nucleoplasmatic staining of Narf (Figure 33 B,C). But, it is not clear if the observed effects were specific or had to be considered as unspecific as the newly generated Narf antibody showed some background signal within stained thorax samples. Still, that the Narf antibody in general work good was shown in different tested conditions e.g. in immunostainings of S2 cells and embryonic amnioserosa cells as well as in western blot analyses (Figure 18). Thereby also larval extract of tubulin driven RNAi expressing animals was tested, showing an efficient down regulation of Narf protein level (Supplement Figure 6). This experiment showed first that the RNAi construct worked and second gave another proof for the establishment of a specific Narf antibody. Furthermore, it was observed that a wing specific Narf knock down induced morphological defects in adult wings (Supplement Figure 5), indicating a loss of function phenotype. RNA sequencing analyses of thorax samples finally revealed an efficient and exon based down regulation of the Narf transcript (\log_2 fold: -3.10) upon muscle specific Narf RNAi expression. As the observed increase in Narf protein level did not originate from an inefficient mediated knock down, the question arose if this effect might be considered as Narf specific.

Due to this it is conceivable that a ubiquitous knock down of Narf during adulthood (Figure 35) induced a cellular stress situation eventually based on a disturbed Fe-S protein maturation. The hypothesis is that this situation led to an elevation of Narf protein level in order to protect the cellular redox homeostasis. Furthermore, it was shown that the yeast homologue Nar1 is required for its own biosynthesis (Balk et al., 2004), suggesting a regulation via a negative feedback mechanism after knocking down. However, if the up regulation of Narf protein level is caused by an increase in gene expression or controlled by increase in protein stability might be shown in the future.

On the other hand, the majority of the flies died even after Narf overexpression, suggesting that the activation of the defense mechanism was too slow or the developed damage already too severe. But, the survival of a distinct subpopulation indicates the capability of this mechanism in stress protection. The fact that these flies even show a prolongation in lifespan compared to control flies indicates the induction of long lasting effects which might improve the cellular defense mechanism against elevated ROS levels.

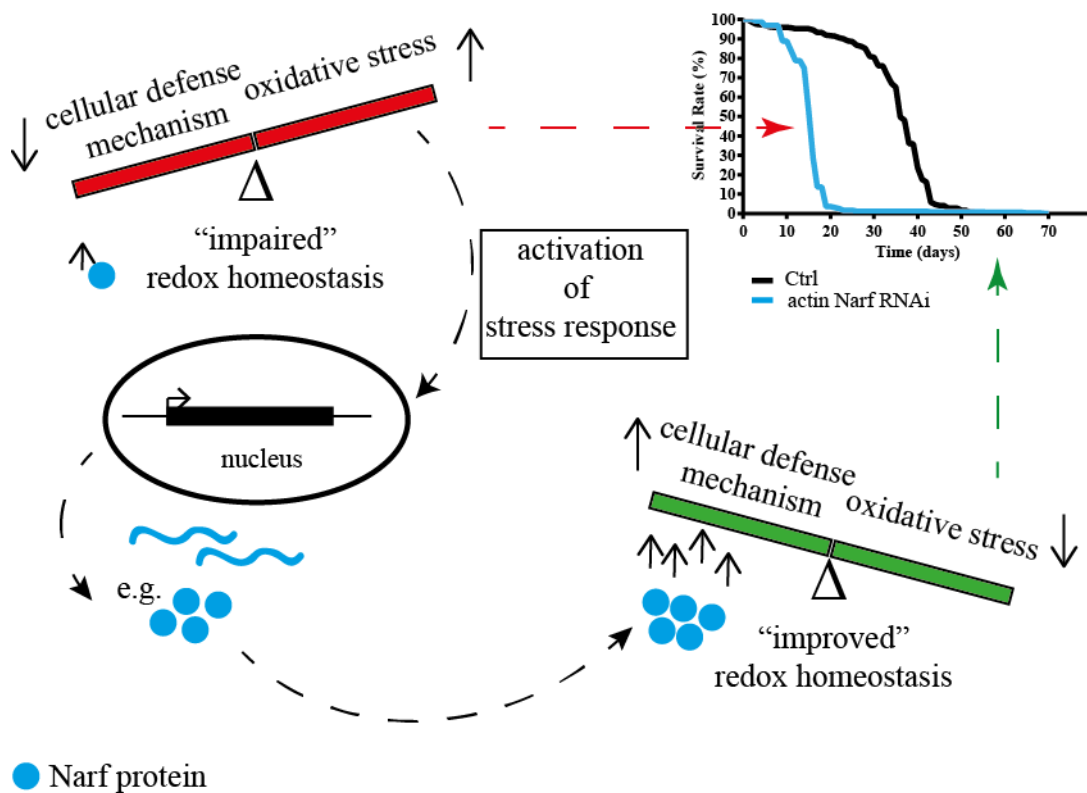


Figure 47: Narf down regulation might increase protein expression via a negative feedback. An ubiquitous down regulation of Narf severely impaired the survival rate of the majority of the flies (red arrow). This was reasoned to an essential function of Narf during adulthood. However, a subpopulation of

approximately 5% survived and even showed a prolongation in lifespan (green arrow). Furthermore a general increase in the Narf protein level was observed upon down regulation. I hypothesize that a ubiquitous knock down of Narf caused a severe stress situation, which led to the activation of a response signaling pathway and by this increased Narf protein levels via a negative feedback loop in order to maintain homeostasis. If this effect is mediated on the DNA, mRNA or protein level is not known. The fact that Narf overexpression achieved an increase in lifespan is consistent to the observed lifespan extension upon overexpression of genomic and inducible transgenes. Thus, Narf might be a new regulator involved in stress response and by this involved in aging processes.

5.2.4 An altered Narf expression in muscle cells probably leads to redox imbalance

Muscle specific experiments showed a decrease in lifespan of approximately 25% in a Narf knock down situation (Figure 34) and a decrease of approximately 20% in Narf overexpressing situations induced with 20 μ M of RU. An increase in gene expression by using 200 μ M of RU further shortened lifespan (Figure 32). Next to this, aging phenotypes such as nuclear morphology changes and a decrease in climbing behavior was observed upon muscle specific overexpression of Narf (WT or H/R) (Figure 29, Figure 30).

However, the biggest problems using phenotypic analyses as a tool to study aging is that a distinct effect might be observed but the molecular reasons behind remain unknown. Due to this RNA sequencing analyses were performed to study changes in gene expression in thorax samples upon altered Narf expression in muscle cells (Figure 36). A comparison of the RNA sequencing analyses showed an overlap in gene expression changes. In case of the overexpressed Narf wild type transgene 177 genes were identified for being changed. Out of these approximately 50% of the candidates were also found upon overexpression of the mutant Narf H/R transgene as well as upon Narf down-regulation. The most interesting candidates were selected based on the log₂fold change on gene expression level. Methuselah-like 8 (log₂fold: + 7.11) and Cyp12d1 (log₂fold: - 6.58) were identified when Narf was muscle-specific down regulated; whereas Cyp4p2 (log₂fold: + 4.59 WT, + 4.64 H/R) was detected upon Narf overexpression.

Methuselah-like 8 is annotated to be involved in aging in *Drosophila* due to its homology with methuselah (mth) which mutant could cause a lifespan extension (Lin et al., 1998). It was shown that methuselah increases lifespan accompanied by a resistance to several kinds of stress including heat, starvation, and oxidative stress (Lin et al., 1998). It was suggested that the wild type methuselah allele has a central role in maintaining homeostasis and metabolism by modulating molecular events in response to stress and that the level of gene

expression plays a critical role in balancing the system (Lin et al., 1998). Methuselah has 15 paralogs, namely methuselah-like 1-15 which functions are largely unknown (Mendoza et al., 2016). There are no evidences that they exhibit the same function (Araujo et al., 2013). Nevertheless, the changes in methuselah-like 8 expression level indicate that a Narf knockdown is inducing stress which might be the reason for the observed shortened lifespan. Furthermore, the gene expression of Cyp12d1 was changed in thorax samples upon Narf down regulation. Cyp12d1 belongs to the group of cytochrome P450 monooxygenases (P450s) which is large, conserved and able to catalyze a variety of enzymatic reactions (reviewed in Sono et al., 1996 and Scott et al., 2001). In *Drosophila* 83 P450 genes exist, which are involved in essential processes as well as in adaptive response to chemical compounds (Tijet et al., 2001). However, the function of Cyp-proteins in insects is not well understood yet. The expression pattern of P450s in *Drosophila* has been studied. It has been shown by performing an RNAi lethality screen that P450s are needed for essential processes which are potentially involved in detoxification (Chung et al., 2009). Thus, 35 P450s genes were identified for being putatively involved in the cellular detoxification system including Cyp6a8, Cyp6w1 and Cyp12d1d which were identified for being changed in their expression profile upon Narf down regulation in this study.

An interesting observation was that a muscle specific overexpression of the two Narf alleles (wild type and mutant H/R) also led to changes in gene expression for P450 monooxygenases (like Cyp4p2 and Cyp4p3). Next to the P450s also GST- (GstE14) and UGT-proteins (Ugt36Bb) were found to be changed. These genes are involved in all three phase of the detoxification system comprising phase I detoxification enzymes especially P450, phase II enzymes such as glutathione S-transferases and phase III enzymes including UDP-glucuronosyltransferases (Misra et al., 2011) have been found to be changed in expression level upon altered Narf expression in muscle cells. The Nuclear factor erythroid 2-related factor 2 (Nrf2) was described for being a transcription factor involved in redox balance by controlling gene expression of detoxifying genes. Nrf2 is associated to the Kelch-like ECH associated protein 1 (Keap-1) which mediates Nrf2 ubiquitinylation followed by degradation (reviewed in Motohashi and Yamamoto, 2004 and Loboda et al., 2016). However, under stressed situations Keap-1 is oxidized which disturbs Nrf2 binding. Thus, Nrf2 translocates to the nucleus and activates the cellular defense mechanism by binding to the ARE sequence (Jain et al., 2010). The Nrf2 transcription factor is quite conserved and can be also found in *Drosophila* where it is called Cap-and-collar C (CncC). A first link of

CncC/Nrf2 to the nuclear lamina in *Drosophila* was made by Dialynas et al., in 2015. There it was shown that a muscle specific overexpression of mutant lamins activated the Nrf2(CncC)/Keap-1 pathway during larval stage by causing reductive stress. Nrf2 mediated gene expression is different in oxidative and reductive stress. Reductive stress prevents Nrf2-Keap1 association by direct competition with p62/SQSTM1-Keap1 association (Komatsu et al., 2010). p62/SQSTM1 is also conserved and can be found in *Drosophila* named as p62/Ref(2)P. It was shown that in mutant lamin expressing larvae as well as in muscular dystrophy affected human patients the protein level for p62 is increased (Dialynas et al., 2015).

In order to analyze if p62/Ref(2)P protein level is elevated upon muscle specific alteration in Narf expression western blot analyses of thorax samples were performed. However, an increase in p62/Ref(2)P protein level was not observed after 17 days of induction (Supplement Figure 7). This might indicate that Narf is not inducing reductive stress but do not exclude the activation of the Nrf2 signaling pathway by oxidative stress. Another hint showing that the Nrf2 pathway might be activated is the observed change in gene expression for Nrf2/CncC target genes.

Misra et al., 2011 analyzed gene expression profile upon xenobiotic exposure in *Drosophila* and identified its target genes. A Comparison of these data with the total list of identified RNA sequencing candidates after muscle specific Narf-RNAi or Narf OE showed that in all cases approximately 15% of the candidates were described for being CncC/Nrf2 dependent.

I hypothesize that the muscle specific alteration of Narf expression could cause an imbalance in redox homeostasis, which lead to the activation of the Nrf2/Keap-1 signaling pathway as a mechanism to defense the stress situation with the observed activation in gene expression. However, it was already reported that CncC is involved in aging due to a decreased ability of target gene expression upon stress in aged flies, suggesting that a constitutional activation of the Nrf2/Keap-1 pathway leads to an exhaustion over time (Rahman et al., 2013).

Consistent to this it might be reasonable that an altered Narf expression induces stress, which causes a constitutional activation of the Nrf2/Keap1 signalling pathway and finally results in a shortened lifespan which might represent an accelerated aging effect.

5.2.5 The human mutation might represent a loss-of function allele

Considering the current knowledge about Narf it seems that the human mutation represents a loss of function allele. The strongest argument for this hypothesis was the detected lifespan prolongation in *Drosophila* upon overexpression. This effect was observed in two independent experiments first by an increase in genomic Narf alleles (Figure 24 B) and second by a tubulin-Gal4 controlled gene expression (Figure 25). Survival rate analyses confirmed that the development of Narf overexpressing flies was not affected, showing that lifespan analyses were performed with representative adults (Figure 24 A). That a gain of function might be beneficial was further indicated by the elevated Narf protein level upon ubiquitous down regulation (Figure 35 B), which was probably responsible for the increase in lifespan of a distinct subpopulation of flies (Figure 35 A).

A mutant version of the *C.elegans* homologue *oxy-4* was identified for being more sensitive to oxidative stress and showing a decrease in lifespan (Fujii et al., 2009). An interesting fact is that the mutation refers to the homologous position of the human patient. It was described that *oxy-4* mutants show a delay in development of 1 to 1.5 days compared to control worms (Fujii et al., 2009). Similar results have been observed upon RNAi treatment (Figure 38), suggesting delayed development is a loss-of function phenotype. However, a decrease in lifespan in RNAi worms was not observed, probably due to a sufficient protein expression level upon inefficient down regulation (Figure 44).

However, an important point which should not be left out of consideration is the fact that in humans two homologues namely Narf (IOP-2) and Narf-like (IOP-1) exist, whereas only one can be found in invertebrates like CG17683 (Narf) in *Drosophila* and Oxy-4 in *C.elegans*. It has been shown in this study that the *Drosophila* homologue localizes to the nuclear envelope as well as to the cytoplasm (Figure 18). Compared to this is the human Narf restricted to the nuclear envelope whereas IOP-1 is predominantly cytoplasmic localized (Barton and Worman 1999, Song and Lee 2008). These data suggest that *Drosophila* Narf takes over functions which are separated in vertebrates. To better understand the molecular nature of the human Narf mutation and its role in aging it will be necessary to further study *Drosophila* Narf gene function and its involvement in signaling pathways.

6 Materials and Methods

6.1 Materials

6.1.1 General Buffers

Table 1: List of buffers

Agent	Ingredients
PBS (1x)	137 mM NaCl, 10 mM Na ₂ HPO ₄ , 2.7 mM KCL, 1.8 mM KH ₂ PO ₄ , [pH 7.4], 1l
Sample buffer (2x)	100 mM Tris-Cl [pH 6.8], 4% SDS, 0.2% bromphenolblue, 20% glycerol, 200 mM DTT
SDS-Page buffer (10x)	0.25 M Tris, 2 M glycine, 1% SDS, 1l
TAE-buffer (50x)	2 M Tris, 50 mM EDTA, 1 M acetic acid [pH 8.5], 1l
Transfer-buffer (1x)	193 mM glycine, 25 mM Tris, 5% methanol, 1l

6.1.2 Chemical reagents

All chemicals used in this study were purchased from AppliChem GmbH (Darmstadt, Germany), Carl ROTH (Karlsruhe, Germany) or Sigma-Aldrich (Steinheim, Germany) unless otherwise stated.

6.1.3 Laboratory services

BestGene (Chino Hills, CA, US)

BioScience (Göttingen, Germany)

Charles River (Wilmington, Massachusetts, US)

Genetivision (Houston, Texas, US)

Hybrigenics (Paris, France)

InDroso (Rennes, France)

6.1.4 Antibiotics

	Stock concentration	Working concentration
Ampicillin	(100 mg/ml in ddH ₂ O)	50 - 100 µg/ml (final)
Kanamycin	(10 mg/ml in ddH ₂ O)	50 µg/ml (final)

6.1.5 Enzymes and Kits

All restriction enzymes used in this study were either purchased from Fermentas/Thermo Fisher scientific (Waltham, USA) or New England Biolabs GmbH (Ipswich, USA).

Enzymes from other sources are listed below.

DNaseI	Roche (Basel, Swiss)
Long PCR Enzyme Mix	Fermentas
Lysozym	AppliChem (Darmstadt, Germany)
M-MLV Reverse transcriptase	Promega (Madison, USA)
PfuS mix DNA Polymerase	expressed and purified in the Großhans lab
Proteinase K	Roche
RQ1 RNase-free DNase	Promega
T4 DNA Ligase	Fermentas
T4 DNA Polymerase	Fermentas
Taq DNA Polymerase	expressed and purified in the Großhans lab

Following Kits were used as described in manufacturer`s instructions.

Arcturus™ PicoPure™ RNA isolation Kit, Thermo Fisher scientific
In-fusion HD cloning kit, Clontech (Mountain View, USA)
MiniElute Gel extraction Kit, Qiagen (Hilden, Germany)
Plasmid Midi Kit Nucleobond Xtra, Macherey-Nagel (Düren, Germany)
Presto™ Mini Plasmid Kit, Geneaid (New Taipei City, Taiwan)
PureLink^R PCR-Purification Kit, Invitrogen (Carlsbad, USA)
SYBR® FAST qPCR Kit Master Mix (2X) Universal, KapaBiosystems

6.1.6 Chromatography

CNBr activated Sepharose 4B, GE Healthcare Life Sciences (Little Chalfont, UK)
Dynabeads MyOne Streptavidin T1 beads, Life technologies (Carlsbad, USA)
Ni-sepharose beads, Amersham Pharmacia Biotech (Little Chalfont, UK)
PD-10 desalting columns, GE Healthcare Life Sciences

6.1.7 Fly stocks

Table 2: Provided flystrains

Name	Genotype	Source/Lab stock number
A) General strains:		
OregonR	+/+	A401
w1118	w	A101
Tft	w ; Tft, c px sp / CyO	A207
BL25709	y ¹ v ¹ P{nos-phiC31\int.NLS}X;P{CarryP}attP40	Bloomington
B) Driverlines:		
actin-Gal4	w ; actin-Gal4 {w+}/CyO	N. Lee/ B118
actinGS-Gal	y w Flp[122]{ry+} ; UAS-GFP / CyO ; act-Gal4-PR[3] / TM6B, Tb Hu	Bloomington/ B121
armadillo-Gal4	arm-GAL4, UAS-lacZ	Wieschaus/ B111
GMR-Gal4	w ; Bcg/CyO; GMR-Gal4{w+}	B104
MHC-GS-Gal	w ; GS-Gal4-Switch[MHC]{w+}	Helfand/ B127
tubulin-Gal4	w ; tubulin-Gal4{w+}LL7 / TM3, Sb	N. Lee/ B119
vestigial-Gal4	w ; vestigial-Gal4{w+}	B108
C) Kugelkern concerning strains:		
kuk	w ; dur+{w+} , kuk15 e ca / dur+{w+}, Df(3R)EX6176{w+} e ca	F026
kukD15 (Δ 15)	w ; Sp / CyO, hb-lacZ{ry+} ; dur+{w+} , kuk15 e ca	F030
UASt-Kuk	w ; UASt-kuk{w+}/CyO, Dr/Tm3,Ser	H.Steffen/ F122
GFP-Kuk; D15	w ;matGal4(67) {w+}, UASp-GFP{w+} /CyO; dur+{w+} , kuk15 e ca / dur+{w+}, Df(3R)EX6176{w+} e ca	F113
D) Narf concerning strains:		
7172	CG17683 ^{NC37} cn ¹ bw ¹ /SM1	Bloomington
7173	CG17683 ^{NC38} cn ¹ bw ¹ /SM1	Bloomington
7176	CG17683 ^{NC70} cn ¹ bw ¹ /SM1	Bloomington
7162	CG17683 ^{NC109} cn ¹ bw ¹ /SM1	Bloomington
v110003/Narf-RNAi	P{KK115708}VIE-260B	VDRC
E) Other fly strains		
twistGFP, Cy0	w; Gla/Cy0,{twi::GFP}	B. Shiloh, Weizmann Institute of Science (Israel)

UAS-GFP	w; UAS ^t -GFP{w+}	Paros/ B204
GFP-cadherin	w; ubi-DE-cadherin-GFP{w+}	T. Lecuit/ B312
F) Fly strains used in RNAi-Screen (see Supplement Table 2)		

Table 3: Flystrains generated in this study

Name	Integration	Injection
GFP-Kuk	Δ 2/3 transposase mediated integration 4 th chromosome	M. Kriebel
GFP-Kuk	Δ 2/3 transposase mediated integration 2 nd chromosome	GenetiVision
KukC567S	Δ 2/3 transposase mediated integration 2 nd chromosome	GenetiVision
GFP-KukC567S	Δ 2/3 transposase mediated integration 2 nd chromosome	GenetiVision
pAttP Narf genomic	BL25709 (2L) 25C6	M. Kriebel
pAttP Narf genomic	VK1(2R) 59D3	GenetiVision
pAttP Narf genomic	P2(3L) 68A4	GenetiVision
pUAS ^t Narf	BL25709 (2L) 25C6	M. Kriebel
pUAS ^t Narf H/R	BL25709 (2L) 25C6	M. Kriebel

6.1.8 Worm strains and RNAi-vectors used in this study

Table 4: Worm strains used in this study

Name	Genotype	Source
N2	wild type	Gruenbaum lab
qa5001(<i>oxy-4</i>)	D373N substitution	M. Fujii
GFP:: <i>Ce-lamin</i>	baf-1p-gfp:: <i>lmn-1</i>	Gruenbaum lab

Table 5: RNAi-vectors used in this study

Name	Genotype	Source
L4440	Empty vector RNAi	Gruenbaum lab
<i>lmn-1</i> RNAi	RNAi against <i>Ce-Lamin</i>	Gruenbaum lab
Y54H5A.4	RNAi against <i>Oxy-4</i>	ORF RNAi Ressource - VIDAL

6.1.9 Media for flies

Fly food

64 g of thread agar were cooked in seven liter water until agar was completely dissolved. Afterwards 0.64 g maize meal, 80 g soya-bean meal, 200 g of baker` yeast, 640 g malt extract and 175 g sugar-beet molasses were added and properly mixed. The food was cooked for another 30 min and cooled down afterwards to 55 – 60 °C. 12 g Nipagin dissolved in 90 ml ethanol and 75 ml propionic acid were finally added. Food was mixed again and filled in fly vials. The food was kept overnight at room temperature to cool down and to solidify. Vial plugging was performed the next day. Fly food vials were stored at 18 °C until usage.

Apple juice agar plates

To prepare one liter of apple juice agar, 17.5 g agar were dissolved in 750 ml water. After autoclaving a mix of 25 g sugar solved in 250 ml of apple juice and 1.5 g of Nipaging dissolved in 10 ml ethanol was added to the agar solution. The mixture was allowed to cool down to 60 °C and apple juice agar was poured to Petri dishes. Plates were kept at 4 °C.

6.1.10 Media for *C.elegans*

NGM plates

To prepare the standard nematode growth medium, 3 g NaCl, 17 g agar and 2.5 g peptone were mixed in an Erlenmeyer flask and dissolved in 975 ml of water. Suspension was autoclaved for 50 min and after cooling down to 55 °C, 1 ml CaCl₂ (1 M), 1 ml cholesterol in 95% ethanol (5 mg/ml), 1 ml MgSO₄ (1 M), 25 ml KPO₄ buffer (1 M) and streptomycin (300 ng/ml) were added. The medium was mixed and dispensed into Petri plates by using a peristaltic pump under steril conditions. Plates have been dried at room temperature for 2 - 3 days and finally stored at 4°C.

RNAi plates

The same protocol for NGM plates was used but streptomycin was replaced by 50 µg/ml ampicillin and 120 µg/ml IPTG.

Seeding plates

5 ml starter culture of bacteria (OP50 or RNAi expressing bacteria) was set up in LB medium by picking a single colony and incubated for overnight, best 8h, at 37 °C. 50 – 100 µl were pipetted under sterile conditions to either NGM or RNAi plates and distributed equally. The plates were let dry over night at room temperature and finally shifted to 4 °C for storage.

6.1.11 Bacterial cell lines

Following *E.coli* strains were used in this study:

DH5α was used for plasmid amplification.

F⁻, ø80dlacZΔM15, Δ(*lacZYA-argF*)U169, *deoR*, *recA1*, *endA1*, *hsdR17*(rK⁻,mK⁺), *phoA*, *supE44*, λ⁻,*thi-1*, *gyrA96*, *relA1*

BL21DE3(rosetta) was used for protein expression.

F⁻ *ompT hsdS_B*(rB⁻ mB⁻) *gal dcm* (DE3) pRARE (Cam^R)

OP50 was used for seeding NGM-plates.

[*ura-*,*strR*,*rnc-*,(delta)*attB::FRT-lacI-lacUV5p-T7*]

6.1.12 Media for bacterial culture

LB-medium

To make one liter of LB-medium, 10 g Bactotryptone, 5 g Yeast extract and 10 g Sodium chloride were dissolved in water, autoclaved and stored at 4 °C.

LB-plates

LB-plates additionally contained 10 g agar and a desired antibiotic which was added after LB-solution was cooled down to 55 °C. LB-plates were poured into Petri dishes and stored at 4 °C.

6.1.13 Oligonucleotides

All oligonucleotides named by numbers were ordered from Eurofins Genomics (Germany). Alphabetically named oligonucleotides were ordered from hylabs (Israel).

Bold letters within oligonucleotide sequence show restriction enzyme sites, big letters were used for vector sequences within infusion primers.

Table 6: Oligonucleotides used for *C.elegans* studies

Name	Sequence 5' → 3'	Description
MKa	taata gggccc atattgtatagttcatccatgcc	Amplification of vectorbackbone Baf1PGFP lmn1 without lmn1 inclusive Bsp120I site
MKb	ata tagtta acctctagaactagtgatccc	Amplification of vectorbackbone Baf1PGFP lmn1 without lmn1 inclusive HpaI sites
MKc	gata gggccc atggaagattctggattcagtgg	Amplification genomic oxy-4 inclusive Bsp120I site
MKd	agata gtaact caccatttcaagacttgagcaac	Amplification genomic oxy-4 inclusive HpaI site
MKe	tgtagaatccgaagctggag	Sequencing for D/N
MKf	actggagaattaacagacgtc	Sequencing for in frame GFP to oxy-4
MKg	tggattcagtggtgctcgttcgac	qPCR Primer oxy-4 (Primermix 1)
MKh	ccactacatgccagacaatcagc	qPCR Primer oxy-4 (Primermix 1 + 4)
MKi	gaaaacgacgaagccggagatgtg	qPCR Primer oxy-4 (Primermix 2 + 7)
MKj	ctccagaagcaccaccatcgtc	qPCR Primer oxy-4 (Primermix 2)
MKk	gacgatggtggtgcttctggag	qPCR Primer oxy-4 (Primermix 3)
MKl	ctccagcttggattctacagtcg	qPCR Primer oxy-4 (Primermix 3 + 7)
MKq	gctccgaatttgactgcataatcc	qPCR Primer oxy-4 (Primermix 4)
MKr	tagctgattgtctggcatgtagtgg	qPCR Primer oxy-4 (Primermix 5)
MKs	ggagaaacagtgacgactgagagc	qPCR Primer oxy-4 (Primermix 5)
MKt	agagaaggtttaagcccctgtgatg	qPCR Primer oxy-4 (Primermix 6)
MKu	caacatctccggcttcgtcgttt	qPCR Primer oxy-4 (Primermix 6)
MK48	gaagagcatggttatcggc	Sequencing Primer oxy-4
MK49	gccgataaccattgctctc	Sequencing Primer oxy-4
lmn-1	gggtccgtgttgcaaaactc	qPCR Primer lmn-1 (Gruenbaum lab)
lmn-1	ctccaattggccactgttgcttc	qPCR Primer lmn-1 (Gruenbaum lab)
pmp-3	cgacgattcatttggtcaacgc	qPCR Primer pmp-3 (Gruenbaum lab)
pmp-3	gatgtcgcgaattgaacctggag	qPCR Primer pmp-3 (Gruenbaum lab)

Table 7: Oligonucleotides used for *Drosophila* studies

Name	Sequence 5' → 3'	Description
Oligonucleotides used for making GFP-transgenes		
MK9	AAGCAAATGGCTAGCtccaagggcga ggagctg	Amplification EGFP from Twe-Vector
MK10	CGCTTGTGTTGCTAGCCTTGTACA GCTCgtccatgcc	Amplification EGFP from Twe-Vector
Oligonucleotides used for Δ15 characterisation		
MK11	atggcgaatgcgggtggtgga	PCR primer call

MK12	tttggtgctggtggaaggtac	PCR primer cal1
MK13	tggactgcacagaggttgagg	PCR primer cher
MK14	ctacacatcgatctggaatggg	PCR primer cher
MK15	atgcgtcgcggttattatcag	PCR primer Keap1
MK16	tcatgtggctgcctcgtg	PCR primer Keap1
MK17	taacatcaacagtcaggtgtggtg	PCR primer Dad
MK18	tcaccgcagatgactaaagtgaac	PCR primer Dad
MK21	taaccacgtaaactggctggg	PCR primer kuk
MK22	ctaccacgcgagaaatacc	PCR primer kuk
MK23	gcgtaatgcgaactggc	PCR primer kuk
MK24	ttggtgatgcatgggtattgaaggc	PCR primer kuk
MK25	atctttccagctgttgattagagccg	PCR primer kuk
MK26	gaaattccaagacgtgaaccatcgtg	Long range PCR primer
MK27	tatggaatggacttgagaccaaggc	PCR primer kuk
MK28	ccgatgaagataacgccttgctaaa	PCR primer kuk
MK29	ttagccaaggcgttatcttcacg	Long range PCR primer
MK30	acgaatttctcacttcagcc	Sequencing primer
MK31	ctcgaacacagacttcag	Sequencing primer
Oligonucleotides used for Narf constructs		
MK32	gaaaaggtatcaaattacagattgttgaggtaatggcc	Site directed mutagenesis - Narf
MK33	ggcattacctcaacaaatctgtaattgatacctttc	Site directed mutagenesis - Narf
MK34	cgagaagacgctatctggc	Sequencing NarfH/R cDNA clone
MK35	catggtaacgggtgtgcag	Sequencing NarfH/R cDNA clone
Mk36	cgaagttatggatcaggcc	Sequencing NarfH/R cDNA clone binds within pFLC vector
MK37	ccacacctatctgatagcg	Sequencing NarfH/R cDNA clone
MK38	cgctatcagataggtgtgg	Sequencing NarfH/R cDNA clone
MK39	gccagatagcgtcttctcg	Sequencing NarfH/R cDNA clone
MK40	ctgcacaccggttaccatg	Sequencing NarfH/R cDNA clone
MK41	cgaagatcagggccttatg	Sequencing NarfH/R cDNA clone binds within pFLC vector
MK42	TTAACCATGGGAGCCtcgaggtgagcagagcg	Infusion primer, generation of a Narf specific antibody
MK43	GATGAGATCTGGATCgccaatttatattaa gcgatatactg	Infusion primer, generation of a Narf specific antibody
MK44	gcgaggttaatggcgtttagc	Amplification Narf genomic construct inclusive repetitive regions
MK45	cctgcgccaatggaatatttagg	Amplification Narf genomic construct inclusive repetitive regions
MK56	gataaggcaaggtcaaagactgg	Sequencing primer (genomic Narf + lethal alleles)
MK57	gagaacttgaccatgcttagctc	Sequencing primer (genomic Narf + lethal alleles)
MK58	ggaggagcacaatacgtcc	Sequencing primer (genomic Narf + lethal alleles)

MK59	acgatagcttggtcactgcac	Sequencing primer (genomic Narf + lethal alleles)
MK60	atgcaaataagctgtgtctgcc	Sequencing primer (genomic Narf + lethal alleles)
Oligonucleotides used for CRISPR approach		
MK61	ggatttatgaatggcgtaacg	Sequencing primer (putative gRNA)
MK62	tcaagaggcgaggttaatgg	Sequencing primer (putative gRNA)
MK63	aaagctagcgggtggcgtaatatgcgctgc	Cloning homology arm left, inclusive NheI site
MK64	aaagcggccgctagtaaaagccgcgcgctaac	Cloning homology arm left, inclusive NotI site
MK65	aaaagatctactaggttcaaacgagtggtc	Cloning homology arm right, inclusive BglII site
MK66	aaaactcgagccatagtgactacaataggg	Cloning homology arm right, inclusive XhoI site
MK67	cttcgcgcgcggctttactaatc	sgRNA homology arm left inclusive BbsI Restriction site
MK68	aaacgattagtaaaagccgcgcgcgc	sgRNA homology arm left inclusive BbsI Restriction site
MK69	cttcgccgagaaggtctgacaact	sgRNA homology arm right inclusive BbsI Restriction site
MK70	aaacagttgtcagacctctcgg	sgRNA homology arm right inclusive BbsI Restriction site
MK71	aatcacttgaggtgaaagtgcg	Sequencing pBFvU6.2B sgHAL,sgHAR Verification of sgHAL
MK72	gactcatcgtcccagagaatcg	Sequencing pBFvU6.2B sgHAL,sgHAR Verification of sgHAR

6.1.14 Plasmid constructs

Table 8: Provided plasmids used in this study

Name	Description	Source
Plasmid constructs used for <i>C.elegans</i> studies		
BAF-1p-GFP lamin	GFP Ce-lamin fusion protein expressed by BAF promoter	Gruenbaum Lab
Plasmid constructs used for <i>Drosophila</i> studies		
Antibody generation		
pGEX6OH	Bacterial expression, pGEX vector with additional N-terminal GST tag and C terminal His6 tag	Großhans lab
pGEX6OHNup153	pGEX6OH digested with BamHI, insertion of 1079 bp concerning Nup153 (isoformA) by infusion cloning (primer: MC15/MC16)	M. Clever

QE80N60	Bacterial expression, QE60 vector with additional N-terminal His6 tag	Prof. Görlich, MPI Göttingen
CRISPR approach		
pHD-DsRed attP	Site specific Integration of transgenes DsRed flanked by two loxP sites Two MCS used for inserting homology arms flanking targeted sequence	Gratz et al., 2014
pBFvU6.2	sgRNA expression by U6 promoter	Kondo and Ueda, 2013
pBFvU6.2B	sgRNA expression by U6 promoter	Kondo and Ueda, 2013
Generation of transgenic flies		
UASattB	Site specific Integration of transgenes	Bischof et al., 2007
pattB	Site specific Integration of transgenes	Bischof et al., 2013
Other Plasmid constructs		
RE37350	cDNA clone of Narf (CG17683) in pFLC vector	Flybase, BDGP DGC clone
CasBAC kuk genomic	Genomic rescue, EcoRV fragment cloned into pCasp4	Großhans lab
pBKS II (+)	Bluescript cloning vector	Short et al., 1988
CS-kug-C567S	CG5157 cDNA from pSK (LD09231) cloned into pCS2 vector via EcoRI-XhoI and XhoI-XhoI	Großhans lab
pBABR-Twine-EGFP	Genomic DNA of <i>twine</i> fused to codon optimized EGFP	Wischaus lab

Table 9: Plasmid constructs generated in this study

Name	Description Source
pFLC cDNA Narf H/R	Introduction of mutation via site-directed-mutagenesis (MK32/33), vector backbone was cleaned by NotI and BamHI digest
pUASattB cDNA Narf	pFLC cDNA Narf digested with BamHI for blunt end cloning and NotI, pUASattB digested with XhoI for blunt end cloning and NotI
pUASattB cDNA Narf H/R	pFLC cDNA Narf H/R digested with BamHI for blunt end cloning and NotI, pUASattB digested with XhoI for blunt end cloning and NotI
pAttB genomic Narf	pAttB digested with BglII and XbaI, genomic construct of CG17683 was amplified (MK44/45) and digested with BglII and NheI
pAttB genomic Narf H/R	pAttBNarf-genomic digested with NdeI and XhoI, missing Insert including AGA mutation and restriction enzyme sites for NdeI and XhoI was synthesized by Eurofins
pHDdsRed attP HAL HAR	HAL region amplified by MK63/MK64 including NheI and NotI restriction enzyme sites, HAR region amplified by MK65/MK66 including BglII and XhoI

	restriction enzyme sites, both fragments cloned into opened pHDDsRedattP vector
pBFvU6.2 sgRNA1	Oligonucleotides MK67 + MK68 were annealed against each other and cloned into pBFvU6.2 vector via BbsI restriction enzyme site
pBFvU6.2B sgRNA2	Oligonucleotides MK69 + MK70 were annealed against each other and cloned into pBFvU6.2B vector via BbsI restriction enzyme site
QE80N60 cDNA Narf	QE80N60 digested with BamHI, introduction of amplified Narf cDNA (MK42/43) by infusion cloning
Cas BAC-kuk-genomic-GFP	Cas BAC-kuk-genomic opened with NheI, introduction of amplified EGFP from pUAS _T -Twn-EGFP vector by infusion cloning
Cas Bac-kuk-genomic-C567S	SpeI fragment from Cas BAC-kuk-genomic cloned into SpeI site of pBKS (pBKS kuk SpeI), NheI-NruI fragment exchanged with corresponding NheI-NruI fragment from CS-kukC567S (pBKSkukC567S), cloned back into SpeI digested Cas BAC-kuk-genomic vector
CasBac-kuk-genomic-C567SGFP	Cas BAC-kuk-genomic-C567S opened with NheI, introduction of amplified EGFP from pUAS _T -Twn-EGFP vector by infusion cloning
Baf1P-GFP oxy-4 wt	Amplification of genomic oxy-4 based on wild strain N2 (MKc/MKd), cloned via Bsp120I and HpaI into Baf-1p-GFP vector amplified on Baf-1p-GFP lamin (MKa/MKb)
Baf1P-GFP oxy-4 D/N	Amplification of genomic oxy-4 based on mutant strain qa5001 (MKc/MKd), cloned via Bsp120I and HpaI into Baf-1p-GFP vector amplified on Baf-1p-GFP lamin (MKa/MKb)

6.1.15 Primary antibodies

1 st Antibody	Host	Dilution		Source
		Staining	Western	
Antibodies used for <i>C.elegans</i> project				
Ce-LaminC (3932)	rabbit	-	1:100	K.Wilson (Gruenbaum lab)
Myosin	mouse	-	1:1.000	Gruenbaum lab
Phalloidin	rabbit	1:200	-	Sigma, P1951
Antibodies used for <i>Drosophila</i> project				
Caspase		1:500	-	AB13847, Abcam
Dlg4	mouse	-	1:100	DSHB
Dm0	mouse	1:200	1:1.000	C. Saumweber

GFP	rabbit	-	1:6.000	Sc-8334, Santa Cruz Biotec.
Kuk affinity purified	rabbit	1:5.000	1:10.000	S. Lawo/ Charles River
Kuk	gp	1:5.000	-	S. Lawo/ Charles River
Nup153	mouse	-	1:1.000	AB24700, Abcam
P62/Ref(2)	rabbit		1:3.000	G. Juhasz
Slam	rabbit	1:5.000	-	Charles River
Tubulin	mouse	-	1:50.000	T5168, Sigma
Antibodies generated during this study				
Narf (polyclonal)	gp	1:500	1:10.000	M.Kriebel/Bioscience
Narf (polyclonal)	rabbit	Tested but unspecific		M.Kriebel/Bioscience
Nup153 (polyclonal)	gp	1:5.000	1:10.000	M.Kriebel/Charles River
Nup153 (polyclonal) affinity purified	rabbit	1:500	1:10.000	M.Kriebel/Charles River

6.1.16 Secondary antibodies

2 nd Antibody	Host	Dilution		Source
		Staining	Western	
Anti-Rabbit IgG(H+L) Cy3	goat	1:200	-	Jackson 111-166-003
Alexa Fluor 488	goat	1:500	-	Molecular Probes, Invitrogen
Alexa Fluor 568	goat	1:500	-	Molecular Probes, Invitrogen
Alexa Fluor 647	goat	1:500	-	Molecular Probes, Invitrogen
Alexa Fluor Phalloidin 488		1:1.000	-	Molecular Probes, Invitrogen
IRDye-680RD	goat, donkey	-	1:20.000	LI-COR Biotechnology
IRDye-800CW	goat, donkey	-	1:20.000	LI-COR Biotechnology

6.1.17 Software

Adobe Illustrator CS6, Adobe

Adobe Photoshop CS6, Adobe

Citavi4, Swiss Academic Software GmbH

GraphPad Prism6, GraphPad Software, Inc.,

ImageJ, Wayne Rasband

Image Studio, LI-COR Biosciences

IntasGDS, Intas Science Imaging

Lasergene, GATC biotech

Microsoft Excel 2013, Microsoft

Microsoft Word 2013, Microsoft

NanoDrop 2000, Thermo Fischer Scientific

OASIS, Yang et al., 2011

Rotor-Gene 6000 Series 1.7, Quiagen

SeqBuilder, DNASTAR

SnapGene, GSL Biotech LLC

UNICORN, GE healthcare

Zen 2012, Carl Zeiss

6.1.18 Equipment

Microscopes:

Axioplan 2 Fluorescence Microscope, Zeiss

LSM 780, Zeiss

MZ12.5, Leica

PrimoVert Inverted Microscope, Zeiss

Stemi 2000 Stereomicroscope, Zeiss

SteREO Lumar V12, Zeiss

SZX12 Fluorescence Stereo Microscope, Olympus

Camera:

AxioCam MRc, Zeiss

Other Equipment:

Äkta pure, GE healthcare

Centrifuges, Eppendorf

ChemiDoc, Biorad

Concentrator, Eppendorf

DynaMagnet, life technologies

Electrophoresis Constant Power Supply, Pharmacia

FemtoJet, Eppendorf

Flaming/Brown Micropipette Puller P97, Sutter Instrument

High Pressure Homogenizer/Microfluidizer- EmulsiFlex-C5, Avestin

Megafuge, Heraeus

NanoDrop 2000c, Thermo Scientific

Odyssey CLx Infrared imaging system, LI-COR Biosciences

Real time PCR machine - rotor gene 6000, Corbett/Quiagen

Thermomixer, Eppendorf

Trans-Blot Semidry, Biorad

Ultrasonics Sonifier-450, Branson

6.1.19 Other materials

Agarose, Invitrogen

Aquapoly mount, Polysciences, Inc.

BSA/Albumin Fraktion V, Roth

Cover Slides, Thermo Scientific

DanKlorix

DAPI, Sigma-Aldrich

Dialysis sleeve, Trans Roth E656.1 MWOC 3,500 Da

DNA ladder (1 kb), Thermo Scientific

dNTPs, Thermo Scientific

Falcon tubes (15 ml, 50 ml), BD Falcon

Filter papers (Ø 110 mm) Macherey-Nagel

Fly cages (Ø 50 mm, Ø 94 mm)

Fly vials, Greiner

Forceps

Formaldehyd (37%), Sigma-Aldrich
Gelatin, Dicto Bacto, 0143-02 ¼ lb
Glass homogenizer, B. Braun Biotech International
Glass pipettes (5 ml – 25 ml), Silber Brandt
Glass slides, Thermo Scientific
Green Taq buffer (10x), Thermo Scientific
Halocarbon oil 700, Sigma-Aldrich
Immersol 518F/W, Zeiss
Microinjection needles TW100F-4, WPI
Mifepristone (RU468), Sigma-Aldrich
Milk powder, Sucofin
Parafilm M, Bemis
Pasteur pipettes, Brandt
Petri dishes, Greiner
Phenol/Chloroform/Isopropanol, Roth
Phusion HF buffer (5x), Thermo Scientific
Pipetman (2 µl, 10 µl, 200 µl, 1000 µl), Gilson
Pipette tips, Sarstedt
Platinum wire
Poly-L-Lysine Solution (0.1%), Sigma-Aldrich
Polypropylene column, Quiagen
Prestained Protein Ladder, Thermo Scientific
Protease Inhibitor Cocktail - Complete Mini (EDTA free), Roche
Proteinase K, Roche
Protran Nitrocellulose Membrane, Amersham
Reaction tubes (1.5 ml, 2.0 ml), Sarstedt
Reaction tubes (5.0 ml), Eppendorf
Reaction tubes (50 µl), Brand
Reaction tubes (500 µl), ELKay
Sodium Hypochlorite solution (15%), Sigma-Aldrich
TRI-reagent, Sigma-Aldrich
TritonX-100, Roth
Tween20, Roth

Viva spin, Sartorius

VoltaLef Oil 10s, Lehmann, Voss & Co.

Weigh Boat, VWR

Whatman 3 mm blotting paper, GE healthcare

Yeast, Dr. Oetker

6.2 Methods

Standard procedures were carried out, according to the protocols described in Sambrook and Russels, 2001 and to established protocols of the Großhans laboratory, unless otherwise stated.

6.2.1 DNA methods

6.2.1.1 Extraction of genomic DNA from *Drosophila*

For getting a good amount of genomic DNA, two male flies were pestelled in 60 μ l of buffer A and centrifuged for 1 min at 14,000 xg. The RNA containing supernatant was discarded. The pellet was washed with 400 μ l buffer A, centrifuged and the supernatant was removed. The pellet was subsequently resuspended in 36 μ l buffer B containing 0.36 μ l proteinase K (20 mg/ml) and 4 μ l of SDS (10%) were added. The sample was mixed properly and incubated for 1-4 hours at 37 °C. After incubation 6 μ l, of sodium chloride (3 M) and 20 μ l of phenol/chloroform were added, mixed and centrifuged for 1 min at 14,000 xg. 40 μ l of the upper phase were transferred to a fresh reaction tube and mixed with 100 μ l ethanol (100%). Centrifugation was done for 5 min at 14,000 xg. The supernatant was discarded and the pellet was washed with 400 μ l of ethanol (70%). After repeating the centrifugation step, the supernatant was removed and the DNA sample was dried by using speed-vac. After dissolving the pellet in 20 μ l TE buffer, the prepared genomic DNA was ready to use as template for subsequent PCR approaches.

Buffer A

30 mM Tris/HCL [pH 8]

100 mM NaCl

19 mM EDTA

0.5% Triton X-100

Buffer B

30 mM Tris/HCL [pH 8]

100 mM NaCl

19 mM EDTA

6.2.1.2 Extraction of genomic DNA from *C.elegans*

This method was performed according to Williams *et al.*, 1994. To isolate genomic DNA, ten worms of each genotype were used and transferred to a PCR tube containing 50 μ l of worm lysis buffer. The samples have been placed at -80°C for 15 min to break down nematode bodies. The tubes were warmed up to room temperature and following incubated at 60 °C for one hour and 95 °C for 15 min. Additional vortexing during incubation steps helped to break down worm bodies. After cooling down to 4 °C and mixing the samples were ready to use. For subsequent PCR analysis, 2.5 μ l were used as template.

Worm lysis buffer

50 mM KCL

0.05% Gelatin

10 mM Tris [pH 8.2]

0.45% Tween 20

60 μ g/ml Proteinase K2.5 mM MgCl₂**6.2.1.3 Polymerase chain reaction (PCR)**

PCR reactions were performed by using Taq - polymerase for general reactions or PfuS - polymerase for reactions with improved proof reading. A PCR reaction was set up with following reagents:

0.5 – 2.5 μ l	fwd Primer	(10 μ M)
0.5 – 2.5 μ l	rev Primer	(10 μ M)
1.0 μ l	dNTP mix	(10 mM)
1x	Buffer	(Green Taq Buffer (10x)/ Phusion HF buffer (5x))
0.3 U/ μ l	Polymerase	(Taq/PfuS)
50 – 200 ng	DNA template	
ad 50 μ l	ddH ₂ O	

Following PCR programs were used for DNA amplification by Taq- or PfuS - polymerase:

	<u>Taq / PfuS</u>	
1. Initial Denaturation:	95 °C, 2 min / 98,5 °C, 30 s	
2. Denaturation:	95 °C, 30 s / 98,5 °C, 5 -10 s	} 25-35 x
3. Annealing:	X °C (Oligonucleotide specific), 30 s	
4. Extension:	72 °C, 1 kb/min / 72 °C, 1kb/15-30s	
5. Final Extension:	72 °C, 10 min	

6.2.1.4 Site directed mutagenesis

Site directed mutagenesis was used to establish a mutant Narf allele with an aminoacid exchange at position 388 from histidine to arginine (CAC to AGA). The PCR-reaction was performed as described before, using PfuS mix polymerase, Primer MK32/33, annealing temperature of 58 °C and an extension time of 2.5 min. The PCR-product was subsequently digested with Dpn, a methylation dependent endonuclease, to remove the vector without mutation, which was used as template. The digested PCR-product was purified by phenol chloroform extraction (6.2.1.5) and transformed to DH5 α electrocompetent cells by electroporation (pulse 4-5 ms, field strength 15.5 kV/cm).

6.2.1.5 Phenol-chloroform extraction

A DNA/RNA sample (e.g. 50 μ l) was first filled up with ddH₂O to fourfold volume. Then, 200 μ l of Phenol/Chloroform/Isopropanol (25:24:1) was added and mixed. The Sample was centrifuged for 5 min at 13,000 xg and the upper phase was transferred to a new reaction tube. 200 μ l of chloroform was added, mixed well and centrifugation was repeated. The DNA was precipitated by taking the upper phase into a new reaction tube and mixing it with 1/10 volume of sodium acetate (3 M) and 2.5 volumes of ethanol (100%). The sample was kept at -20 °C for overnight or at -80 °C for at least 30 min. After centrifugation at fullspeed (14.000 xg, 30min, 4 °C), the supernatant was removed and the pellet was washed with 200 μ l of ethanol (70%). The centrifugation was repeated, the supernatant removed and the pellet was dissolved in 10 – 30 μ l of ddH₂O.

6.2.1.6 DNA Sequencing

DNA sequencing, used for the *C.elegans* studies, was performed by the company hylabs (Israel). Sequencing for the *Drosophila* studies was done by Eurofins Genomics (Germany).

6.2.2 RNA methods

6.2.2.1 RNA extraction

RNA isolation from *Drosophila* thorax samples for subsequent RNAseq analysis was performed as described in the RNA isolation kit instructions.

To extract RNA from *C.elegans* for subsequent qPCR analysis, first the worms had to be washed in M9 buffer for several times. After the final wash, 5 ml of DEPC treated double distilled water were added and the samples were centrifuged. The supernatant was discarded and 2 ml of TRI-reagent per 1 ml of worm pellet were added, gently mixed and frozen for overnight at -80 °C. The worm bodies were following broken by three cycles of crushing, thawing the samples in 42 °C and freezing them in liquid nitrogen. The samples were subsequently centrifuged for 15 min with 12,000 xg at 4 °C. The supernatant was transferred to a new vial and RNA was extracted as described in 6.2.1.5.

6.2.2.2 RNAseq analysis

RNA samples were isolated and handed to the Microarray and Deep-Sequencing Facility in Göttingen for subsequent analysis.

6.2.2.3 Reverse transcription

To make cDNA for subsequent qPCR analysis the following protocol was used:

1. 2 µg isolated RNA
 4 µl RQ1 DNase (1U/µl)
 2 µl Reaction buffer (10x)
 ad 20 µl DEPC ddH₂O
 → Incubation for 30 min at 37 °C
2. 2 µl RQ1 DNase Stop solution
 → Incubation for 10 min at 65 °C
3. 1 µl Oligo(dT) (100 pmol/l)
 → Incubation for 5 min at 70 °C
4. 10 µl dNTP mix (10 mM)
 10 µl M-MLV buffer (5x)
 2 µl M-MLV reverse transcriptase (200 U/µl)
 1.25 µl Ribonucleotide inhibitor
 ad 50 µl ddH₂O
 → Incubation for 60 min at 42 °C

5. The newly generated cDNA was finally stored at -20 °C.

6.2.2.4 Quantitative real-time PCR (qRT-PCR)

All qPCR reactions were performed in triplets. For each reaction the following components were used to prepare a qPCR mastermix:

1 µl	cDNA (1/10 dilution)
3.5 µl	Primermix (fwd, rev, 1 µM)
12.5 µl	SYBr green qPCR mix (Roche)
ad 25 µl	ddH ₂ O

For detecting of oxy-4, lmn-1 and pmp-3 mRNA levels, the following qPCR program was used:

- | | | |
|--------------------------|-------------------------------------|--------|
| 1. Initial denaturation: | 95°C, 3 min | |
| 2. Denaturation: | 95°C, 10 s | } 40 x |
| 3. Annealing: | 60°C, 15 s | |
| 4. Elongation: | 72°C, 30 s | |
| 5. Melting curve: | 55°C – 95°C, 10 s (increase 0.5 °C) | |

6.2.3 Biochemical methods

6.2.3.1 Nuclei fractionation

Staged embryos were collected, dechorionated, weighted, frozen in liquid nitrogen and stored at -80 °C until the fractionation experiment was performed. To minimize protein degradation during fractionation, all steps were performed on ice or at 4 °C with precooled buffers. Embryos were suspended in HEPES buffer in a ratio of 150 mg of embryos to 1 ml of buffer. Embryos were crushed by douncing 6 times with a potter and 20 µl were saved for western blot analysis and named as “total”. To pellet nuclei and other cell components, the sample was centrifuged for 5 min at 1.000 xg. The supernatant was removed and centrifuged with high speed (14,000 xg) for 10 min and a “cytoplasm” fraction was saved. Nuclei were subsequent fractionated by using a sucrose gradient. The pellet was resuspended in 1 ml HEPES buffer with 0.25 M sucrose and layered over a 5 ml cushion of HEPES buffer with 0.35 M sucrose. Centrifugation was performed at 1,400 xg in a swing out rotor for 5 min. After discarding supernatant the nuclei pellet was resuspended in 1 ml HEPES buffer with 0.35 M sucrose and layered over a 5 ml cushion of HEPES buffer with 0.8 M

sucrose. The centrifugation step was repeated with 2,000 xg for 5 min. To enhance the nuclei separation, the last sucrose step was done twice. After nuclei isolation, the pellet was washed two times in 1 ml Hepes buffer. Samples were saved before and after centrifugation (4,000 xg, 5 min) and named as “isolated nuclei” and “washing step”. Kugelkern solubilization was done by incubating the nuclei pellet for at least 15 min on a wheel in 1 ml Hepes buffer with 1% TritonX-100 and 150 mM sodium chloride. The sample was centrifuged for 15 min with 14,000 xg. A volume amount representing 4,500 embryos was saved as “input” sample. The remaining sample was used for subsequent immunoprecipitation experiments. This method was modified according to established protocols of the Lamond laboratory (online available at <http://www.trinklelab.com/pubpdf/CellFractionation.pdf>).

Hepes Buffer

15 mM Hepes

5 mM MgCl₂

10 mM KCL

[pH 7.4] (KOH)

Sucrose was added in a final concentration of 0.25 M, 0.35 M or 0.8 M.

To all Hepes buffers, 1x protease inhibitor cocktail, 1 mM DTT and 0.1 mM PMSF were added freshly.

6.2.3.2 GFP-protein pulldown using GFP dynabeads

To analyze biochemical interaction partners of Kugelkern, GFP-Kuk expressing embryos were collected and nuclei fractionation was performed as described in 6.2.3.1. After taking an “input” sample for western blot analysis, the rest of the fraction sample was incubated with 50 nM of biotinylated GFP binding protein (gift from Prof. Görlich) for one hour on ice. 20 µl of Magnetic Streptavidin T1 dynabeads, resuspended by gentle vortexing, were taken for binding assay. The beads were washed trice in 1x PBS containing 0.1% BSA and concentrated by using a magnetic field. Proteinlysate with bound GFP binder was transferred to the beads and incubated for one hour on the wheel. After incubation, an “unbound” sample was taken and beads were washed trice with Hepes buffer (6.2.3.1). To minimize unspecific binding, the GFP binder was cleaved off from beads via an intrinsic cleavage site. Therefore, 100 µM of Sumostar Protease (gift from Prof. Görlich, MPI for Biophysical Chemistry, Göttingen), diluted in 1x PBS, were added to the dynabeads and

incubated again for one hour at 4°C on a wheel. Afterwards, samples of the supernatant, representing the “cleaved” fraction and the “beads”, were analyzed by western blot.

6.2.3.3 Protein precipitation

Fractionation samples that exceed a volume of 20 µl were precipitated by adding TCA in a final concentration of 15%. Samples were incubated first at -20 °C and second on ice for 15 min. Next, a centrifugation was performed at 14,000 xg for 10 min. The supernatant was removed and the protein pellet was washed twice with ice-cold acetone, followed by a centrifugation step. The pellet was finally resuspended in an appropriate volume of 2x sample buffer. In the case that sample buffer color turned to yellow, pH was adjusted by adding a drop of 1 M Tris pH > 8. The samples were boiled at 95 °C for 3 – 5 min and used for SDS-page.

6.2.3.4 Western Blot

6.2.3.4.1 Sample preparation

To analyze different samples via western blot it is essential to load an appropriate amount of protein. Following protocols were used in this study.

Embryos and larvae: 15 embryos or larvae were collected in 10 µl of water, freezed in liquid nitrogen and macerated. Afterwards 10 µl of 2x sample buffer were added. Samples were vortexed, boiled for 3 min at 95 °C and centrifuged for 1 - 2 min at 14.000 xg. For following analysis the lysate of 10 embryos and L1 larvae, 1.5 L2 larvae and 0.5 L3 larvae were used.

Fly extract: 10 male flies were collected and macerated in 50 µl water. One volume of 2x sample buffer was added. The samples were vortexed, boiled for 3 min at 95 °C and centrifuged for 10 min at 14.000 xg. The lysate of one fly was used for subsequent analysis.

Thoraces: 10 thoraces were prepared (compare 6.2.5.5) and macerated in 50 µl 1x sample buffer and sample volume was filled up to 70 µl of 1x sample buffer. The samples were vortexed, boiled for 3 min at 95 °C and centrifuged for 2 - 3 min at 14.000 xg. The lysate of 1.5 – 2.5 thoraces was used for subsequent analysis.

Worm extract: 25 worms were collected in a reaction tube and washed several times with M9 buffer. The supernatant was completely removed. The worms were frozen in liquid nitrogen and macerated after adding 25 µl of 1x sample buffer. The sample was boiled for 3 min at 95 °C and centrifuged for 2 - 3 min at 14.000 xg. The lysate of 10 worms was used for western blot analysis.

6.2.3.4.2 Western blot

The samples were prepared as described before and loaded on a 10% SDS-gel, unless otherwise stated. The SDS-gel electrophoresis was performed at 17 mA. Proteins were following blotted to a nitrocellulose membrane for 1.5 hours at 60 mA by using a semi-dry transfer. Unspecific antibody binding was minimized by blocking with 5% milk/1x PBS for 1 hour at room temperature. Primary antibodies were diluted in 1% milk/1x PBS with 0.1% Tween20 and incubated for one hour at room temperature or overnight at 4 °C. Membrane was first rinsed and then washed three times for five minutes in 1x PBS/0.1% Tween20. Incubation and washing steps were repeated for the secondary antibody. Bound secondary antibodies coupled with fluorescence were finally detected using Odyssey CLx Imaging system.

6.2.4 Antibodygeneration

6.2.4.1 Expression of recombinant proteins

Plasmid DNA coding for the protein was transformed into the *E.coli* strain BL21DE (rosetta). A 100 ml LB^{Amp} culture was set up and incubated at 37 °C for overnight. To express recombinant proteins in a large scale, 1 l LB^{Amp} culture was inoculated with the overnight culture to an optical density (OD) of 0.1. The culture was afterwards incubated at 37°C until it reached an OD-value of 0.5. A 1 ml sample for subsequent SDS-page was taken, centrifuged for 1 min at 14,000 xg and dissolved in 1x sample buffer. Protein expression was then induced by adding 1 mM of IPTG to the culture and incubating it for 1 - 4 hours at 18 °C. In between, further samples were taken. Cell collection was performed by centrifugation at room temperature for 20 min at 4,800 xg. Cell lysis was improved by a preceding overnight freezing step at -20 °C. Cells were afterwards thawed on ice and 10 ml lysis buffer per 1 g pellet were added and thoroughly suspended. A sample was taken, centrifuged and sample buffer was added to the supernatant (soluble fraction) and the pellet (insoluble fraction). Then, protease inhibitor PMSF (final concentration 1mM), Lysozym (final: 1 mg/ml) and a spatula tip of DNase were added. The cell suspension was mixed and incubated for 30 min on ice. A sample of the soluble and insoluble fraction was taken. Next, cells were disrupted by sonification (pulse: 50, power 5, cycles of one minute sonification and two minutes pause were repeated three times) or using the Microfluidizer and samples were taken. For soluble proteins, the supernatant was transferred to a new vial, centrifuged

for 10 min at 14.000 xg and 4 °C and purified as described in 6.2.4.2. Insoluble proteins, present in the pellet, were purified under denatured conditions (see 6.2.4.3).

Lysis buffer:

20 mM Na-phosphate, pH 8.0

500 mM NaCl

20 mM Imidazole

6.2.4.2 Native protein purification via His-tag

Before protein purification a Ni-His-Trap column was prepared and after purification regenerated as described in manufacturer`s instruction. Protein sample was loaded in a constant flow rate of 0.5-1 ml/min using the Äkta-system. The flow through was collected. The column was washed with washing buffer using more than 10 column volumes (CV). Elution was achieved by establishing an imidazole gradient between wash- and elution buffer. Elution fractions were collected every 0.5 CV. Samples of all purifications steps were taken and analyzed in a SDS-Page. Elution fractions, containing the desired protein, were pooled and a buffer exchange was performed using PD10 columns following manual instructions. To finally store the purified protein 50% of glycerol was added and the sample was kept at -80 °C.

Wash buffer:

20 mM Na-phosphate, pH 8.0

500 mM NaCl

40 mM Imidazole

Elution buffer:

20 mM Na-phosphate, [pH 8.0]

500 mM NaCl

500 mM Imidazole

6.2.4.3 Denatured protein purification via His-tag

Insoluble proteins, present in the pellet, were first suspended in 25 ml of lysis buffer and mixed for one hour at room temperature. The suspension was centrifuged for 10 min at 10,000 xg and the solubilized pellet extract was added to 3 ml of Ni-sepharose beads, which

were equilibrated with lysis buffer before. Binding was allowed under rotation at room temperature for 30 – 60 min. Next, the beads suspension was loaded onto a drop column. The flow-through was collected and the beads were washed three times with 6 ml washing buffer. Proteins were eluted in 15 1 ml fractions of elution buffer. Eluates were analyzed by SDS-Page and the identified protein containing fractions were kept at 4 °C for further usage. The buffers were prepared according to “The QIAexpressionist™”, 5th edition 2003.

Lysis buffer

100 mM NaH₂PO₄

10 mM TrisCl

6 M GuHCl

[pH 8.0], NaOH

Wash buffer

100 mM NaH₂PO₄

10 mM TrisCl

8 M Urea

[pH 6.3], HCl

Elution buffer

100 mM NaH₂PO₄

10 mM TrisCl

8 M Urea

[pH 4.5], HCl

6.2.4.4 Immunisation

Polyclonal antibodies were produced by either Charles River (Wilmington, USA) or BioScience (Göttingen, Germany). Received final sera were tested in western-blot analysis as well in immunostainings and if necessary further purified.

6.2.4.5 Antibody affinity purification

Antibody affinity purification is a method based on the specific interaction of an antibody and its antigen. To specifically isolate the desired antibody it is necessary to couple

the antigen against CNBr-activated Sepharose 4B. This method was performed according to manufacturer`s instruction.

Protein preparation

As denatured purified proteins were kept in 8 M urea, which would react with the BrCN groups, it was necessary to remove the urea. Therefore, a dialysis sleeve was prepared as mentioned in manual`s description and a dialysis against coupling buffer (three times 100 volumes) was performed.

Coupling buffer

100 mM NaHCO₃

300 mM NaCl

1% SDS

[pH 8.3], NaOH

Preparation of CnBr-activated Sepharose 4B

1 g of dry Sepharose 4B was swelled in 10 ml of 1 mM HCl for 15 minutes. The swollen beads (gel) were washed on a sintered glass filter with 200 ml of 1 mM HCl.

Coupling of antigen and beads

The gel was equilibrated in 5 ml coupling buffer per 1 g of dry beads and immediately afterwards the protein suspension was added in a 2:1 buffer to gel ratio. Beads suspension was mixed for 3 hours at room temperature or at 4 °C for overnight. The beads were allowed to settle down, supernatant was removed and tested for its protein concentration (A₂₈₀) to confirm efficient binding. To minimize unspecific binding, the beads were blocked for 2 hours at room temperature in blocking buffer. The suspended beads were poured into a column where they were washed for five times each with washing buffer I, II and 1x PBS.

Blocking buffer

0.1 M Tris/HCl

[pH 8.0]

Wash buffer I

0.1 M Na acetate

0.5 M NaCl

[pH 4.0]

Wash buffer II

0.1 M Tris/HCl

0.5 M NaCl

[pH 8.0]

Antibody affinity chromatography

5 – 10 ml of the final serum were centrifuged at 14,000 xg for 30 min at 4 °C and the cleared serum was applied to the prepared affinity column. The flow through was collected and loaded again up to seven times. The column was washed with 10 CV of 1x PBS followed by 10 CV of 1x PBS + 300 mM NaCl. Elution buffer was added and elution fractions of 900 µl were collected in reaction tubes containing 100 µl neutralization buffer. The protein concentration of the elution fractions was measured and protein containing samples were pooled. The antibody was finally concentrated to 1 mg/ml using Viva spin columns. 0.02% of Na-azide was added and the antibody was stored at 4 °C.

Neutralisation buffer:

1 M Tris/HCl

[pH > 9.0]

Elution buffer:

50 mM Glycine

[pH 2.5]

Affinity column regeneration

The used column was washed with 10 CV of washing buffer I, II and 1x PBS and finally stored in 1x PBS + 0.01% Sodium azide at 4 °C.

6.2.4.6 Generation of a nuclear pore complex (NPC) specific antibody

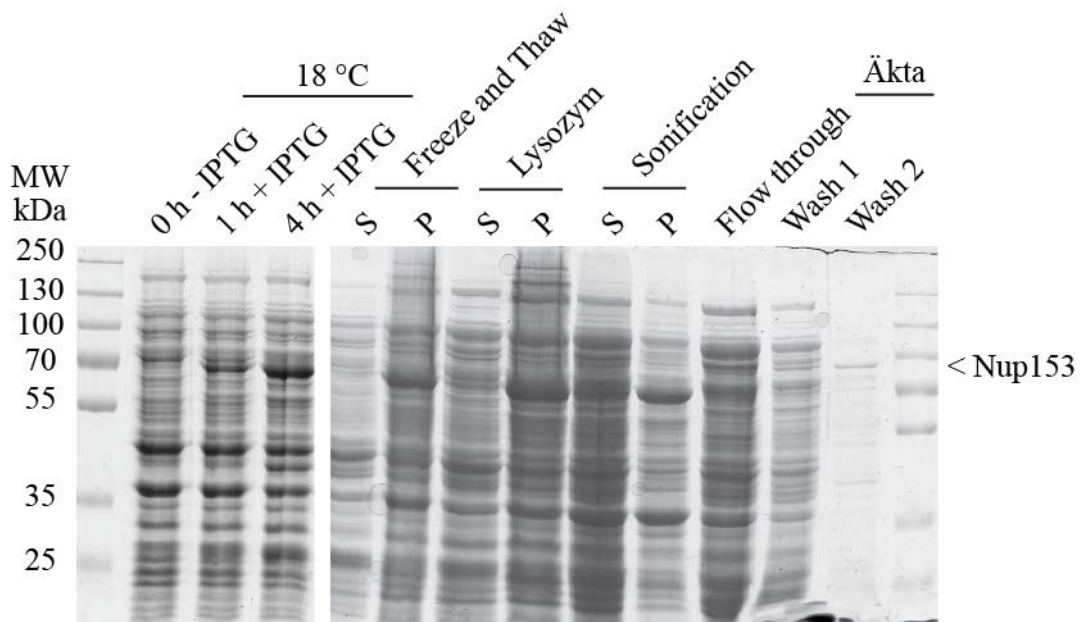
To generate a Nup153 specific antibody, 352 amino acids of the PA-isoform were used. The corresponding DNA sequence was cloned into pGEX-60H vector by M. Clever. The recombinant protein was expressed for 4 hours at 18 °C and purification was performed under native conditions using His-tag. Immunisation was done by Charles River into guinea pig and rabbit. The Nup153 (rabbit) antibody was affinity purified and concentrated to 1 mg/ml. Immunofluorescence and western blot analysis confirmed that the anti-Nup153 antibody can be used as a marker for nuclear pore complexes. However, it is likely that the antibody also recognizes other proteins of the NPCs as the aminoacid sequence contains several phenylalanine-glycine repeats (FG-repeats), which are evolutionary conserved within nucleoporins (Figure 48).

```

VMNKSSDEECIACQTPNSQARNNSNESALISSISSSSASFGSLSRPSSRSSSGSTSTC
GSVCSGSIVSISSTTESAKALSAKKVPPKPDAGFQQLVAAQKTSTWECEACLAKND
MSRKTCICCEQMMPEAFNPAATTANSAASSVPKFRFGFSHVKEVVKPSVETTTTPA
PTSAQFSFGFGQSNQGDVADSKKTEAPKTFMFGVSKVEEPKTVSFGTGIKETTAT
SSTEATAPTPAAAAPAPVQFVFKAPTATTASSLTTTISTTSNAPALGGFSFGAPSSS
STVSSSTTSTSANPAAVKPMFSWSGAGSAVSSSTSSSQQPVAKAPTLFGVSSSTVT
TTTTSTKVFAF
    
```

Figure 48: Amino acid sequence used for Nup153 antibody

Green colored amino acids show evolutionary conserved FG-repeats.



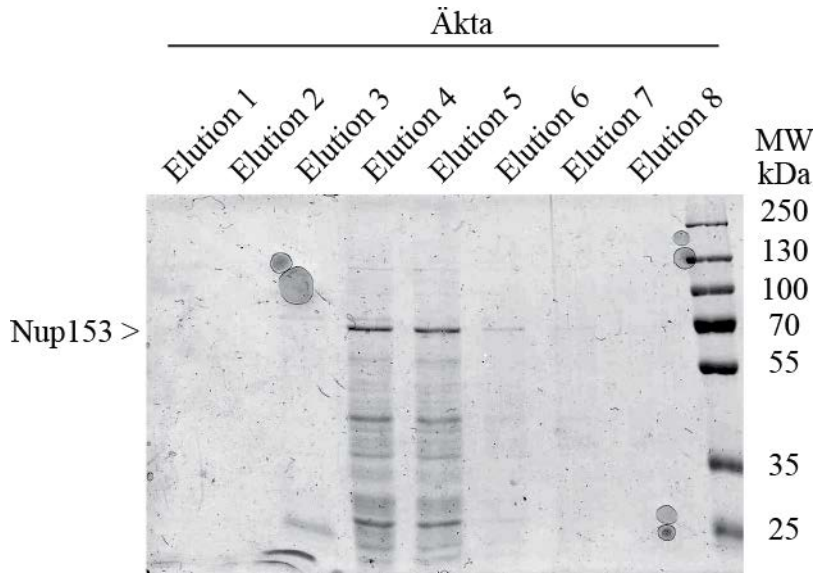


Figure 49: Expression and purification of the pGEX-60H-Nup153 protein

Nup153 was expressed for 4 hours at 18 °C. Preparation of cell lysates was performed by freezing and thawing the sample followed by lysozyme treatment and sonification. The success of cell disruption was proved by loading a sample of the soluble fraction (S - supernatant) and insoluble fraction (P - pellet) of each step. Purification was done under native conditions via His-Tag. Elution was established by using an imidazole gradient. The protein was eluted between 240 mM and 395 mM of imidazole (elution fraction 4 and 5). Sample analysis was performed using a 10% SDS-gele.

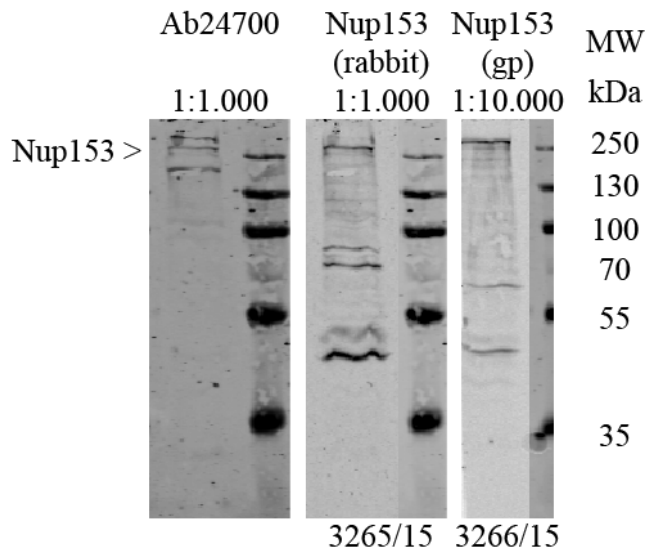


Figure 50: Specificity of the generated Nup153 antibody

The western blot analysis shows that the antibodies bind to Nup153 protein. A commercial available antibody (Ab24700) which stains for Nup153, Nup214 and p62 was used as comparison.

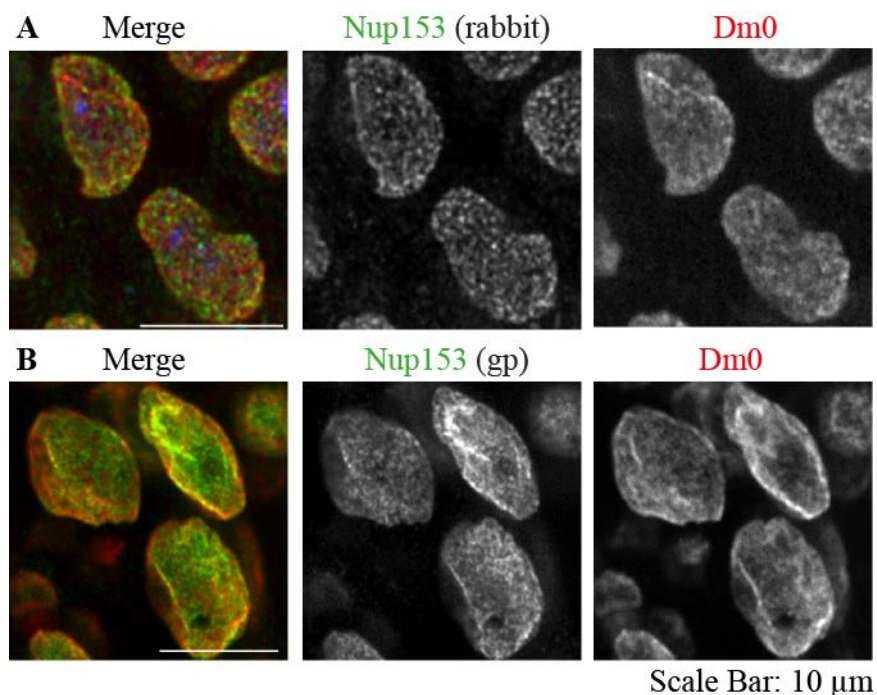


Figure 51: Nup153 antibody stains specific nuclear pore complexes

Immunofluorescence analysis of amnioserosa cells with antibodies against Dm0 as a marker for the nuclear envelope and Nup153 A) generated in rabbit and B) in guinea pig.

6.2.5 Staining methods

6.2.5.1 Embryo fixation

Embryos of desired stages were dechorionized on apple-juice plates by treating them with 50% of Klorix for 90 s. The embryos were collected in a net and washed several times with water to remove the Klorix completely. Afterwards, embryos were transferred to a scintillation vial containing 5 ml heptane, 4.5 ml 1x PBS and 0.5 ml formaldehyde (37%) and fixed for 20 min at room temperature under constant shaking. The lower phase was removed, 5 ml of methanol were added and embryos were vortexed for 30 s to remove the vitellin membrane. Devitellinized embryos were collected and transferred to a reaction tube. The embryos were washed with methanol for several times and finally stored at -20°C .

6.2.5.2 Embryo immunostaining

In methanol stored embryos were rinsed several times and washed once for 5 min with 1 ml 1x PBS/0.1% Tween (PBT). Blocking was performed by incubation of 1 hour in 500 μl PBT containing 5% BSA at room temperature. All incubations were done under constant rotation. Primary antibodies were diluted in the indicated ratio in 500 μl of PBT

with 1% BSA and incubated for 2 hours at room temperature or overnight at 4 °C. The embryos were rinsed three times and washed for four times for each 15 minutes with 500 µl PBT. Secondary antibody incubation and following washing steps were performed using the same procedure. Embryos were stained with DAPI (1:250, 0.2 mg/ml) for 7 – 10 minutes, rinsed three times and washed once for 5 minutes with PBT. Mounting was done by using Aquapolymount medium.

6.2.5.3 Imaginal discs preparation and fixation

To prepare imaginal discs, L3 larvae were dissected in ice-cold 1x PBS by holding them with forceps at the anterior end and tearing two thirds of the larvae away. Mouth hooks with attached and colorless appearing imaginal discs were pulled out. The tissue was collected in staining tubes containing 1x PBS. Fixation was performed by incubating samples in 4% paraformaldehyde in 1x PBS for 40 minutes at room temperature under constant shaking.

6.2.5.4 Imaginal discs immunostaining

The fixated samples were washed once in 1x PBS/0.3% Triton X-100 for 20 minutes and blocked with 5% BSA in 1 x PBS/0.3% Triton X-100 for one hour at room temperature. All incubation steps were carried out under constant horizontal shaking. Primary antibodies were diluted in the indicated ratio in 500 µl of 1x PBS/1% BSA/0.1% Tween and incubated overnight at 4 °C. The samples were washed three times with 1x PBS/0.3% Triton X-100 for 20 minutes each. Secondary antibody incubation and following washing steps were performed as for the first antibody. Samples were stained with DAPI (1:250, 0.2 mg/ml) for 7 – 10 minutes, rinsed three times and washed twice for 10 minutes with 1x PBS/0.3% Triton X-100. Finally, larvae mouth hooks with attached imaginal discs were transferred to a drop of 1x PBS on a glass slide and excess tissue was removed with forceps. Aquapolymount medium was added to the isolated imaginal discs and samples were mounted with a cover slide and dried over night at 4 °C.

6.2.5.5 Thorax muscle fixation and immunostaining

For every staining, 7 – 10 thoraces were prepared by removing head, legs and abdomen from anesthetized flies. The samples were collected in a reaction tube on ice. Fixation was achieved by incubating thoraces with 4% formaldehyde in 1 x PBS/0.3% Triton X-100 for 20 minutes at room temperature under constant shaking. Samples were washed two times with 1x PBS for 5 minutes each and transferred to sticky tape with the ventral side

up. Muscle tissue was deposited by cutting thoraces midsagittally. The thorax halves were transferred back to a 500 µl reaction tube and blocked with 5% BSA in 1x PBS/0.3% Triton X-100 for one hour at room temperature. Antibody stainings were performed as described in 6.2.5.2. This method was modified according to Weitkunat et al., 2014.

6.2.5.6 Phalloidin staining of worms

Worms were collected at the desired developmental stages and washed with M9-Buffer. Permeabilisation took place by freezing worms in liquid nitrogen. The samples were thawed at room temperature and consecutively fixed by methanol and acetone incubation for 5 min at -20 °C each. After incubating worms in blocking solution for 20 min, the samples were stained with fluorescent phalloidin for one hour at room temperature. The samples were washed three times with 1x PBS containing 3% BSA and mounted in 2% of n-propyl galate in glycerol on agarose slides. This method was performed according to established protocols of the Gruenbaum laboratory.

M9 Buffer

KH ₂ PO ₄	22 mM
Na ₂ HPO ₄	42 mM
NaCl	86 mM

Blocking solution

10% milk
3% bovine serum albumin
0.1% Tween20 (v/v)
in 1x PBS

6.2.5.7 Immunostaining of worms

Cleaned slides had to be coated first with 50 – 100 µl of poly Lysine solution (0.1% v/v). After 30 min of incubation, excess solution was removed and slides were let to dry completely. Around 20 worms of the desired stage were transferred by a platinum wire to a drop of 10 µl of M9 buffer which was placed on the poly lysine area. Afterwards a 24 x 50 mm cover slip was placed perpendicular to the slide. To break nematodes tissue, gentle pressure was given at the slide edges. The samples were following frozen by liquid nitrogen and the cover slip was removed afterwards. Fixation was done successively by

methanol and acetone incubation each for 15 min at -20 °C. Remaining's of fixation solution was removed by a washing step with 1x PBS/0.01% Tween20 (PBS-T) for 10 min at room temperature. The worm samples were then blocked in 1x PBS/0.1% milk solution for 15 min at room temperature. Antibody staining was performed by pipetting 50 µl of the diluted antibody to the sample, covering it with parafilm and incubating at 4 °C for overnight in a humidity chamber. The glass slides were then quickly washed in 1x PBS to carefully remove the parafilm. Three washing steps in 1x PBS each for 20 min followed. Then, 50 µl of the diluted secondary antibody were pipetted to the samples. The samples were covered with parafilm and incubation took place for 3 hours at room temperature in a humidity chamber. Washing steps were repeated and DAPI (1:1.000, 1 mg/ml) staining was performed by pipetting 100 µl of to the samples and incubating it for 10 min at room temperature. The sample were finally incubated for at least 10 min in 1x PBS and mounted in a drop of 2% n-propyl galate in glycerol on agarose slides. This method was performed according to established protocols of the Gruenbaum laboratory.

6.2.6 Fly work methods

6.2.6.1 Wing preparation

To study gain-of-function and loss-of-function effects on wing development, wings were removed from the adult fly body and mounted into a medium consisting of Hoyers medium and lactate acid in a 1:1 ratio. The samples were incubated overnight at a temperature of 50 °C and analyzed.

6.2.6.2 Lifespan

To analyze the lifespan of a distinct fly population newly hatched male flies were collected every 2 - 3 days. For each genotype, three to four replicates with each ~ 75 males were collected under short anesthesia and transferred to a fly cage with a filter. Cages were closed with plates containing fly food. Induction with the GeneSwitch system was carried out by adding additional mifepriston (RU-486) with concentrations ranging from 2 to 200 µM directly to fly food. Fly cages were kept at 25 °C with a humidity of 70% and a day/night cycle of 12 hours. New fly food was provided every 2 - 3 days and death events were counted at the same time. Escaped flies were noted as censored. Survival data were analyzed by using OASIS (Yang et al., 2011) an online application tool for survival analysis

(log-rank test) and data were illustrated by using GraphPad Prism6. Lifespan assays were performed according to Brandt et al., 2008.

6.2.6.3 Negative geotaxis

To analyze climbing behavior over time newly hatched male flies (0 – 3 days) were collected and kept in cage at 25 °C with a humidity of 70% and a day/night cycle of 12 hours during experimental analysis. The climbing assay was performed once a week. Therefore, 25 males were shortly anesthetized and transferred individually to vertical climbing tubes. After flies were completely awake, males were tapped to the bottom and immediately 10 s test time started. Climbing high was noted and measurements were repeated 3 - 4 times for each fly. Mean values were determined and the climbing high of control flies in the first week was set as 100% negative geotaxis. This method was performed according to Gargano et al., 2005.

6.2.6.4 Survival rate assay

Flies were kept at 25 °C. 100 embryos of each genotype were collected without dechorionization and transferred to fresh apple-juice plates coated with yeast. To distinguish between homozygous and heterozygous genotypes an embryo sorting, based on GFP expression, was performed if necessary. Hatched L1 larvae were counted and moved to fly food vials where following pupae and hatched adults were counted as well. Finally, percentage of the survival rate during development was analyzed.

6.2.6.5 Microinjection of *Drosophila* embryos

Early w1118 embryos were collected, dechorionated, arranged in line and transferred to a cover slide with n-Heptane. The embryos were incubated for 7 min in a desiccation chamber and subsequently covered with 10S VoltaLef oil. An injection mix, consisting of the desired DNA and a helper plasmid with a 3:1 ratio, was prepared and injected into the posterior pole of the embryos with a final concentration of 0,3 – 0,8 µg/µl. Injected embryos were transferred to a humidity chamber and kept at 18°C. First larvae were collected, transferred to normal fly food vials and G0 - flies were separately crossed to w1118 flies. Offsprings were scored for red eyes and individual white⁺ flies were used to establish transgenic fly lines.

For site specific integration, a vector, containing the desired DNA and an attP site, were injected in a final concentration of 0.1 µg/ul to embryos containing a genomic attB-site.

6.2.7 Worm work methods

Worm work methods were performed according to Dobrzynska et al., 2016, unless otherwise stated.

6.2.7.1 Synchronizing worms

Worms carrying embryos were collected by washing NGM plates with M9-buffer. Animals were washed 2-3 times by spinning them down (2.500 xg) and adding new M9 buffer. The supernatant was removed and replaced by bleach solution. The worms were opened by vortexing for around 4 min. In order to remove the bleach solution, worms were washed up to 5 times with M9 buffer. Embryos were spinned down (16.000 xg) and collected in 20 – 50 µl of M9-buffer. About 10 µl were subsequently seeded per NGM or feeding plate. If it was necessary to synchronize worms to L1 stage, eggs were transferred into a 4 ml M9-buffer containing 15 ml falcon and incubated over night at 20 °C. L1 worms were collected and transferred to plates.

Bleach solution

2 Volumes Water

1 Volume Sodium Hypochlorite Solution (15%)

6.2.7.2 Oxygen sensitivity assay

Worm eggs were isolated and cultured on OP50 seeded NGM plates and incubated for 5 days in the presence of 75% of oxygen at 20 °C. Control worms were grown under normoxic conditions. Afterwards the developmental stages of the hatched worms were determined. This method was performed according to Fujii et al., 2009.

6.2.7.3 Time course analysis

To analyze worm development under distinct conditions, nematodes were first synchronized to L1 stage (6.2.7.1), transferred to either NGM or RNAi plates and grown for three days at 20 °C. At different time points, worms were taken for microscopic analysis. To prevent strong nematode movement, worms were mounted in levamisol (2 mM). Worm length was measured by using ImageJ and the data analysis was performed with GraphPad Prism6.

6.2.7.4 Pumping experiment

For studying pumping rates, worm eggs were isolated and grown on OP50 seeded NGM plates at 20 °C until they reached adulthood. Plates were changed regularly in between. At day 1, 3 and 5 of adulthood, 30 worms were equally distributed to new NGM plates and the grinder movement of the terminal bulb within the worm pharynx was counted for one minute under binocular observation. This assay was performed according to Raizen et al., 2005.

6.2.7.5 Lifespan assay

Worms were bleached and isolated eggs were transferred to RNAi plates seeded with oxy-4 RNAi, lmn-1 RNAi or L4440 (empty vector) expressing bacteria. Approximately 100 L4 larvae were separated with ongoing RNAi treatment and survival rate was determined every second day. Animals were considered as dead when they did not longer react after gently touching with a platinum wire. Dead and missing worms were considered as censored. Lifespan analysis were performed at 20 °C.

6.2.7.6 Microinjection of *C.elegans*

To fix worms for injection procedure, agarose pads were prepared. Therefore 2% of agarose were dissolved in water, boiled and 100 µl of hot agarose were placed to a glass slide and quickly covered by a cover slip. The agarose was let solidify and prepared slides were stored till usage.

For the generation of transgenic worms, young hermaphrodites were picked and transformed to the agarose pads and the worms were covered with halocarbon oil 700 to prevent drying. Afterwards, an injection-mix, consisting of a visible marker and the desired DNA was injected into one or both of the gonad arms. The concentrations were ranging from 5 ng/µl – 125 ng/µl for Baf-1P-GFP oxy-4 and 10 ng/µl – 100 ng/µl for the marker. The injected worms were recovered and released from the agarose pad by adding a drop of M9 buffer and transferred separately to a fresh NGM plate using a platinum wire. The worms were grown at 20 °C and the offspring were scored by fluorescence for successful injection.

6.2.8 Microscopy

6.2.8.1 Fluorescence recovery after photobleaching (FRAP)

In order to determine the turnover rate of GFP-Kuk (C567S) under control of the endogenous promoter, a circular area at the surface of GFP expressing embryos during

cellularization was bleached using 100% laser power, 15 iterations at a scan speed of 6. To compare GFP-Kuk and a non-farnesylable mutant GFP-kukC567S, embryos at a similar stage of cellularization were chosen. Fluorescence of two areas outside and one area inside of the bleached region were measured to determine the background signal. Subsequent analysis was done by using ImageJ.

7 References

- Araújo, Ana Rita; Reis, Micael; Rocha, Helder; Aguiar, Bruno; Morales-Hojas, Ramiro; Macedo-Ribeiro, Sandra et al. (2013): The *Drosophila melanogaster* methuselah gene. A novel gene with ancient functions. In: *PloS one* 8 (5), e63747.
- Bahadorani, Sepehr; Hur, Jae H.; Lo Jr, Thomas; Vu, Kevin; Walker, David W. (2010): Perturbation of mitochondrial complex V alters the response to dietary restriction in *Drosophila*. In: *Aging cell* 9 (1), S. 100–103.
- Balk, J.; Pierik, A. J.; Netz, D. AguilarJ; Mühlenhoff, U.; Lill, R. (2005): Nar1p, a conserved eukaryotic protein with similarity to Fe-only hydrogenases, functions in cytosolic iron-sulphur protein biogenesis: Portland Press Limited.
- Balk, Janneke; Pierik, Antonio J.; Netz, Daili J Aguilar; Mühlenhoff, Ulrich; Lill, Roland (2004): The hydrogenase-like Nar1p is essential for maturation of cytosolic and nuclear iron-sulphur proteins. In: *The EMBO journal* 23 (10), S. 2105–2115.
- Bank, Erin M.; Ben-Harush, Kfir; Feinstein, Naomi; Medalia, Ohad; Gruenbaum, Yosef (2012): Structural and physiological phenotypes of disease-linked lamin mutations in *C. elegans*. In: *Journal of Structural Biology* 177 (1), S. 106–112.
- Bar, Daniel Z.; Gruenbaum, Yosef (2010): Reversal of age-dependent nuclear morphology by inhibition of prenylation does not affect lifespan in *Caenorhabditis elegans*. In: *Nucleus* 1 (6), S. 499–505.
- Bar, Daniel Z.; Neufeld, Ester; Feinstein, Naomi; Gruenbaum, Yosef (2009): Gliotoxin reverses age-dependent nuclear morphology phenotypes, ameliorates motility, but fails to affect lifespan of adult *Caenorhabditis elegans*. In: *Cell motility and the cytoskeleton* 66 (10), S. 791–797.
- Barton, Racine M.; Worman, Howard J. (1999): Prenylated prelamin A interacts with Narf, a novel nuclear protein. In: *Journal of Biological Chemistry* 274 (42), S. 30008–30018.
- Beumer, Kelly J.; Trautman, Jonathan K.; Mukherjee, Kusumika; Carroll, Dana (2013): Donor DNA utilization during gene targeting with zinc-finger nucleases. In: *G3: Genes, Genomes, Genetics* 3 (4), S. 657–664.

Bischof, Johannes; Björklund, Mikael; Furger, Edy; Schertel, Claus; Taipale, Jussi; Basler, Konrad (2013): A versatile platform for creating a comprehensive UAS-ORFeome library in *Drosophila*. In: *Development* 140 (11), S. 2434–2442.

Bischof, Johannes; Maeda, Robert K.; Hediger, Monika; Karch, François; Basler, Konrad (2007): An optimized transgenesis system for *Drosophila* using germ-line-specific φ C31 integrases. In: *Proceedings of the National Academy of Sciences* 104 (9), S. 3312–3317.

Biteau, Benoit; Karpac, Jason; Supoyo, Stephen; DeGennaro, Matthew; Lehmann, Ruth; Jasper, Heinrich (2010): Lifespan extension by preserving proliferative homeostasis in *Drosophila*. In: *PLoS genetics* 6 (10), e1001159.

Bossie, Cynthia A.; Sanders, Marilyn M. (1993): A cDNA from *Drosophila melanogaster* encodes a lamin C-like intermediate filament protein. In: *Journal of Cell Science* 104 (4), S. 1263–1272.

Brandt, Annely; Krohne, Georg; Großhans, Jörg (2008): The farnesylated nuclear proteins KUGELKERN and LAMIN B promote aging-like phenotypes in *Drosophila* flies. In: *Aging cell* 7 (4), S. 541–551.

Brandt, Annely; Papagiannouli, Fani; Wagner, Nicole; Wilsch-Bräuninger, Michaela; Braun, Martina; Furlong, Eileen E. et al. (2006): Developmental control of nuclear size and shape by Kugelkern and Kurzkern. In: *Current biology* 16 (6), S. 543–552.

Brandt, Annely; Vilcinskas, Andreas (2013): The fruit fly *Drosophila melanogaster* as a model for aging research. In: *Yellow Biotechnology I: Springer*, S. 63–77.

Brent, Roger; Ptashne, Mark (1985): A eukaryotic transcriptional activator bearing the DNA specificity of a prokaryotic repressor. In: *Cell* 43 (3), S. 729–736.

Broers, J. L.V.; Ramaekers, F. C.S.; Bonne, G.; Yaou, R. Ben; Hutchison, C. J. (2006): Nuclear lamins. Laminopathies and their role in premature aging. In: *Physiological Reviews* 86 (3), S. 967–1008.

Bruick, Richard K.; McKnight, Steven L. (2001): A conserved family of prolyl-4-hydroxylases that modify HIF. In: *Science* 294 (5545), S. 1337–1340.

Capell, Brian C.; Erdos, Michael R.; Madigan, James P.; Fiordalisi, James J.; Varga, Renee; Conneely, Karen N. et al. (2005): Inhibiting farnesylation of progerin prevents the

characteristic nuclear blebbing of Hutchinson-Gilford progeria syndrome. In: *Proceedings of the National Academy of Sciences of the United States of America* 102 (36), S. 12879–12884.

Cavazza, Christine; Martin, Lydie; Mondy, Samuel; Gaillard, Jacques; Ratet, Pascal; Fontecilla-Camps, Juan C. (2008): The possible role of an [FeFe]-hydrogenase-like protein in the plant responses to changing atmospheric oxygen levels. In: *Journal of inorganic biochemistry* 102 (5), S. 1359–1365.

Chevallier, Philippe (1993): Pest sequences in nuclear proteins. In: *International journal of biochemistry* 25 (4), S. 479–482.

Chung, Henry; Sztal, Tamar; Pasricha, Shivani; Sridhar, Mohan; Batterham, Philip; Daborn, Phillip J. (2009): Characterization of *Drosophila melanogaster* cytochrome P450 genes. In: *Proceedings of the National Academy of Sciences* 106 (14), S. 5731–5736.

Copeland, Jeffrey M.; Cho, Jaehyoung; Lo, Thomas; Hur, Jae H.; Bahadorani, Sepehr; Arabyan, Tagui et al. (2009): Extension of *Drosophila* life span by RNAi of the mitochondrial respiratory chain. In: *Current Biology* 19 (19), S. 1591–1598.

Corbin, Monique V.; Rockx, Davy A. P.; Oostra, Anneke B.; Joenje, Hans; Dorsman, Josephine C. (2015): The iron-sulfur cluster assembly network component NARFL is a key element in the cellular defense against oxidative stress. In: *Free Radical Biology and Medicine* 89, S. 863–872.

Coulthard, Alistair B.; Alm, Christina; Cealiac, Iulia; Sinclair, Don A.; Honda, Barry M.; Rossi, Fabrizio et al. (2010): Essential loci in centromeric heterochromatin of *Drosophila melanogaster*. I: the right arm of chromosome 2. In: *Genetics* 185 (2), S. 479–495.

Dechat, Thomas; Adam, Stephen A.; Taimen, Pekka; Shimi, Takeshi; Goldman, Robert D. (2010): Nuclear lamins. In: *Cold Spring Harbor perspectives in biology* 2 (11), a000547.

Dechat, Thomas; Pfliegerhaa, Katrin; Sengupta, Kaushik; Shimi, Takeshi; Shumaker, Dale K.; Solimando, Liliana; Goldman, Robert D. (2008): Nuclear lamins. Major factors in the structural organization and function of the nucleus and chromatin. In: *Genes & development* 22 (7), S. 832–853.

Dechat, Thomas; Shimi, Takeshi; Adam, Stephen A.; Rusinol, Antonio E.; Andres, Douglas A.; Spielmann, H. Peter et al. (2007): Alterations in mitosis and cell cycle progression caused

by a mutant lamin A known to accelerate human aging. In: *Proceedings of the National Academy of Sciences* 104 (12), S. 4955–4960.

Dialynas, George; Shrestha, Om K.; Ponce, Jessica M.; Zwerger, Monika; Thiemann, Dylan A.; Young, Grant H. et al. (2015): Myopathic lamin mutations cause reductive stress and activate the nrf2/keap-1 pathway. In: *PLoS genetics* 11 (5), e1005231.

Dobrzynska, Agnieszka; Askjaer, Peter; Gruenbaum, Yosef (2016): Chapter Twenty-Two-Lamin-Binding Proteins in *Caenorhabditis elegans*. In: *Methods in enzymology* 569, S. 455–483.

Dong, Jinsheng; Lai, Ruby; Nielsen, Klaus; Fekete, Christie A.; Qiu, Hongfang; Hinnebusch, Alan G. (2004): The essential ATP-binding cassette protein RLI1 functions in translation by promoting preinitiation complex assembly. In: *Journal of Biological Chemistry* 279 (40), S. 42157–42168.

Eckersley-Maslin, Melanie A.; Bergmann, Jan H.; Lazar, Zsolt; Spector, David L. (2013): Lamin A/C is expressed in pluripotent mouse embryonic stem cells. In: *nucleus* 4 (1), S. 53–60.

Erber, Andreas; Riemer, Dieter; Hofemeister, Helmut; Bovenschulte, Marc; Stick, Reimer; Panopoulou, Georgia et al. (1999): Characterization of the Hydra lamin and its gene. A molecular phylogeny of metazoan lamins. In: *Journal of molecular evolution* 49 (2), S. 260–271.

Eriksson, Maria; Brown, W. Ted; Gordon, Leslie B.; Glynn, Michael W.; Singer, Joel; Scott, Laura et al. (2003): Recurrent de novo point mutations in lamin A cause Hutchinson-Gilford progeria syndrome.

Fields, Stanley; Song, Ok-kyu (1989): A novel genetic system to detect protein-protein interactions. In: *Nature* 340 (6230), S. 245–246.

Fujii, Michihiko; Adachi, Noritaka; Shikatani, Kazuki; Ayusawa, Dai (2009): [FeFe]-hydrogenase-like gene is involved in the regulation of sensitivity to oxygen in yeast and nematode. In: *Genes to Cells* 14 (4), S. 457–468.

Gargano, Julia Warner; Martin, Ian; Bhandari, Poonam; Grotewiel, Michael S. (2005): Rapid iterative negative geotaxis (RING). A new method for assessing age-related locomotor decline in *Drosophila*. In: *Experimental gerontology* 40 (5), S. 386–395.

- Gari, Kerstin; Ortiz, Ana María León; Borel, Valérie; Flynn, Helen; Skehel, J. Mark; Boulton, Simon J. (2012): MMS19 links cytoplasmic iron-sulfur cluster assembly to DNA metabolism. In: *Science* 337 (6091), S. 243–245.
- Gilchrist, Susan; Gilbert, Nick; Perry, Paul; Östlund, Cecilia; Worman, Howard J.; Bickmore, Wendy A. (2004): Altered protein dynamics of disease-associated lamin A mutants. In: *BMC cell Biology* 5 (1), S. 46.
- Gonzalez-Suarez, Ignacio; Redwood, Abena B.; Gonzalo, Susana (2009): Loss of A-type lamins and genomic instability. In: *Cell Cycle* 8 (23), S. 3860–3865. In: *PNAS* 109 (41), S. 16666-16671.
- Gordon, L. B., Kleinman, M. E., Miller, D. T., Neuberg, D. S., et al. (2013). Clinical trial of a farnesyltransferase inhibitor in children with Hutchinson-Gilford progeria syndrome.
- Gosh, S. and Zhou, Z. (2014) Genetics of aging, progeria and lamin disorders. *Curr Opin Genet Dev.* 26, S. 41-46.
- Gratz, Scott J.; Ukken, Fiona P.; Rubinstein, C. Dustin; Thiede, Gene; Donohue, Laura K.; Cummings, Alexander M.; O'Connor-Giles, Kate M. (2014): Highly specific and efficient CRISPR/Cas9-catalyzed homology-directed repair in *Drosophila*. In: *Genetics* 196 (4), S. 961–971.
- Gruenbaum, Yosef; Foisner, Roland (2015): Lamins. Nuclear intermediate filament proteins with fundamental functions in nuclear mechanics and genome regulation. In: *Annu. Rev. Biochem.* 84, S. 131–164.
- Gruenbaum, Yosef; Goldman, Robert D.; Meyuhas, Ronit; Mills, Erez; Margalit, Ayelet; Fridkin, Alexandra et al. (2003): The nuclear lamina and its functions in the nucleus. In: *International review of cytology* 226, S. 1–62.
- Gruenbaum, Yosef; Landesman, Yosef; Drees, Barry; Bare, John W.; Saumweber, Harald; Paddy, Michael R. et al. (1988): *Drosophila* nuclear lamin precursor Dm0 is translated from either of two developmentally regulated mRNA species apparently encoded by a single gene. In: *The Journal of cell biology* 106 (3), S. 585–596.
- Hackstein, J. H.P. (2005): Eukaryotic Fe-hydrogenases-old eukaryotic heritage or adaptive acquisitions?: Portland Press Limited.

- Haithcock, Erin; Dayani, Yaron; Neufeld, Ester; Zahand, Adam J.; Feinstein, Naomi; Mattout, Anna et al. (2005): Age-related changes of nuclear architecture in *Caenorhabditis elegans*. In: *Proceedings of the National Academy of Sciences of the United States of America* 102 (46), S. 16690–16695.
- He, Ying; Jasper, Heinrich (2014): Studying aging in *Drosophila*. In: *Methods* 68 (1), S. 129–133.
- Huang, Jianhe; Song, Daisheng; Flores, Adrian; Zhao, Quan; Mooney, Sharon M.; Shaw, Leslie M.; Lee, Frank S. (2007): IOP1, a novel hydrogenase-like protein that modulates hypoxia-inducible factor-1 α activity. In: *Biochemical Journal* 401 (1), S. 341–352.
- Ivan, Mircea; Kondo, Keiichi; Yang, Haifeng; Kim, William; Valiando, Jennifer; Ohh, Michael et al. (2001): HIF α targeted for VHL-mediated destruction by proline hydroxylation: implications for O₂ sensing. In: *Science* 292 (5516), S. 464–468.
- Jaakkola, Panu; Mole, David R.; Tian, Ya-Min; Wilson, Michael I.; Gielbert, Janine; Gaskell, Simon J. et al. (2001): Targeting of HIF α to the von Hippel-Lindau ubiquitylation complex by O₂-regulated prolyl hydroxylation. In: *Science* 292 (5516), S. 468–472.
- Jain, Ashish; Lamark, Trond; Sjøttem, Eva; Larsen, Kenneth; Bowitz, Awuh, Jane Atesoh; Øvervatn, Aud et al. (2010): p62/SQSTM1 is a target gene for transcription factor NRF2 and creates a positive feedback loop by inducing antioxidant response element-driven gene transcription. In: *Journal of Biological Chemistry* 285 (29), S. 22576–22591.
- Jiang, Huaqi; Patel, Parthiv H.; Kohlmaier, Alexander; Grenley, Marc O.; McEwen, Donald G.; Edgar, Bruce A. (2009): Cytokine/Jak/Stat signaling mediates regeneration and homeostasis in the *Drosophila* midgut. In: *Cell* 137 (7), S. 1343–1355.
- Jinek, Martin; Chylinski, Krzysztof; Fonfara, Ines; Hauer, Michael; Doudna, Jennifer A.; Charpentier, Emmanuelle (2012): A programmable dual-RNA-guided DNA endonuclease in adaptive bacterial immunity. In: *Science* 337 (6096), S. 816–821.
- Johnson, Deborah C.; Dean, Dennis R.; Smith, Archer D.; Johnson, Michael K. (2005): Structure, function, and formation of biological iron-sulfur clusters. In: *Annu. Rev. Biochem.* 74, S. 247–281.

Kispal, Gyula; Sipos, Katalin; Lange, Heike; Fekete, Zsuzsanna; Bedekovics, Tibor; Janáky, Tamás et al. (2005): Biogenesis of cytosolic ribosomes requires the essential iron-sulphur protein Rli1p and mitochondria. In: *The EMBO journal* 24 (3), S. 589–598.

Kitten, G. T.; Nigg, E. A. (1991): The CaaX motif is required for isoprenylation, carboxyl methylation, and nuclear membrane association of lamin B2. In: *The Journal of cell biology* 113 (1), S. 13–23.

Kolb, Thorsten; Maaß, Kendra; Hergt, Michaela; Aebi, Ueli; Herrmann, Harald (2011): Lamin A and lamin C form homodimers and coexist in higher complex forms both in the nucleoplasmic fraction and in the lamina of cultured human cells. In: *nucleus* 2 (5), S. 425–433.

Komatsu, Masaaki; Kurokawa, Hirofumi; Waguri, Satoshi; Taguchi, Keiko; Kobayashi, Akira; Ichimura, Yoshinobu et al. (2010): The selective autophagy substrate p62 activates the stress responsive transcription factor Nrf2 through inactivation of Keap1. In: *Nature cell biology* 12 (3), S. 213–223.

Kondo, Shu; Ueda, Ryu (2013): Highly improved gene targeting by germline-specific Cas9 expression in *Drosophila*. In: *Genetics* 195 (3), S. 715–721.

Krohne, G. (1998): Lamin assembly in vivo. In: *Sub-cellular biochemistry* 31, S. 563–586.

Lieber, Michael R. (2010): The mechanism of double-strand DNA break repair by the nonhomologous DNA end-joining pathway. In: *Annu. Rev. Biochem.* 79, S. 181–211.

Lill, Roland (2009): Function and biogenesis of iron-sulphur proteins. In: *Nature* 460 (7257), S. 831–838.

Lin, Yi-Jyun; Seroude, Laurent; Benzer, Seymour (1998): Extended life-span and stress resistance in the *Drosophila* mutant methuselah. In: *Science* 282 (5390), S. 943–946.

Liu, Yiyong; Rusinol, Antonio; Sinensky, Michael; Wang, Youjie; Zou, Yue (2006): DNA damage responses in progeroid syndromes arise from defective maturation of prelamin A. In: *J Cell Sci* 119 (22), S. 4644–4649.

Loboda, Agnieszka; Damulewicz, Milena; Pyza, Elzbieta; Jozkowicz, Alicja; Dulak, Jozef (2016): Role of Nrf2/HO-1 system in development, oxidative stress response and diseases. An evolutionarily conserved mechanism. In: *Cellular and Molecular Life Sciences* 73 (17), S. 3221–3247.

- McClintock, Dayle; Ratner, Desiree; Lokuge, Meepa; Owens, David M.; Gordon, Leslie B.; Collins, Francis S.; Djabali, Karima (2007): The mutant form of lamin A that causes Hutchinson-Gilford progeria is a biomarker of cellular aging in human skin. In: *PLoS One* 2 (12), e1269.
- Mendoza, Alexandre de; Jones, Jeffery W.; Friedrich, Markus (2016): Methuselah/Methuselah-like G protein-coupled receptors constitute an ancient metazoan gene family. In: *Scientific reports* 6.
- Meneely, Philip (2014): Genetic Analysis: Genes, Genomes, and Networks in Eukaryotes: Oxford University Press.
- Misra, Jyoti R.; Horner, Michael A.; Lam, Geanette; Thummel, Carl S. (2011): Transcriptional regulation of xenobiotic detoxification in *Drosophila*. In: *Genes & development* 25 (17), S. 1796–1806.
- Moir, Robert D.; Yoon, Miri; Khuon, Satya; Goldman, Robert D. (2000): Nuclear Lamins a and B1. In: *The Journal of cell biology* 151 (6), S. 1155–1168.
- Mondy, Samuel; Lenglet, Aurore; Cosson, Viviane; Pelletier, Sandra; Pateyron, Stéphanie; Gilard, Françoise et al. (2014): GOLLUM [FeFe]-hydrogenase-like proteins are essential for plant development in normoxic conditions and modulate energy metabolism. In: *Plant, cell & environment* 37 (1), S. 54–69.
- Motohashi, Hozumi; Yamamoto, Masayuki (2004): Nrf2-Keap1 defines a physiologically important stress response mechanism. In: *Trends in molecular medicine* 10 (11), S. 549–557.
- Moulson, Casey L.; Fong, Loren G.; Gardner, Jennifer M.; Farber, Emily A.; Go, Gloriosa; Passariello, Annalisa et al. (2007): Increased progerin expression associated with unusual LMNA mutations causes severe progeroid syndromes. In: *Human mutation* 28 (9), S. 882–889.
- Muñoz-Alarcón, Andrés; Pavlovic, Maja; Wismar, Jasmine; Schmitt, Bertram; Eriksson, Maria; Kylsten, Per; Dushay, Mitchell S. (2007): Characterization of lamin mutation phenotypes in *Drosophila* and comparison to human laminopathies. In: *PLoS One* 2 (6), e532.
- Nakamura, Miyuki; Buzas, Diana Mihaela; Kato, Akira; Fujita, Masahiro; Kurata, Nori; Kinoshita, Tetsu (2013): The role of *Arabidopsis thaliana* NAR1, a cytosolic iron-sulfur

cluster assembly component, in gametophytic gene expression and oxidative stress responses in vegetative tissue. In: *New Phytologist* 199 (4), S. 925–935.

Nicholson, Louise; Singh, Gunisha K.; Osterwalder, Thomas; Roman, Gregg W.; Davis, Ronald L.; Keshishian, Haig (2008): Spatial and temporal control of gene expression in *Drosophila* using the inducible GeneSwitch GAL4 system. I. Screen for larval nervous system drivers. In: *Genetics* 178 (1), S. 215–234.

Nicolet, Yvain; Cavazza, Christine; Fontecilla-Camps, J. C. (2002): Fe-only hydrogenases: structure, function and evolution. In: *Journal of inorganic biochemistry* 91 (1), S. 1–8.

Pendás, Alberto M.; Zhou, Zhongjun; Cadiñanos, Juan; Freije, José M. P.; Wang, Jianming; Hultenby, Kjell et al. (2002): Defective prelamin A processing and muscular and adipocyte alterations in *Zmpste24* metalloproteinase-deficient mice. In: *Nature genetics* 31 (1), S. 94–99.

Pesavento, Patricia A.; Stewart, Russell J.; Goldstein, L. S. (1994): Characterization of the KLP68D kinesin-like protein in *Drosophila*. Possible roles in axonal transport. In: *The Journal of cell biology* 127 (4), S. 1041–1048.

Pollex, R. L.; Hegele, R. A. (2004): Hutchinson-Gilford progeria syndrome. In: *Clinical genetics* 66 (5), S. 375–381.

Progeria Research Foundation (PRF) webpage <http://www.progeriaresearch.org/>

Rahman, Mohammed Mahidur; Sykiotis, Gerasimos P.; Nishimura, Mayuko; Bodmer, Rolf; Bohmann, Dirk (2013): Declining signal dependence of Nrf2-MafS-regulated gene expression correlates with aging phenotypes. In: *Aging cell* 12 (4), S. 554–562.

Raizen, David; Song, Bo-mi; Trojanowski, Nick; You, Young-Jai (2005): Methods for measuring pharyngeal behaviors.

Ray, Krishanu; Perez, Sharon E.; Yang, Zhaohuai; Xu, Jenny; Ritchings, Bruce W.; Steller, Hermann; Goldstein, Lawrence S. B. (1999): Kinesin-II is required for axonal transport of choline acetyltransferase in *Drosophila*. In: *The Journal of cell biology* 147 (3), S. 507–518.

Rechsteiner, Martin; Rogers, Scott W. (1996): PEST sequences and regulation by proteolysis. In: *Trends in biochemical sciences* 21 (7), S. 267–271.

- Riemer, Dieter; Stuurman, Nico; Berrios, Miguel; Hunter, Cecil; Fisher, Paul A.; Weber, Klaus (1995): Expression of Drosophila lamin C is developmentally regulated. Analogies with vertebrate A-type lamins. In: *Journal of Cell Science* 108 (10), S. 3189–3198.
- Rogers, Scott; Wells, Rodney; Rechsteiner, Martin (1986): Amino acid sequences common to rapidly degrade proteins. The PEST hypothesis. In: *Science* 234, S. 364–369.
- Rudolf, Jana; Makrantonis, Vasso; Ingledew, W. John; Stark, Michael, JR; White, Malcolm F. (2006): The DNA repair helicases XPD and FancJ have essential iron-sulfur domains. In: *Molecular cell* 23 (6), S. 801–808.
- Rusiñol, Antonio E.; Sinensky, Michael S. (2006): Farnesylated lamins, progeroid syndromes and farnesyl transferase inhibitors. In: *Journal of Cell Science* 119 (16), S. 3265–3272.
- Salceda, Susana; Caro, Jaime (1997): Hypoxia-inducible Factor 1 α (HIF-1 α) Protein Is Rapidly Degraded by the Ubiquitin-Proteasome System under Normoxic Conditions ITS STABILIZATION BY HYPOXIA DEPENDS ON REDOX-INDUCED CHANGES. In: *Journal of Biological Chemistry* 272 (36), S. 22642–22647.
- Sambrook, Joseph; Russell, David W. (2001): Molecular cloning. A laboratory manual. 2001: Cold Spring Harbor Laboratory Press, Cold Spring Harbor, New York.
- Sandre-Giovannoli, Annachiara de; Bernard, Rafaele; Cau, Pierre; Navarro, Claire; Amiel, Jeanne; Boccaccio, Irene et al. (2003): Lamin a truncation in Hutchinson-Gilford progeria. In: *Science* 300 (5628), S. 2055.
- Scaffidi, Paola; Misteli, Tom (2005): Reversal of the cellular phenotype in the premature aging disease Hutchinson-Gilford progeria syndrome. In: *Nature medicine* 11 (4), S. 440–445.
- Schulze, Sandra R.; Curio-Penny, Beatrice; Speese, Sean; Dialynas, George; Cryderman, Diane E.; McDonough, Caitrin W. et al. (2009): A comparative study of Drosophila and human A-type lamins. In: *PLoS One* 4 (10), e7564.
- Scott, Jeffrey G.; Wen, Zhimou (2001): Cytochromes P450 of insects. The tip of the iceberg. In: *Pest management science* 57 (10), S. 958–967.
- Semenza, Gregg L. (1999): Regulation of mammalian O₂ homeostasis by hypoxia-inducible factor 1. In: *Annual review of cell and developmental biology* 15 (1), S. 551–578.

- Short, Jay M.; Fernandez, Joseph M.; Sorge, Joseph A.; Huse, William D. (1988): λ ZAP. A bacteriophage λ expression vector with in vivo excision properties. In: *Nucleic acids research* 16 (15), S. 7583–7600.
- Sinensky, Michael; Fantle, K.; Trujillo, M.; McLain, T.; Kupfer, A.; Dalton, M. (1994): The processing pathway of prelamin A. In: *Journal of Cell Science* 107 (1), S. 61–67.
- Song, Daisheng; Lee, Frank S. (2008): A role for IOP1 in mammalian cytosolic iron-sulfur protein biogenesis. In: *Journal of Biological Chemistry* 283 (14), S. 9231–9238.
- Song, Daisheng; Lee, Frank S. (2011): Mouse knock-out of IOP1 protein reveals its essential role in mammalian cytosolic iron-sulfur protein biogenesis. In: *Journal of Biological Chemistry* 286 (18), S. 15797–15805.
- Song, Daisheng; Tu, Zheng; Lee, Frank S. (2009): Human ISCA1 interacts with IOP1/NARFL and functions in both cytosolic and mitochondrial iron-sulfur protein biogenesis. In: *Journal of Biological Chemistry* 284 (51), S. 35297–35307.
- Sono, Masanori; Roach, Mark P.; Coulter, Eric D.; Dawson, John H. (1996): Heme-containing oxygenases. In: *Chemical Reviews* 96 (7), S. 2841–2888.
- Stehling, Oliver; Vashisht, Ajay A.; Mascarenhas, Judita; Jonsson, Zophonias O.; Sharma, Tanu; Netz, Daili J. A. et al. (2012): MMS19 assembles iron-sulfur proteins required for DNA metabolism and genomic integrity. In: *Science* 337 (6091), S. 195–199.
- Steinman, Howard M. (1980): The amino acid sequence of copper-zinc superoxide dismutase from bakers' yeast. In: *Journal of Biological Chemistry* 255 (14), S. 6758–6765.
- Sturtz, Lori A.; Diekert, Kerstin; Jensen, Laran T.; Lill, Roland; Culotta, Valeria Cizewski (2001): A fraction of yeast Cu, Zn-superoxide dismutase and its metallochaperone, CCS, localize to the intermembrane space of mitochondria a physiological role for Sod1 in guarding against mitochondrial oxidative damage. In: *Journal of Biological Chemistry* 276 (41), S. 38084–38089.
- Stuurman, Nico; Heins, Susanne; Aebi, Ueli (1998): Nuclear lamins. Their structure, assembly, and interactions. In: *Journal of Structural Biology* 122 (1-2), S. 42–66.
- Sykoti, Gerasimos P.; Bohmann, Dirk (2008): Keap1/Nrf2 signaling regulates oxidative stress tolerance and lifespan in *Drosophila*. In: *Developmental cell* 14 (1), S. 76–85.

- Tijet, Nathalie; Helvig, Christian; Feyereisen, René (2001): The cytochrome P450 gene superfamily in *Drosophila melanogaster*. Annotation, intron-exon organization and phylogeny. In: *Gene* 262 (1), S. 189–198.
- Ullrich N. J., Kieran, M. W., Miller, D. T., Gordon, L. B., et al. (2013). Neurologic features of Hutchinson-Gilford progeria syndrome after lonafarnib treatment. *Neurology* 81 (5), S. 427-430.
- Vidak, Sandra; Foisner, Roland (2016): Molecular insights into the premature aging disease progeria. In: *Histochemistry and cell biology* 145 (4), S. 401–417.
- Weitkunat, Manuela; Schnorrer, Frank (2014): A guide to study *Drosophila* muscle biology. In: *Methods* 68 (1), S. 2–14.
- Wiesel, Naama; Mattout, Anna; Melcer, Shai; Melamed-Book, Naomi; Herrmann, Harald; Medalia, Ohad et al. (2008): Laminopathic mutations interfere with the assembly, localization, and dynamics of nuclear lamins. In: *Proceedings of the National Academy of Sciences* 105 (1), S. 180–185.
- Yamada, Ryuichi; Deshpande, Sonali A.; Keebaugh, Erin S.; Ehrlich, Margaux R.; Soto Obando, Alina; Ja, William W. (2017): Mifepristone reduces food palatability and affects *Drosophila* feeding and lifespan. In: *The Journals of Gerontology: Series A* 72 (2), S. 173–180.
- Yang, Jae-Seong; Nam, Hyun-Jun; Seo, Mihwa; Han, Seong Kyu; Choi, Yonghwan; Nam, Hong Gil et al. (2011): OASIS. Online application for the survival analysis of lifespan assays performed in aging research. In: *PLoS One* 6 (8), e23525.
- Yarunin, Alexander; Panse, Vikram Govind; Petfalski, Elisabeth; Dez, Christophe; Tollervey, David; Hurt, Eduard C. (2005): Functional link between ribosome formation and biogenesis of iron-sulfur proteins. In: *The EMBO journal* 24 (3), S. 580–588.
- Young, S. G., Yang, S. H., Davies, B. S., Jung, H. J., Fong, L. G. (2013) Targeting protein prenylation in progeria. *Sci Transl Med.* 5 (171): 171ps3
- Young, Stephen G.; Fong, Loren G.; Michaelis, Susan; others (2005): Prelamin A, Zmpste24, misshapen cell nuclei, and progeria—new evidence suggesting that protein farnesylation could be important for disease pathogenesis. In: *J Lipid Res* 46 (12), S. 2531–2558.

Young, Stephen G.; Meta, Margarita; Yang, Shao H.; Fong, Loren G. (2006): Prelamin A farnesylation and progeroid syndromes. In: *Journal of Biological Chemistry* 281 (52), S. 39741–39745.

Zaremba-Czogalla, Magdalena; Piekarowicz, Katarzyna; Wachowicz, Katarzyna; Koziół, Katarzyna; Dubińska-Magiera, Magda; Rzepecki, Ryszard (2012): The different function of single phosphorylation sites of *Drosophila melanogaster* lamin Dm and lamin C. In: *PLoS One* 7 (2), e32649.

Zhao, Wei; Fang, Bing Xiong; Niu, Yu Jie; Liu, Yi Na; Liu, Bin; Peng, Qi et al. (2014): Nar1 deficiency results in shortened lifespan and sensitivity to paraquat that is rescued by increased expression of mitochondrial superoxide dismutase. In: *Mechanisms of aging and development* 138, S. 53–58.

Zuela, Noam; Zwerger, Monika; Levin, Tal; Medalia, Ohad; Gruenbaum, Yosef (2016): Impaired mechanical response of an EDMD mutation leads to motility phenotypes that are repaired by loss of prenylation. In: *J Cell Sci* 129 (9), S. 1781–1791.

8 Supplement Data

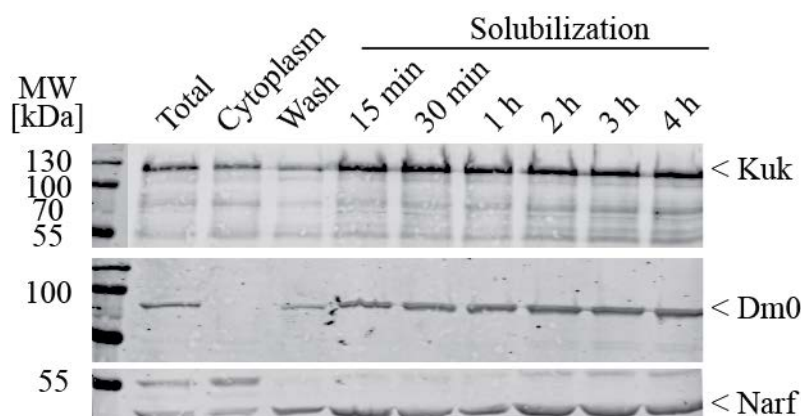
```

ATCACAAAGGTATATTTGAAACAAAAAATTTAAAGATACATATTTATATGACATTTTTATATGTTTCTCGCG
CATTATTTGTTTGTATCCAATTTATTTATTTAGATAACGTTTATTAGTCTTAAATTAGTAGTCAATATTTTC
TACTCAACAAAACCCACAAAAGTCTATAATCACAAAAAATCAGTCAAATGCCATTTAAATAATTGGTTAGAGT
ATGTAGCAATCCGGATAAAGTAAAAATGAACTTTTCGCATTTATCTGGCATCGAGCTGTCTGGGAAAATCCAT
CTCTTGGCATTCTAGACGAATTTCTTCACTTCAGCCcatgatgaaataacataagggtgggcccgctcggcaaga
gacatccacttaacgatgcttgcaataagtgcgagtgaaaggaatagtagtattctgagtgctgattgagctg
agtgagacagcgatgatgattgattgattaacccttagcatgtccgtggggttgaattaactcataagcttggc
tgcaggtcgacctcgagggtaccaatgaacaggacctaacgcacagtcacgttattgtttacataaatgattt
ttttactattcaaaacttactctgtttgtgtactcccactggtagccttcttttatcttttctggttcagg
ctctatcacccggttttcaaaaaaaattcgtccgcacacaacctttcctctcaacaagcaaacgtgcactgaa
ttaaagtgataacttcggtaagcttcggctatcgacgggaccaccttagttatttcatcatgGGCGGGACAA
CGCCTAGTCCAAACGAACAGCGCCTGTCTGAACAACCTTCTCTTCCCCGTGCTGAGCGACATCCAGCGAAAGT
ACTCCGGCGGAGGATCTGCAGGAAGCGGAGGATCAGGCGGCCGTAACATAGGCGTCCGCAGCGACATCCGGCGA
CCTGAAGTCTGTGTTTCGAGCTGGCCGAACGTTCCAGTCCGGGAGTGAGCGACCTATTTATGAAAGAGCTGATC
CACATGCTCGTTCCTGGTTACTCGGAGACGCGAATCAATACGATCATGGACCGCGCCATACGCAACCGCAAGT
AGCTGGCGAAGCCGTAGCAAATTCGATTCCAAGCAGCCTATTTTAATATATACACAACCTTTATTAACGACAC
CGAGACAACACAACTGAAACGCTGGAGCAGACATATTCGACATTTAGTGGCCAACAGAGGACCGGGAGCGA
TGTACATGTATTTCAATTGAACAGTTAT

```

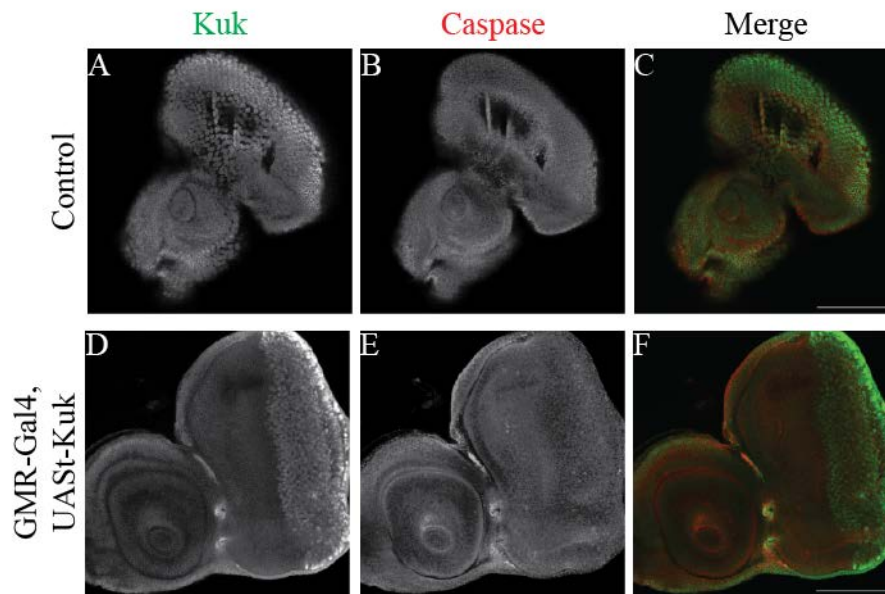
Supplement Figure 1: The deletion of $\Delta 15$ a kuk deficient fly line

The genomic breakpoints of the deletions were analyzed by PCR, including the neighboring genes of *kuk*. Final characterization was done by a long range PCR (MK26/MK29) followed by a subsequent sequencing analysis. The sequencing results revealed a depletion of ~ 5.5 kb within the genomic locus of *kuk* (upper case) and *GckIII* (bold upper case). Furthermore, an insertion of 465 bp (lower case) due to initially performed transposon remobilization was found.

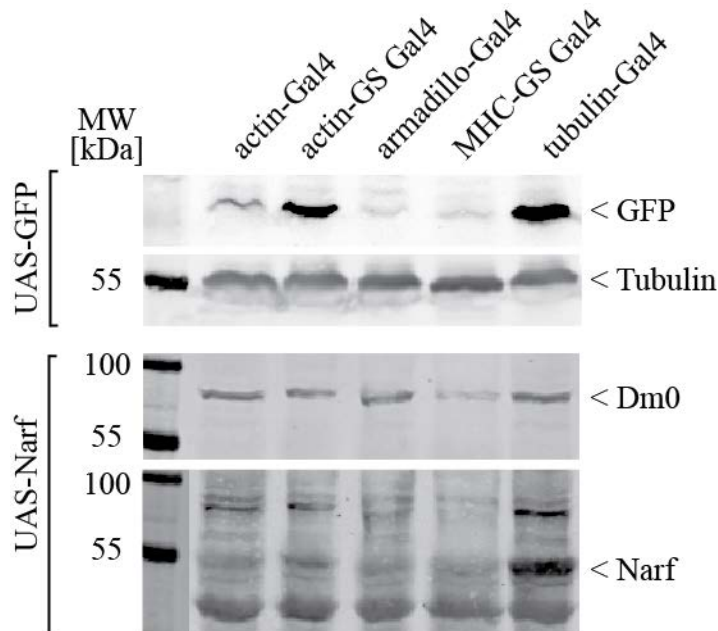


Supplement Figure 2: Kugelkern is stable for at least four hours after solubilization

Western blot analysis of nuclei extract incubated for maximal 4 hours with 150 mM NaCl and 1% TritonX100 for solubilization. A nuclei fractionation with 150 mg wild type embryos was performed and a protein amount of 30 embryos was loaded for the total and the cytoplasm sample. The wash fraction was loaded after protein precipitation with trichloroacetic acid. For each time point after solubilization a sample with a theoretical protein amount of 2.250 embryos was taken and loaded after protein precipitation.

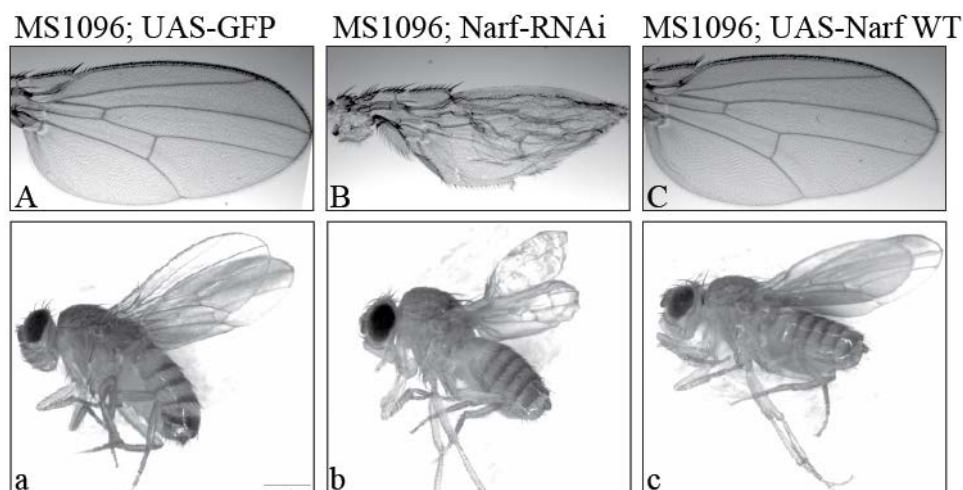


Supplement Figure 3: Kugelkern overexpression did not induce apoptosis in larval eye-discs
 Immunofluorescence stainings for Caspase-3 and Kugelkern in eye-antennal imaginal discs from L3 larvae. Discs from flies expressing GFP-cadherin under the ubiquitin promoter were used as control and stained in the same tube. Eye specific overexpression of Kugelkern elevated Kuk protein level (D) but did not increase the signal for activated Caspase (E) compared to control discs (A and B). Scale bar: 100 μ m

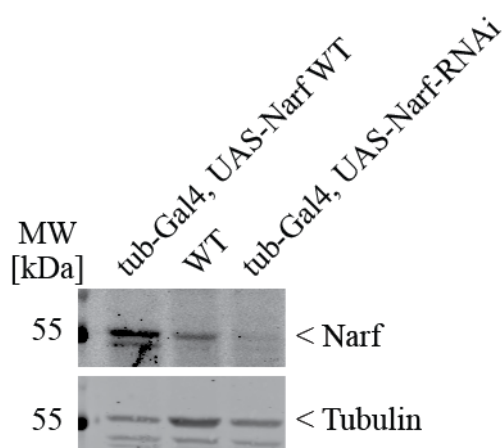


Supplement Figure 4: Strongest Narf expression was achieved using the tubulin-Gal4 driver
 Western blot analyses of total fly extract from GFP and Narf expressing animals controlled by different driver lines. Samples were taken after flies reached day 10 of adulthood. RU-dependent gene expression was induced with 20 μ M of RU for 7 days using 1-3 days old males. The lysate of one fly was loaded and stained for GFP

and Narf. Dm0 and α -tubulin were used as loading controls. The strongest Narf gene expression was achieved using tubulin-Gal4.

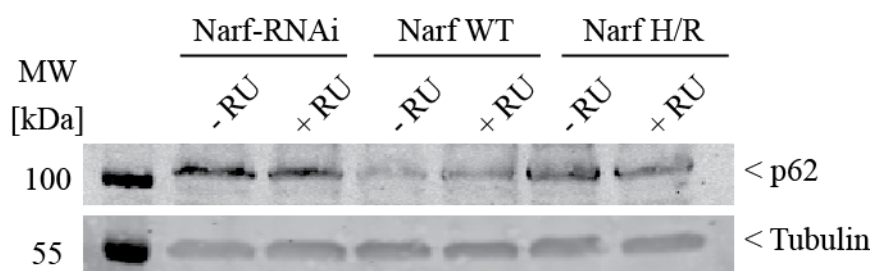


Supplement Figure 5: Wing specific down-regulation of Narf induced morphological defects. Representative wing pictures of flies expressing UAS-GFP (A), Narf-RNAi (B) or UAS-Narf (C) wing specifically controlled by MS1096-Gal4. Expression of a long hairpin structure specific for Narf led to aberrant wing phenotypes (B) compared to GFP expressing control flies (A). An overexpression of Narf had no effects on wing development (C).



Supplement Figure 6: Narf-RNAi efficiently down regulated larval expressed Narf

Western blot analysis of larvae extract stained for Narf and α -tubulin which was used as loading control. Ubiquitous expression of a long hairpin structure specific for Narf efficiently down regulated Narf protein level in L3 larvae compared to the wild type control. However, the larvae extract of the RNAi sample was a mix of RNAi expressing and non-expressing larvae extract as the used tubulin-Gal4 driver line was kept over a non GFP-tagged balancer chromosome. The lysate of 0.75 L3 larva was loaded.



Supplement Figure 7: p62/Ref(2)P protein level is not affected upon altered Narf expression

Western blot analyses of thorax samples from Narf-RNAi or UAS-Narf (WT or H/R) expressing flies controlled by the MHC-GS Gal driver line. The lysate of 1.5 thoraxes was loaded and stained for p62/Ref(2)P and α -tubulin, which was used as loading control. RU-dependent gene expression was induced with 200 μ M of RU for 17 days using 1-3 days old males. In none of the tested situation an increase in protein level for p62 was detected compared to non-induced control flies.

1	MLSKMASNTSGGGGTTSGTGTGRRLPLSLSGGSTVTRLQQSSGSNGRSNSPQNGNKKITE	60
61	SFLPVKKSNQPRTTSTGSGSSQNGVSKPTNGKDKSQNGSSTGKDQKVEKSKDKLPEKKA	120
121	KEVGAENKDKDGAAEMTDMEVVVENKQKEVVSENKQNEVSENKEVVSENKEVVSENKEV	180
181	ASEKKVVVAEVP SDKDDNGETTKDDATVESTAPASQTPADA AVI IDEVVFIPDLSTPTKD	240
	OO	
241	RKSTRKSGSQKSPISKASNAPVQKIKTEAVSSSTSGSLTPQEDVDMEPLQVDASPIRS	300
	+++++	
301	VHGNLNAVPTATSTPGRSLFSFRGSNKQSTEVELAAQTSSSPAGTPARTFAQISGRRSIR	360
	OOOOOOOOOOOOOOOOOOOOOOOO	
361	PIDSLTPSKIGTYRCGNSDLDTSNCTNASMNATVGSEIPNSSSFSFSFFGRGRKRERTPP	420
	OO	OOO
421	PLTASQSTSDLGHDVDMSPPKRARFDLFLSNLASFLLRSRFSKATIGTPTRLRLPEPNS	480
	OOOOOOOOOOOO	OO
		OOOOO
481	SGVEEQHLNTSTTGVPPEEVDVEEQPAEDVTVGQEAGAEIIPAKKDVEDKNVNGQDGDKE	540
	OOOOOO ++++++	O
541	SSDGENIDPVVEVADVA AVAAEGRSIC SIM	570
	OO	

Supplement Figure 8: The amino acid sequence of Kuk contains two potential PEST-motifs

Amino acid analysis of Kugelkern using the software epestfind led to the identification of nine PEST-motifs. Motifs indicated with a score value $> +5$ are potential PEST-sequences and indicated by a (+). PEST-sequences with a score $< +5$ are below the threshold are termed as poor motifs (0). Kugelkern has two potential PEST-motifs with 30 amino acids between position 268 and 299 (PEST score: 7.24) and 36 amino acids between position 487 and 524 (PEST score: 9.56).

```
1  MSSKSRRAGTATPQPGNTSTPRPPSAGPQPPPPSTHSQTASSPLSPTRHSRVAEKVELQN 60
61  LNDRLATYIDRVRNLETENSRLTIEVQTTTRDVTRET'TNIKNIFEELLETRRLDDDTAR 120
121 DRARAEIDIKRLWEENEELKNKLDKKTKECTTAEGNVRMYESRANELNKNYNQANADRKK 180
181  LNEDLNEALKELERLRKQFEETRKNLEQETLSRVDLENTIQSLREELSFKDQIHSQEINE 240
241  SRRIKQTEYSEIDGRLSSEYDAKQSLQELRAQYEEQMQRINDEIQSLYEDKIQRLQEA 300
301  AARTSNSTHKSIEELRSTRVRIDALNANINELEQANADLNARIRDLERQLDNDREHRHGQE 360
361  IDLLEKELIRLREEMTQQKEYQDLMDIKVSLDLEIAAYDKLLVGEEARLNITPATNTAT 420
421  VQSFSQSLRNSTRATPSRRTPSAAVKRKRAVDESEDHSVADYYVSASAKGNVEIKEIDP 480
481  EGKQVRLFNKGSEEVVAIGGWQLQRLINEKGPSTTYKFHRSVRIEPNGVITVWSADTKASH 540
      OOOOOOOOOOOO
541  EPPSSLVMKSQKWVSADNTRTILLNSEGEAVANLDRIKRIVSQHTSSSRLSRRRSVTAVD 600
601  GNEQLYHQGDPPQSNEKCAIM 622
      OOOOOOOOOO
```

Supplement Figure 9: The amino acid sequence of lamin Dm0 contains no potential PEST-motif

Amino acid analysis of lamin Dm0 using the software epestfind led to the identification of two poor PEST-motifs with 14 amino acids between position 522 and 537 (PEST score: -11.79) and 10 amino acids between position 607 and 618 (PEST score -2.64). Both PEST-motifs have a score of $< +5$ and are below the threshold.

Supplement Table: 1: Top 50 candidate list: $\Delta 15$, embryo 6-8 hours

group	gene id	gene name	Chr	function	log2 fold
0	FBgn0051813		.		-26,70
0	FBgn0028855				-23,81
0	FBgn0051300	CG31300	3R	transferase activity, transferring phosphorus-containing groups	-23,75
0	FBgn0033275	CG14756	2R		-12,32
0	FBgn0052475	mthl8	3L	G-protein coupled receptor activity	-11,25
0	FBgn0035208	CG9184	3L		-10,72
0	FBgn0033721	CG13159	2R		-10,57
3	FBgn0039073				-10,54
0	FBgn0052640				-9,99
0	FBgn0035621	CG10591	3L		-9,77
2,4,5	FBgn0036789	AstC-R2	3L	neuropeptide receptor activity	-9,72
3	FBgn0052318	CG32318	3L	ATP binding	-9,20
0	FBgn0261341	verm	3L	protein binding	-9,17
0	FBgn0029728	CG2861	X		-8,70
0	FBgn0037447	Neurochondrin	3R	binding	-8,29
7	FBgn0003710	tipE	3L	plasma membrane	-8,20
0	FBgn0039795	Spn100A	3R	extracellular space	-8,11
3	FBgn0038610	CG7675	3R	oxidoreductase activity	-7,83
0	FBgn0038581	CG14314	3R	transferase activity, transferring phosphorus-containing groups	-7,78
0	FBgn0038476	kuk	3R	lipid particle	-7,60
0	FBgn0035495	CG14989	3L		-7,48
0	FBgn0003382	sha	2R	molecular_function	-7,33
3,7	FBgn0038734				-7,32
0	FBgn0031088	CG15322	X		-7,11
3	FBgn0034756	Cyp6d2	2R	oxidation-reduction process	-6,84
0	FBgn0260874	Ir76a	3L	sensory dendrite	4,91
3,7	FBgn0003996	w	X	transmembrane signaling receptor activity	4,97
2	FBgn0031461	daw	2L	determination of adult lifespan	5,12
2	FBgn0032484	kek4	2L	axonogenesis	5,15
0	FBgn0262104	CG42857	3R	cellular_component	5,18
0	FBgn0265912				5,24
3,4	FBgn0034085	Ptp52F	2R	protein binding	5,24
3,7	FBgn0037973	CG18547	3R	oxidoreductase activity	5,43
0	FBgn0265533				5,45
1,3	FBgn0001149	GstD1	3R	protein binding	6,02
0	FBgn0038294	Mf	3R	chaeta development	7,10
3	FBgn0015038	Cyp9b1	2R	oxidation-reduction process	7,15
0	FBgn0037408	NPFR	3R	integral component of membrane	7,27
6	FBgn0037986	CG14736	3R	membrane	7,50
3,7	FBgn0037975	CG3397	3R	oxidoreductase activity	7,69
2,6	FBgn0031585	CG2955	2L	protein binding	7,70
0	FBgn0051286				7,72
0	FBgn0052010				8,01
0	FBgn0004911				8,06
0	FBgn0267248				8,13
3	FBgn0051683				8,81
0	FBgn0266219				8,91
2,4,5,7	FBgn0038840	CG5621	3R	cell junction	10,17
2	FBgn0052581	CG32581	X	protein binding	10,43
0	FBgn0038718				11,35

Supplement Table: 2: List of commercial available fly-lines used in the RNAi-screen

	name	VDRC		name	VDRC
1	APC1	110290/KK II	69	Lamin Dm0	107419
2	Axs	6137	70	Lamin ds RNA	45635
3	baf	102013	71	lamin ds RNA	107419
4	Bcell associated protein3	KK106452	72	LaminDm0	45635
5	bocksbeutel	24189	73	LAP1	18600/80 II
6	bocksbeutel	24191	74	LAS1	KK105415
7	btz, barensz	38722	75	LBR	39468
8	Caf-1 180	20151	76	LBR	110508/KK II
9	Caf-1, p55	26455	77	Lipin	107707/KK II
10	CdsA	5121	78	Lk6	32885
11	CG12013	100790/KK	79	Mad	12635
12	CG1274	104006/KK	80	Mad	110517/KK II
13	CG13887	106452/KK	81	MAN1	108906/KK II
14	CG14444	110678/KK	82	mbo	47693
15	CG14696	100232/KK	83	msp-300	50192
16	CG16944	104576/KK	84	MSP300	107183/KK
17	CG1742	109140/KK	85	Mtor	24265
18	CG17991	1277	86	Mtor	24265
19	CG31460	103626/KK	87	n.a.	21604
20	CG3149	47560	88	n.a.	1277
21	CG3167	108906/KK	89	Ndc1	3408
22	CG32297	34506	90	Ndc1	101264/KK
23	CG33129	107365/KK	91	Nesprin	107183/KK II
24	CG44154	108236/KK	92	Notch	27229 (80) III
25	CG44254	109119/KK	93	Notch	100002/KK II
26	CG6136	109421/KK	94	Notch	27229
27	CG6743	110759/KK	95	nucleophosmin	KK102920
28	CG6773	110428/KK	96	nucleoplasmin	GD22623
29	CG6961	109951/KK	97	Nup 50	100564
30	CG6962	KK110163	98	Nup107	22407
31	CG7830	105649/KK	99	Nup153	47155
32	CG8111	101348/KK	100	Nup153	2340
33	CG8112	100347/KK	101	Nxt1	52631
34	CG8679	30778	102	Otefin	105308
35	CG8679	30778	103	Otefin	1095308/KK II
36	CG9159	109910/KK	104	p53	38235
37	CG9323	44984	105	p53	10692
38	CG9662	100769/KK	106	p53	38235
39	cup	18179	107	P66 Simyang	13066

Supplement Data

40	Cup	18179	108	p66, simjang	13066
41	Delta	109491/KK II	109	Phosphatidyl- inositolglycan anchor	KK107643
42	Delta	109491	110	picolo	GD44974
43	D-MAN1	11149	111	Pnt	105390/KK
44	dMyc	106066/KK	112	Pontin/Ruv BL1	KK105408
45	dMyc	2947/GD	113	prohibitin	GD12360
46	E(bx)	46645	114	prohibitin 2	GD32361
47	EGFR	107130/KK	115	quemao	47001
48	erlin 2A	GD44273	116	Reptin	KK103483
49	erlin 2B	KK 101392	117	RFC2	KK108452
50	fs(1)YA	12232	118	sbr	32690
51	Fs(2)Ket	22348	119	Scalloped	101497/KK
52	Ftase	47000	120	SHMT	19206
53	Ftase	47001	121	STAT92E	43867
54	GCL	28897	122	Su (H)	103597/KK II
55	GV1	107768	123	Su(var)2-10	30709
56	Hairless	100046	124	Su(Var)3-9	33834
57	Hopscotch	40037	125	Su(Var)3-9	39377
58	HP1aSu(var)2-5	31995	126	TMEM 209	GD45648
59	HP1b	26097	127	TMEM194A	105905
60	HP1c	50520	128	TMEM209	KK105105
61	Hp1c	27782	129	Ugt1	16467
62	iswi	6208	130	Ulp1	31744
63	Klar	32836	131	ulp1	106625
64	Klaroid	3990/80	132	WD repeat 18	KK105616
65	Klaroid	108236/KK	133	Wts	9928/80
66	Klarsicht	32836/80	134	Wts	106174/KK
67	Kuk	106855/KK II	135	Y37H913	21928
68	kuk ds RNA	34959	136	Yortz barentsz	38722

Supplement Table: 3: Top 50 candidate list – Narf WT
MHC-GS Gal4; UAS-Narf WT + 200 μ M RU, Thorax sample 10 d

group	gene_id	gene_name	Chr	function	log2 fold
1	FBgn0262115	CG17683	2R	neurogenesis	7,08
1	FBgn0004034	y	X	cytoplasm	5,24
1	FBgn0033395	Cyp4p2	2R	oxidation-reduction process	4,59
1	FBgn0052640	CG32640	X	response to heat	4,45
0	FBgn0037964	CG14731	3R	metabolic process	3,92
1	FBgn0266310				3,87
1	FBgn0263744				3,70
1	FBgn0262430				3,65
1	FBgn0003082	phr	2R	DNA repair	3,56
1	FBgn0266094				3,53
0	FBgn0267680				3,46
0	FBgn0053160	CG33160	3L	proteolysis	3,40
0	FBgn0262789				3,25
1	FBgn0262386				3,14
0	FBgn0037972	CG10005	3R	cellular_component	3,11
0	FBgn0053159	CG33159	3L	proteolysis	3,07
0	FBgn0004379	Klp67A	3L	mitotic spindle organization	2,98
1	FBgn0032551	CG18636	2L	proteolysis	2,96
1	FBgn0042102	CG18745	3R		2,93
1	FBgn0038353	CG5399	3R		2,93
0	FBgn0262452				2,89
1	FBgn0262413				2,85
0	FBgn0052277	CG32277	3L	proteolysis	2,83
1	FBgn0038391	GATAe	3R	RNA polymerase II transcription factor activity	2,83
0	FBgn0265186	CG44251	2R		2,80
0	FBgn0264569				-2,52
0	FBgn0265949				-2,52
0	FBgn0050287	CG30287	2R	proteolysis	-2,52
0	FBgn0264810	Pburs	2L	G-protein coupled receptor signaling pathway	-2,52
0	FBgn0040261	Ugt36Bb	2L	metabolic process	-2,54
0	FBgn0069354	Porin2	2L	regulation of anion transport	-2,55
1	FBgn0040359	CG11380	X		-2,55
0	FBgn0038191	CG9925	3R	zinc ion binding	-2,58
0	FBgn0032804	CG13081	2L	cellular_component	-2,61
1	FBgn0033628	CG13203	2R		-2,68
0	FBgn0050395	CG30395	2R	molecular_function	-2,74
1	FBgn0265813				-2,88
1	FBgn0039009	CG13842	3R		-2,94
1	FBgn0025776	ind	3L	nucleus	-2,96
1	FBgn0262150	CG42876	2L		-3,11
0	FBgn0031559	CG3513	2L	serine-type endopeptidase inhibitor activity	-3,18
1	FBgn0038315	CG14866	3R	carbohydrate binding	-3,19
1	FBgn0263250	CG43393	2R	cellular_component	-3,41
1	FBgn0053302	Cpr31A	2L	structural constituent of chitin-based cuticle	-3,43
1	FBgn0266156				-3,46
1	FBgn0050121				-3,50
1	FBgn0030105	CG15369	X	cysteine-type endopeptidase inhibitor activity	-3,56

1	FBgn0262721	CG43165	2L	serine-type inhibitor activity	endopeptidase	-3,60
1	FBgn0058469					-5,53
1	FBgn0265912					-6,52

Supplement Table: 4: Top 50 candidate list – Narf H/R
MHC-GS Gal4; UAS-Narf H/R + 200 μ M RU, Thorax sample 10 d

group	gene_id	gene_name	Chr.	function	log2 fold
1	FBgn0262115	CG17683	2R	neurogenesis	6,60
1	FBgn0004034	y	X	cytoplasm	5,68
1	FBgn0033395	Cyp4p2	2R	oxidation-reduction process	4,64
1	FBgn0052640	CG32640	X	response to heat	4,49
1	FBgn0003082	phr	2R	DNA repair	3,71
0	FBgn0026760	Tehao	2L	protein binding	3,71
1	FBgn0266310				3,64
1	FBgn0263744				3,51
0	FBgn0050049	CG30049	2R	cellular_component	3,30
1	FBgn0042102	CG18745	3R		3,26
0	FBgn0013692				3,24
1	FBgn0038353	CG5399	3R		3,22
1	FBgn0262430				3,21
0	FBgn0036419	CG13482	3L		3,12
1	FBgn0266094				3,06
1	FBgn0038391	GATAe	3R	RNA polymerase II transcription factor activity	2,99
0	FBgn0002570	Mal-A1	2R	cation binding	2,97
0	FBgn0040299	Myo28B1	2L	protein binding	2,97
1	FBgn0032551	CG18636	2L	proteolysis	2,94
1	FBgn0262413				2,93
0	FBgn0034294	Muc55B	2R	biological_process	2,88
0	FBgn0040363	CG11384	X	integral component of membrane	2,84
0	FBgn0030756	CG9903	X	membrane	2,81
1	FBgn0262386				2,78
0	FBgn0265104				2,76
0	FBgn0016974				-2,67
1	FBgn0025776	ind	3L	nucleus	-2,67
0	FBgn0083946	lobo	3R	molecular_function	-2,70
1	FBgn0033628	CG13203	2R		-2,70
0	FBgn0036410	CG8100	3L	extracellular region	-2,71
0	FBgn0051025	Ppi1	3R	protein phosphatase 1 binding	-2,71
0	FBgn0039469	TwlC	3R	structural constituent of chitin-based cuticle	-2,73
1	FBgn0262150	CG42876	2L		-2,76
0	FBgn0267728	otk2	2R	protein binding	-2,80
0	FBgn0029848	Btd	X	histone biotinylation	-2,81
0	FBgn0037078	CG12971	3L	cellular_component	-2,88
1	FBgn0030105	CG15369	X	cysteine-type inhibitor activity	endopeptidase -2,90
1	FBgn0039009	CG13842	3R		-2,90
0	FBgn0033597	Cpr47Ea	2R	structural constituent of chitin-based cuticle	-2,91
1	FBgn0262721	CG43165	2L	serine-type inhibitor activity	endopeptidase -2,91
0	FBgn0037323	CG2663	3R	transporter activity	-2,94
1	FBgn0265813				-3,02

Supplement Data

1	FBgn0040359	CG11380	X		-3,19
1	FBgn0263250	CG43393	2R	cellular_component	-3,27
1	FBgn0050121				-3,47
1	FBgn0038315	CG14866	3R	carbohydrate binding	-3,60
1	FBgn0053302	Cpr31A	2L	structural constituent of chitin-based cuticle	-3,66
1	FBgn0266156				-3,78
1	FBgn0058469				-5,93
1	FBgn0265912				-6,11

Supplement Table: 5: Top 50 candidate list – Narf RNAi
MHC-GS Gal4; UAS-Narf RNAi + 20 μ M RU, Thorax sample 10 d

group	gene_id	gene_name	Chr	function	log2 fold
0	FBgn0262811	CG43182	X	cellular_component	-8,77
1	FBgn0004034	y	X	cytoplasm	-6,61
0	FBgn0053503	Cyp12d1-d	2R	mitochondrion	-6,58
0	FBgn0266822				-5,29
0	FBgn0003996	w	X	transmembrane signaling receptor activity	-5,01
1	FBgn0052640	CG32640	X	response to heat	-4,86
0	FBgn0032968	CG11634	2L	cellular_component	-4,33
1	FBgn0266253				-4,32
0	FBgn0262945				-4,30
1	FBgn0039299	CG11854	3R	extracellular space	-4,23
1	FBgn0036419	CG13482	3L		-4,17
1	FBgn0034293	CG14495	2R		-4,12
1	FBgn0265186	CG44251	2R		-4,00
0	FBgn0051600	CG31600	2L	cellular_component	-3,82
0	FBgn0262007	CG42825	3L	integral component of membrane	-3,71
1	FBgn0003082	phr	2R	DNA repair	-3,67
0	FBgn0004191				-3,62
1	FBgn0039298	to	3R	molecular_function	-3,57
1	FBgn0032235	CG5096	2L	protein binding	-3,51
1	FBgn0042102	CG18745	3R		-3,40
0	FBgn0053532	lectin-37Da	2L	extracellular region	-3,38
1	FBgn0265185	CG44250	2R		-3,36
0	FBgn0033733	CG8834	2R	metabolic process	-3,34
1	FBgn0034031	CG12963	2R		-3,34
1	FBgn0036320	CG10943	3L		-3,33
1	FBgn0085410	TrissinR	2L	G-protein coupled receptor activity	3,18
0	FBgn0035865	CG7201	3L		3,22
0	FBgn0002609	E(spl)m3-HLH	3R	nucleus	3,23
1	FBgn0262000	CG42818	2L		3,25
1	FBgn0034994	Ir60a	2R	integral component of membrane	3,30
1	FBgn0036790	AstC-R1	3L	integral component of membrane	3,30
0	FBgn0030204	Or9a	X	integral component of membrane	3,36
1	FBgn0266899				3,41
0	FBgn0266842				3,44
1	FBgn0032337	AstCC	2L	hormone activity	3,48
1	FBgn0267728	otk2	2R	protein binding	3,50
1	FBgn0267727	Pen	2L	binding	3,50
0	FBgn0038221	CG3259	3R	cilium	3,51
1	FBgn0083946	lobo	3R	molecular_function	3,51

1	FBgn0051025	Ppi1	3R	protein phosphatase 1 binding	3,55
1	FBgn0022981	rpk	3R	integral component of membrane	3,69
1	FBgn0030105	CG15369	X	cysteine-type endopeptidase inhibitor activity	3,71
0	FBgn0051683	CG31683	2L	lipid metabolic process	3,87
0	FBgn0035880	CG17352	3L	early endosome	3,93
0	FBgn0038915	CG17819	3R	GTP binding	4,02
1	FBgn0053302	Cpr31A	2L	structural constituent of chitin-based cuticle	4,15
1	FBgn0263250	CG43393	2R	cellular_component	4,33
1	FBgn0058469				5,14
1	FBgn0265912				5,97
0	FBgn0052475	mthl8	3L	G-protein coupled receptor activity	7,11

Supplement Table description information:

Supplement Table: 1:

group 1 – antioxidant activity

group 2 – binding

group 3 – catalytic activity

group 4 – reporter activity

group 5 – signal transducer activity

group 6 – structural molecule activity

group 7 – transporter activity

Supplement Table 3/4:

group 0 – Candidate was specifically identified for one overexpressed Narf allele

group 0 – Candidate was identified within top50 lists of one Narf allele and can be found within total list of the other Narf allele

group 1 – Candidate was identified within top50 lists of both Narf alleles

Supplement Table: 5

group 0 – Candidate was specifically identified for the Narf knockdown situation

group 1 – Candidate was also identified within total lists of one or both overexpressed Narf alleles

List of Figures

Figure 1: The deletion of a <i>kuk</i> deficient line comprise 5.5 kb within the genomic locus.....	- 17 -
.....	
Figure 2: The <i>kuk</i> deficient line $\Delta 15$ represents a protein null allele.....	- 18 -
Figure 3: Differentially expressed genes in <i>kuk</i> -depleted embryos	- 20 -
Figure 4: <i>kuk</i> -depleted animals show a decreased survival rate and lifespan.....	- 21 -
Figure 5: Genomic GFP-Kuk transgenes did not rescue the <i>kuk</i> -depleted phenotype....	- 23 -
Figure 6: Protein degradation occurs at the C-terminal end of GFP-Kuk.....	- 24 -
Figure 7: UAS/Gal4 expressed GFP-Kuk rescued the <i>kuk</i> depletion phenotype.....	- 25 -
Figure 8: Solubilization promoted GFP-Kuk degradation	- 27 -
Figure 9: FRAP analysis of wild type and mutant GFP Kuk	- 29 -
Figure 10: Scheme of the performed RNAi-screen.....	- 31 -
Figure 11: Kugelkern overexpression caused wing morphological defects.....	- 32 -
Figure 12: Kuk overexpression induced eye-defects primary independent of apoptosis-	- 34 -
Figure 13: Genetic interaction partners of <i>kuk</i> remain unidentified	- 36 -
Figure 14: Protein expression and purification of QE80N60-Narf	- 38 -
Figure 15: The antibody stained specific for Narf.....	- 39 -
Figure 16: Narf localized to the nuclear envelope.....	- 41 -
Figure 17: The lethal alleles NC38 and NC109 contained the described mutations.....	- 42 -
Figure 18: Characterization of different Narf lethal alleles.....	- 43 -
Figure 19: Narf protein level is decreased dramatically in NC38 homozygous larvae...-	- 44 -
Figure 20: Position of the human patient situation is conserved in <i>Drosophila</i>	- 45 -
Figure 21: Generation of genomic Narf alleles	- 46 -
Figure 22: Overexpression of genomic Narf increased survival rate	- 48 -
Figure 23: Ubiquitous overexpression of Narf prolonged <i>Drosophila</i> lifespan	- 49 -
Figure 24: Generation of a conditional Narf null allele by CRISPR/Cas9.....	- 52 -
Figure 25: The GeneSwitch system enables spatial and dose-dependent gene expression.....	- 54 -
.....	
Figure 26: The GeneSwitch Gal4 system enabled Narf overexpression.....	- 56 -
Figure 27: Narf overexpression affected nuclear size	- 58 -
Figure 28: Narf overexpression might affect negative geotaxis behavior.....	- 60 -
Figure 29: RU468 treatment did not affect <i>Drosophila</i> lifespan	- 61 -
Figure 30: Narf overexpression during adulthood affected <i>Drosophila</i> lifespan	- 63 -

Figure 31: Narf knock-down did not affect nuclear size	65 -
Figure 32: Muscle specific knockdown of Narf decreased lifespan.....	66 -
Figure 33: Ubiquitous down regulation of Narf during adulthood severely affected survival rate	68 -
Figure 34: Gene expression is changed in altered Narf expressing situations	70 -
Figure 35: oxy-4 mutants were sensitive to oxidative stress	73 -
Figure 36: Developmental delay of oxy-4 mutants under normoxic conditions	74 -
Figure 37: Striated muscle structure was normal in oxy-4 mutant worms	75 -
Figure 38: oxy-4 mutants showed a decline in pharyngeal pumping	76 -
Figure 39: oxy-4 mutant worms were normal in non-striated muscle structure.....	76 -
Figure 40: Nuclear morphology was not affected in oxy-4 mutant worms at larval stag-	78 -
Figure 41: A lack of farnesylation in Ce-lamin did not result in a protein shift.	79 -
Figure 42: Inefficient knockdown of oxy-4.....	80 -
Figure 43: Lifespan analyses of oxy-4 mutants with additional lmn-1 RNAi treatment	81 -
Figure 44: Amino acid sequence used for Nup153 antibody	122 -
Figure 45: Expression and purification of the pGEX-60H-Nup153 protein	123 -
Figure 46: Specificity of the generated Nup153 antibody.....	123 -
Figure 47: Nup153 antibody stains specific nuclear pore complexes	124 -
Supplement Figure 1: The deletion of $\Delta 15$ a kuk deficient fly line	145 -
Supplement Figure 2: Kugelkern is stable for at least four hours after solubilization ..	145 -
Supplement Figure 3: Kugelkern overexpression did not induce apoptosis in larval eye-discs	146 -
Supplement Figure 4: Strongest Narf expression was achieved using the tubulin-Gal4 driver.....	146 -
Supplement Figure 5: Wing specific down-regulation of Narf induced morphological defects.....	147 -
Supplement Figure 6: Narf-RNAi efficiently down regulated larval expressed Narf...-	147 -
Supplement Figure 7: p62/Ref(2)P protein level is not affected upon altered Narf expression	148 -
Supplement Figure 8: The amino acid sequence of Kuk contains two potential PEST-motifs	148 -
Supplement Figure 9: The amino acid sequence of lamin Dm0 contains no potential	149

List of Tables

Table 1: List of buffers	- 95 -
Table 2: Provided flystrains.....	- 97 -
Table 3: Flystrains generated in this study	- 98 -
Table 4: Worm strains used in this study	- 98 -
Table 5: RNAi-vectors used in this study.....	- 98 -
Table 6: Oligonucleotides used for C.elegans studies.....	- 101 -
Table 7: Oligonucleotides used for Drosophila studies.....	- 101 -
Table 8: Provided plasmids used in this study	- 103 -
Table 9: Plasmid constructs generated in this study.....	- 104 -
Supplement Table: 1: Top 50 candidate list: $\Delta 15$, embryo 6-8 hours.....	- 150 -
Supplement Table: 2: List of commercial available fly-lines used in the RNAi-screen.....	- 151 -
Supplement Table: 3: Top 50 candidate list – Narf WT.....	- 153 -
Supplement Table: 4: Top 50 candidate list – Narf H/R	- 154 -
Supplement Table: 5: Top 50 candidate list – Narf RNAi	- 155 -